

Performance Improvement of MEMS Accelerometers in Vibration Based Diagnosis

A thesis submitted to

The University of Manchester

For the degree of

Doctor of Philosophy (PhD)

in the Faculty of Engineering and Physical Sciences

2011

Abdellatef E. O. Badri

School of Mechanical, Aerospace and Civil Engineering

(This page is intentionally left blank)

TABLE OF CONTENTS

Table of Contents	3
List of Figures	7
List of Tables	12
Nomenclature	13
List of Abbreviations.....	14
List of Publications	15
Abstract	17
Declaration	18
Copyright Statement.....	19
Acknowledgments.....	20
Dedication	21
 CHAPTER 1 INTRODUCTION	 22
1.1 Overview.....	22
1.2 Objectives	25
1.3 Research Review	26
1.4 Outline of the Thesis.....	28
 CHAPTER 2 LITERATURE REVIEW	 30
2.1 Accelerometers.....	30
2.1.1 Piezoelectric Accelerometers	32
2.1.2 Capacitive type Accelerometers.....	35
2.2 MEMS Accelerometers	38
2.2.1 Sensing Mechanisms in MEMS Accelerometers	39
2.2.2 Capacitive Micro-accelerometer	41
2.2.3 Design Parameters for Capacitive MEMS Accelerometers	43
2.3 MEMS Fabrication Technology	49
2.3.1 Bulk Micromachining	49
2.3.2 Surface Micromachining.....	49
2.3.3 LIGA	50
2.4 MEMS Packing.....	50

2.5 Previous Works.....	51
2.5.1 General Applications.....	52
2.5.2 MEMS Accelerometers in Condition Monitoring.....	55
2.6 Summary	60
 CHAPTER 3 TEST SETUP.....	 61
3.1 Introduction	61
3.1.1 Accelerometer Specifications.....	61
3.1.2 Calibration Procedures.....	62
3.2 Test Setup	63
3.2.1 Test Rig Configuration.....	65
3.2.2 Methodology of Testing.....	66
3.3 The MEMS Accelerometers.....	68
3.3.1 MEMS 1 Accelerometer	68
3.3.2 MEMS 2 Accelerometer	70
3.3.3 MEMS 3 Accelerometer	70
3.3.3.1 Packing MEMS 3 Accelerometer.....	71
3.4 The Reference Accelerometer.....	72
 CHAPTER 4 PERFORMANCE EVALUATION OF MEMS ACCELEROMETERS.....	 73
4.1 Introduction	73
4.2 MEMS Accelerometers	75
4.3 Test Setup	75
4.4 Testing and Results.....	77
4.4.1 Periodic Excitation.....	77
4.4.2 Random Excitation.....	79
4.4.3 Impulse Excitation	80
4.4.4 Further Analysis.....	81
4.5 Comments.....	82
4.6 MEMS 1 Accelerometer	83

4.6.1	MEMS 1 Sinusoidal Excitation	83
4.6.2	MEMS 1 Random Excitation	85
4.6.3	MEMS 1 Sweep-sine Excitation	87
4.7	MEMS 2 Accelerometer	89
4.7.1	MEMS 2 Sinusoidal Excitation	89
4.7.2	MEMS 2 Random Excitation	91
4.7.3	MEMS 2 Sweep-sine Excitation	93
4.8	Comparison between Random and Sweep-sine Measurements.....	95
4.9	Conclusion	96
CHAPTER 5	CORRECTION IN TIME DOMAIN	97
5.1	Introduction	98
5.2	The Experiment Arrangement	99
5.3	The Experimental Results	99
5.4	Proposed Correction Method	102
5.5	Application of the Proposed Method	104
5.6	Conclusion	107
CHAPTER 6	CORRECTION IN FREQUENCY DOMAIN	109
6.1	Introduction	110
6.2	The Proposed Correction Method.....	111
6.2.1	Generation of Characteristic Function (CF)	112
6.2.2	Correction in Frequency Domain	115
6.3	Test Examples	116
6.3.1	Case I: MEMS 1 Accelerometer	117
6.3.1.1	The Sweep-sine Signal	121
6.3.1.2	The Sinusoidal Signals	123
6.3.2	Case II: MEMS 2 Accelerometer	130
6.4	Practical Application of the Correction Method.....	134

6.5	Enhancing the Frequency Range of Measurement for an Accelerometer	137
6.6	Conclusion	139
CHAPTER 7 ACCELEROMETER MODELLING.....		140
7.1	Introduction	141
7.2	A conventional Piezoelectric Accelerometer.....	142
7.3	A Capacitive Type MEMS Accelerometer	143
7.4	Earlier Studies on MEMS Accelerometers Performance.....	145
7.5	Limitations in the existing design of MEMS accelerometer.....	146
7.5.1	3-D Finite Element Model	146
7.5.2	Conversion of the Capacitance into Voltage	148
7.5.2.1	Modulation and Demodulation	149
7.5.2.2	Modulation and Demodulation Experiment.....	150
7.6	Possible Improvement in Mechanical Design.....	152
7.7	Conclusions	156
CHAPTER 8 CONCLUSIONS AND FUTURE WORK.....		158
8.1	Conclusions	158
8.2	Achieved Objectives.....	159
8.3	Overall Conclusion	161
8.4	Future Work	161
REFERENCES		162

LIST OF FIGURES

Figure 2.1 General layout of an accelerometer	31
Figure 2.2 The conventional piezoelectric accelerometer	33
Figure 2.3 Capacitive sensing methods	36
Figure 2.4 Differential or Push-pull displacement sensor	38
Figure 2.5 Capacitive Micro-accelerometer with differential capacitor	41
Figure 2.6 Lateral comb configurations: (a) before and (b) after movement	43
Figure 2.7 Transient response of the proof mass with and without PCB when subject to a mechanical shock [81]	53
Figure 2.8 Functional layout of the measurement system [87]	55
Figure 2.9 Block diagram of acceleration sensor transmitter [88]	56
Figure 2.10 Average coherence for all data acquired during the tests [90]	57
Figure 2.11 Sensor device mounted on a shaker for frequency testing [93]	58
Figure 2.12 Wireless sensor node for vibration monitoring [95]	59
Figure 3.1 Test Setup	64
Figure 3.2 Test rig Configuration.....	66
Figure 3.3 (a) Diagram connections of data acquisition programme, (b) Display front panel	67
Figure 3.4 MEMS 1 accelerometer	69
Figure 3.5 MEMS 3 accelerometer	71
Figure 3.6 (a) MEMS 3 packing structure, (b) final packing	72
Figure 4.1 A typical MEMS accelerometer construction: (a) piezoresistive using cantilever design, (b) capacitive based on membrane design [61]	75
Figure 4.2 Test setup.....	76
Figure 4.3 Measured acceleration responses by MEMS 3 accelerometer and the reference (PCB) accelerometer at 66Hz for the excitation level 0.3g.....	78
Figure 4.4 Measured acceleration responses by MEMS 3 accelerometer and the reference (PCB) accelerometer at 66Hz for the excitation level 0.75g	78
Figure 4.5 Measured acceleration responses by MEMS 3 accelerometer and the reference (PCB) accelerometer at 157Hz for the excitation level 0.65g	78
Figure 4.6 Measured acceleration responses by MEMS 3 accelerometer and the reference (PCB) accelerometer at 157Hz for random excitation	79
Figure 4.7 A typical measured FRF for the random excitation	80

Figure 4.8 A comparison of measured responses by MEMS 3 accelerometer and the PCB accelerometer when the shaker armature excited by impacts from a hammer.....	81
Figure 4.9 Coherence plots between the measured responses by MEMS 3 accelerometer and the reference accelerometer (a) Random test; (b) Impact test.....	82
Figure 4.10 MEMS 1 spectrum at 145Hz.....	84
Figure 4.11 FRF for MEMS 1 at 145 Hz	84
Figure 4.12 MEMS 1 spectrum at 375Hz.....	85
Figure 4.13 MEMS 1 FRF at 375Hz.....	85
Figure 4.14 MEMS 1 time domain signals and their spectra for random excitation	86
Figure 4.15 MEMS 1 FRF for random excitation.....	87
Figure 4.16 MEMS 1 time domain signals and their spectra for the sweep-sine excitation.....	88
Figure 4.17 MEMS 1 FRF for sweep-sine excitation.....	89
Figure 4.18 MEMS 2 spectrum at 237Hz.....	90
Figure 4.19 MEMS 2 FRF at 237Hz.....	90
Figure 4.20 MEMS 2 spectrum at 377.5Hz	91
Figure 4.21 MEMS 2 FRF at 377.5Hz.....	91
Figure 4.22 MEMS 2 time domain signals and their spectra for the random excitation	92
Figure 4.23 MEMS 2 FRF for random excitation.....	93
Figure 4.24 MEMS 2 time domain signals and their spectra for the sweep-sine excitation.....	94
Figure 4.25 MEMS 2 FRF for sweep-sine excitation.....	94
Figure 4.26 Comparison of the FRF plots between MEMS 1 accelerometer and the reference accelerometer due to sweep-sine and random excitations	95
Figure 5.1 Measured responses of the MEMS and reference accelerometers	100
Figure 5.2 FRF plot between MEMS and reference accelerometers, (a) Amplitude, (b) Phase	101
Figure 5.3 Inverse FRF (the FCF curve) plot- Comparison of original and fitted curves,	102
Figure 5.4 Poles and Zeros Map	105
Figure 5.5 The designed filter transfer function (TF) for phase and amplitude (dash line) and comparison with the CF (solid line with dots)	105
Figure 5.6 The corrected MEMS measured response (line with dots) compared with the reference accelerometer (solid line).....	106
Figure 5.7 Amplitude spectrum of corrected MEMS response (line with dots) compared with reference accelerometer (solid line).....	107

Figure 5.8 FRF plot of the MEMS accelerometer (after correction) with respect to the reference accelerometer, (a) Amplitude, (b) Phase	107
Figure 6.1 Test setup (a) picture, (b) schematic	113
Figure 6.2 Measured acceleration responses of the MEMS 1 and reference accelerometer	117
Figure 6.3 Acceleration responses in frequency domain for the MEMS 1 and reference accelerometer, (a) Amplitude Spectra, (b) FRF Amplitude and Phase	118
Figure 6.4 Comparison of the MEMS 1 responses due to Sine (line with dot) and Chirp-sine (line with circle) excitations, (a) FRF Amplitude, (b) FRF Phase	120
Figure 6.5 The CF in the frequency range (0-400 Hz) for the MEMS 1 accelerometer with respect to the reference accelerometer	121
Figure 6.6 Amplitude spectra of the MEMS 1 (before correction) and the reference accelerometer for the linear sweep-sine excitation	122
Figure 6.7 Comparison Amplitude spectra of the MEMS 1 (after correction, line with dot) and the reference accelerometer (solid line) for the linear sweep-sine excitation ...	122
Figure 6.8 FRF plot between the MEMS 1 (after correction) and the reference accelerometer for the linear sweep-sine excitation	123
Figure 6.9 Comparison of the amplitude spectra of the MEMS 1 (line with circle) and the reference accelerometer (line with plus) for the sinusoidal signal at 20 Hz, (a) before correction, (b) after correction	124
Figure 6.10 FRF plots the MEMS 1 with respect to the reference accelerometer for the sinusoidal signal at 20 Hz (indicated by circle), (a) before correction, (b) after correction	125
Figure 6.11 Comparison of the amplitude spectra of the MEMS 1 (line with circle) and the reference accelerometer (line with plus) for the sinusoidal signal at 145 Hz, (a) before correction, (b) after correction	126
Figure 6.12 FRF plots the MEMS 1 with respect to the reference accelerometer for the sinusoidal signal at 145Hz (indicated by circle), (a) before correction, (b) after correction	127
Figure 6.13 Comparison of the amplitude spectra of the MEMS 1 (line with circle) and the reference accelerometer (line with plus) for the sinusoidal signal at 377Hz, (a) before correction, (b) after correction	128

Figure 6.14 FRF plots the MEMS 1 with respect to the reference accelerometer for the sinusoidal signal at 377Hz (indicated by circle), (a) before correction, (b) after correction	129
Figure 6.15 Comparison of the MEMS 2 responses due to Sine (line with dot) and Sweep-sine (line with circle) excitations, (a) FRF Amplitude, (b) FRF Phase	131
Figure 6.16 Amplitude spectra for the MEMS 2 and reference accelerometers for the linear sweep-sine excitation	132
Figure 6.17 The CF in the frequency range (0-400 Hz) for the MEMS 2 accelerometer with respect to the reference accelerometer.....	132
Figure 6.18 Comparison of the amplitude spectra and FRF of the MEMS 2 (line with circle) and the reference accelerometer (line with star) for the sinusoidal signal at 237.5 Hz, (a) & (b) before correction, (c) & (d) after correction	133
Figure 6.19 Comparison of the amplitude spectra and FRF of the MEMS 2 (line with circle) and the reference accelerometer (line with star) for the sinusoidal signal at 377Hz, (a) & (b) before correction, (c) & (d) after correction	134
Figure 6.20 The experimental rig.....	135
Figure 6.21 Mounting of the MEMS and the reference accelerometers at the bearing-2 of the rig.....	135
Figure 6.22 Typical comparison of the amplitude spectrum for the MEMS accelerometer (a) before correction with the reference accelerometer (b) for the rig	136
Figure 6.23 FRF plot of the MEMS accelerometer before correction) with respect to the reference accelerometer, (a) Amplitude, (b) Phase	136
Figure 6.24 Typical comparison of the amplitude spectrum for the MEMS accelerometer (a) after correction with reference accelerometer (b) for the rig.....	137
Figure 6.25 FRF plot of the MEMS accelerometer (after correction) with respect to the reference accelerometer, (a) Amplitude, (b) Phase	137
Figure 6.26 Characteristic response curves of a typical accelerometer for two different mounting resonance frequencies	138
Figure 7.1 The conventional piezoelectric accelerometer	143
Figure 7.2 Typical constructional details of a capacitive type MEMS accelerometer [112]	144
Figure 7.3 A 3D model for a typical MEMS accelerometer.....	147
Figure 7.4 The 1 st mode shape in vertical direction.....	148
Figure 7.5 zoomed view	148

Figure 7.6 Block diagram for synchronised detection circuit	149
Figure 7.7 Modulation and demodulation experiment facility.....	150
Figure 7.8 Amplitude of FRF (a), Phase of FRF (b)	151
Figure 7.9 Simple model	152
Figure 7.10 FE Model	153
Figure 7.11 Mode shapes	153
Figure 7.12 Modified design.....	154
Figure 7.13 1st mode shape for the modified designs compared with original design.....	156

LIST OF TABLES

Table 3.1 MEMS 1 Specifications	69
Table 3.2 MEMS 3 Specifications	70
Table 3.3 Reference accelerometer Specifications.....	72
Table 6.1 Comparison of the FRF Amplitude and Phase for MEMS 1 due to Sine and Sweep-sine excitations with respect to the reference accelerometer	119
Table 6.2 Comparison of the FRF Amplitude and Phase for MEMS 2 due to sine and sweep- sine excitations with respect to the reference accelerometer	130
Table 7.1 Amplitude and phase values for the FRF.....	151
Table 7.2 Physical dimensions and material properties of the MEMS accelerometer.....	152
Table 7.3 Dimensions of modified designs and expected improvement	154
Table 7.4 Natural frequencies for mode shapes of modified designs	155

NOMENCLATURE

Notation	Description
f	Frequency
f_n	Natural frequency
ω	Angular frequency
C	Capacitance
C_t	Total capacitance
C_f	Fringe capacitance
ϵ_0	Permittivity of free space
ϵ	Relative permittivity
Q	Charge
V	Voltage
$V_{pull-in}$	Pull-in voltage
m	Proof mass
k	Mechanical spring constant
k_{elec}	Electric spring constant
K_T	Total spring constant
L_m	Mass length
W_m	Mass width
L_f	Moving finger length
W_f	Moving finger width
N_f	Number of moving fingers
h	Device thickness
L_b	Beam length
W_b	Beam width
ρ	Density
E	Young's modulus
ζ	Damping factor
N	Total number of data points
μ	Poisson's ratio

LIST OF ABBREVIATIONS

MEMS	Micro-Electro-Mechanical-System
ICP	Integrated Circuit Piezoelectric
DC	Direct Current
RMS	Root Mean Square
IC	Integrated Circuit
CMOS	Complementary Metal Oxide Semiconductors
LIGA	Lithography-Galvanoforming-Molding
CF	Characteristic Function
FFT	Fast Fourier Transform
FRF	Frequency Response Function
FCF	Filter Characteristic Function
A_{CF}	Amplitude of CF
Θ_{CF}	Phase of CF
TF	Transfer Function
PSD	Power Spectral Density
FE	Finite element
FEA	Finite Element Analysis

LIST OF PUBLICATIONS

Journal Publications

1. *Paper title “Performance evaluation of MEMS accelerometers”*
Authors: A. Albarbar, A. Badri, Jyoti K Sinha
Status: Published in the Journal of Measurement, Volume 42, Issue 5, June 2009, Pages 790-795

2. *Paper title “A Typical Filter Design to Improve the Measured Signals from MEMS Accelerometer”*
Authors: Abdellatef Badri, Jyoti K Sinha, A. Albarbar
Status: Published in the journal of Measurement, 43 (2010) 1425–1430

3. *Paper title “Enhancing the Frequency Range of Measurement for an Accelerometer”*
Authors: Abdellatef Badri, Jyoti K Sinha, A. Albarbar
Status: Published in the Journal of Noise & Vibration Worldwide, Volume 40, Number 6, June 2009

4. *Paper title “A Method to Calibrate the Measured Responses by MEMS Accelerometers”*
Authors: Abdellatef Badri, Jyoti K Sinha, A. Albarbar
Status: published in the Journal of Strain Journal (2010), doi: 10.1111/j.1475-1305.2010.00764.x

5. *Paper title “Dynamics of MEMS Accelerometer and Possible Design Modification for Future Improvement”*
Authors: Abdellatef Badri, Jyoti K Sinha, A. Albarbar
The Journal of Measurement
Status: Submitted

Conference Publications

1. *Paper title “Correcting Amplitude and Phase measurement of accelerometer in Frequency Domain”*
Authors: Abdellatef Badri, Jyoti K Sinha

The Fifth International Conference on Condition Monitoring and Machinery Failure Prevention Technologies-CM/MFPT 15 Jul 2008 - 18 Jul 2008

Status: Published

2. *Paper title “Improvement in measured signals of MEMS accelerometer”*

Authors: Abdellatef Badri, Jyoti K Sinha

3rd International Conference on Integrity, Reliability and Failure, Porto/Portugal, 2024 July 2009

Status: Published

3. *Paper title “Dynamics of MEMS accelerometer”*

Authors: Abdellatef Badri, Jyoti K Sinha

The 17th International Congress on Sound & Vibration, Cairo, July 2010

Status: published

ABSTRACT

The University of Manchester

Abdellatef E. O. Badri

PhD Mechanical Engineering

Performance Improvement of MEMS Accelerometers in Vibration Based Diagnosis

2011

Vibration measurement and analysis has been an accepted method since decades to meet a number of objectives - machinery condition monitoring, dynamic qualification of any designed structural components, prediction of faults and structural aging-related problems, and several other structural dynamics studies and diagnosis. However, the requirement of the vibration measurement at number of locations in structures, machines and/or equipments makes the vibration measurement exorbitant if conventional piezoelectric accelerometers are used. Hence, there is a need for cheaper and reliable alternative for the conventional accelerometers. The Micro-Electro-Mechanical Systems (MEMS) accelerometers are one such cheap alternative. However, a significant deviation in the performance of the MEMS accelerometers has been observed in earlier research studies and also confirmed by this presented study when compared with well known conventional accelerometer. Therefore, two methods have been suggested to improve the performance of the existing MEMS accelerometers; one for correction in time domain and other in frequency domain. Both methods are based on the generation of a characteristic function (CF) for the MEMS accelerometer using well known reference accelerometer in laboratory tests. The procedures of both methods have been discussed and validations of these methods have been presented through experimental examples. In addition, a Finite Element (FE) model of a typical MEMS accelerometer has been developed and modal analysis has been carried out to understand the dynamics of capacitive type MEMS accelerometer and to identify the source of errors. It has been observed that the moving fingers behave like a cantilever beam while the fixed fingers showed rigid body motion. This cantilever type of motion seems to be causing non-parallel plates effect in the formed capacitors between moving and fixed fingers which results in errors in the vibration measurement. Hence, design modifications on finger shape have been suggested to remove the cantilever motion and results showed remarkable improvement. Moreover, the effect of using synchronous amplitude modulation and demodulation in the readout circuit has been studied. The experimental study showed that this circuit also introduces errors in amplitude and phase of the output signal compared with the input signal. Thus, in the new design of MEMS accelerometers, improvements in both mechanical design and electronic circuit are required.

DECLARATION

I hereby declare that no portion the work referred to in the thesis has been submitted in support of an application for another degree or qualification of this or any other university or other institute of learning.

COPYRIGHT STATEMENT

- I. The author of this thesis (including any appendices and/or schedules to this thesis) owns certain copyright or related rights in it (the “Copyright”) and s/he has given The University of Manchester certain rights to use such Copyright, including for administrative purposes.
- II. Copies of this thesis, either in full or in extracts and whether in hard or electronic copy, may be made **only** in accordance with the Copyright, Designs and Patents Act 1988 (as amended) and regulations issued under it or, where appropriate, in accordance with licensing agreements which the University has from time to time. This page must form part of any such copies made.
- III. The ownership of certain Copyright, patents, designs, trademarks and other intellectual property (the “Intellectual Property”) and any reproductions of copyright works in the thesis, for example graphs and tables (“Reproductions”), which may be described in this thesis, may not be owned by the author and may be owned by third parties. Such Intellectual Property and Reproductions cannot and must not be made available for use without the prior written permission of the owner(s) of the relevant Intellectual Property and/or Reproductions.
- IV. Further information on the conditions under which disclosure, publication and commercialisation of this thesis, the Copyright and any Intellectual Property and/or Reproductions described in it may take place is available in the University IP Policy (see <http://www.campus.manchester.ac.uk/medialibrary/policies/intellectual-property.pdf>), in any relevant Thesis restriction declarations deposited in the University Library, The University Library’s regulations (see <http://www.manchester.ac.uk/library/aboutus/regulations>) and in The University’s policy on presentation of Theses.

ACKNOWLEDGMENTS

I would like to thank my supervisor Dr. **Jyoti K. Sinha** for his continuous support, guidance, and encouragement all along this research study. I also appreciate the assistance of Mr. Paul Townsend, Technical Coordinator for his assistance in preparing test facilities. Special thanks to my colleague Israr Ullah for day-to-day work and discussions.

.

DEDICATION

I dedicate this work to my mother (died in 1995), my father, my wife, my kids, and my family who encouraged me to proceed for this Ph.D. study.

CHAPTER 1

INTRODUCTION

1.1 Overview

Vibration measurement and analysis has been the accepted method to meet a number of objectives; it plays a significant role in machine condition monitoring [1-9], dynamic qualification of newly designed structural components [10-13], prediction of faults and structural aging-related problems [14–15], and several other structural dynamics studies and diagnoses [16–18]. One reason for its wide usage is its capability to monitor vibrating machines without interrupting normal operations. In addition, the vibrating mechanisms of most machinery and structures are fundamentally well-known, giving rise to the possibility of detecting many faults in accordance with the characteristics of the vibration responses. Furthermore, the progress of vibration signal processing techniques, computing capabilities and reliable performance of vibration instrumentation such as wide band transducers and portable analysers has caused this technique to be extensively used around the world.

In condition monitoring of machines, as an example, accelerometers are often used to measure the acceleration responses of the vibrating components to obtain vibration waveforms, which may lead to detection of incipient fault conditions of machines by analysing the vibration signals. These waveforms are interpreted and processed in a variety of ways such as the root mean square (RMS) and variance of the signal in the time domain, and power spectrum analysis in the frequency domain. Wavelet and higher

order spectral analyses are recent signal analysis techniques used to examine vibration waveforms and then decide on machine condition [19].

Vibration has traditionally been sensed using piezoelectric accelerometers or ICP type accelerometers. These accelerometers are referred a conventional accelerometers. They are accurate and reliable, but have two inherent problems: they are difficult to mass-produce and they have high source impedance, which means that their signals must be very carefully amplified as close as possible to the sensor itself. Moreover, the use of the traditional piezoelectric accelerometers for simultaneous multiple data collection points was considered to be impractical; this is mainly because of their cost and the price of the associated electronic signal conditioning units. Other types such as piezoresistive accelerometers have limited resolution and can be used only for low and medium frequencies; this is also a disadvantage of the electrodynamic type. The capacitive type has low resolution and fragile. Commercially, several types of accelerometers manufactured by many well-known manufacturers are available all over the world.

Obviously, the quality of the vibration-based diagnosis mainly depends on the measured responses using accelerometers. Therefore, good performance and reliability of the commercially available accelerometers is very important. In addition, the use of conventional accelerometers for multiple data collection points may increase the complexity of monitoring system because of the associated electronic units that externally connect to the accelerometers. Consequently, the need for cheaper and reliable devices was recognized.

Researchers over the years have developed micro-fabricated systems for measuring temperature, pressure, force, position, torque, flow, magnetic field, humidity, gas composition, biological gas/liquid molecular concentration and acceleration [20]. The use of Micro-Electro-Mechanical Systems (MEMS) accelerometers is one of the available options that came to light because of their low cost and small size. MEMS accelerometers are produced using the same process as integrated circuit manufacturing; this allows the sensor, actuator, and the signal conditioning electronic circuits to be integrated into a single chip.

MEMS can generally be characterized as miniature systems involving one or more micro-machined components or structures. The inherently small size of MEMS enables high level functions by virtue of the large-scale integration process. This permits multiple functions or capabilities integrated on the same silicon chip or package for greater utility. However, the use of MEMS accelerometers is still limited in the field of condition monitoring, although there had been some research going on in their use in structural monitoring. The main reason is that the performance of most devices is not ready to penetrate this market as they are designed and manufactured for other application such as automotive, consumer electronics, and biomedical area where they are only used to detect the event of impact or motion. The stability, sensitivity, lifetime, mechanical strength, ease of operation and installation, are not attractive enough for using them in machine condition monitoring, also there are some concerns about the effect of noise and temperature on their accuracy. A few earlier researches have compared the performance of MEMS and conventional accelerometers, mainly related to the frequency content in the spectrum of the measured signals [21-24]. It has been

observed that the frequency content in the spectrum of the measured signal from the MEMS accelerometer is the same as in the spectrum obtained from the conventional accelerometer if measured at the same location by both accelerometers. However a significant deviation has been noticed in the amplitude and phase. In practice, many vibration based diagnoses for machines and structures have been utilizing the frequency domain data for the system and fault identifications. However, one of the complicated issues in machinery diagnostics is the fact that two very different waveforms can yield similar spectra as their phase relationships are ignored when viewed in the frequency domain. Hence, the phase relationships between the frequency at the running speed of the machine and its harmonics in the time domain may be acceptable when considering factors of lost production, and the unnecessary costs replacing machine parts that may not have been defective in the first place.

1.2 Objectives

The aim of this research is initially to understand the behaviour of MEMS accelerometers and then explore the possibility of improving the performance of MEMS accelerometers to meet the requirements needed for vibration measurements. Hence the objectives are:

1. Compare MEMS accelerometer performance with conventional accelerometer.
2. Improve the measured response in time domain by designing a new filter to correct the phase and amplitude linearity for the existing MEMS accelerometer.

3. Other approach -Improve the measured response in frequency domain for the existing MEMS accelerometer.
4. Explore the possibility of design modification in the present MEMS accelerometer in order to improve its performance.

1.3 Research Review

As previously mentioned, the aims of the present research are to improve the performance of MEMS accelerometers for vibration-based diagnosis applications by correcting the responses of the existing MEMS accelerometers both in time and frequency domains, and study the dynamics of these accelerometers to identify the possible sources of errors in order to propose suitable solutions. In the present work, the performance of capacitive type MEMS accelerometers has been compared with reference conventional accelerometer. The comparison is based on the computation of the Frequency Response Function (FRF) with the measured signals by the reference accelerometer used as the input and by the MEMS accelerometer as the output. It has been observed that MEMS accelerometers show some deviation, both in amplitude and phase of the FRF, for all types of vibration signals.

Vibration signal analysis in the time domain can prevent a misdiagnosis of a rotating machinery problem. Therefore, a method to improve responses of the MEMS accelerometers in the time domain has been developed. The method is based on the use of especially designed filter which its Characteristics Function (CF) matching the CF of the MEMS accelerometer that is generated by comparing the response of the MEMS

accelerometer with the reference accelerometer. The novel method can correct the deviation in both amplitude and phase as it is examined by the FRF before and after correction.

MEMS accelerometers also showed significant deviation of amplitude and phase even in the frequency domain when compared with a reference accelerometer. Hence, a method for correcting the measured MEMS accelerometer signals in the frequency domain has been presented and validated through experimental application on a rotating test rig. The method provided significant improvement in MEMS measured signals when comparing its amplitude and phase with the amplitude and phase of the reference accelerometer in response to different types of controlled vibration signals. The method also can be used to extend the frequency bandwidth of any accelerometer.

To investigate the source of the observed errors, a dynamic study of the capacitive type MEMS accelerometer has been presented. The study included a fine mesh FE model (3-D model) with two moving fingers and three fixed fingers considering the fingers shape design used in the existing accelerometers. It has been observed that the moving fingers behave like a cantilever beam which leads to non-parallel plate effect. Hence, a simple FE model; with a spring, a moving mass, and two moving fingers; has been developed in order to modify the design of the fingers. A few modifications on finger shape design have been suggested which showed remarkable improvement. Also, the effect of using synchronous amplitude modulation and demodulation in the readout circuit has been studied. The experimental study showed that this circuit introduces errors in amplitude and phase of the output signal compared with the input signal.

1.4 Outline of the Thesis

This thesis is not presented in the classical format of PhD thesis. Rather, it is presented in the alternative format with its core context provided in the form of published/submitted papers. However, it should be noted that as in the classical format, the alternative format requires that all the references at the end of each paper be collected together and grouped under “References” at the end of the thesis.

Chapter Two: presents the concepts and working principles of conventional and MEMS accelerometers, and the earlier research studies on the applications of MEMS accelerometers in the field of condition monitoring.

Chapter Three: provides a summary of the papers included in this thesis.

Chapter Four: provides a detailed description of the test set up and lists the test equipments and tools used in data collection and processing.

The following four chapters, Chapter 5 to Chapter 8, are constituted of eight published or submitted papers that report the candidate’s own work.

Chapter Five: presents the performance evaluation of MEMS accelerometers compared with a well known conventional accelerometer.

Chapter Six: presents a correction method of the MEMS accelerometer measured signals in time domain by design of a typical filter.

Chapter Seven: presents the proposed method to correct the MEMS accelerometer responses in frequency domain and how this method can be used to extend the frequency bandwidth of any accelerometer.

Chapter Eight: presents the possible improvements in the mechanical design of the MEMS accelerometer using finite element analysis.

Chapter Nine: concludes the thesis with summary and suggestions for further work.

CHAPTER 2

LITERATURE REVIEW

This chapter presents the concepts of conventional accelerometers that are currently used in machine and structure condition monitoring. Basic principles of capacitive type MEMS accelerometers, review of other types of MEMS accelerometers, and fabrication processes are also discussed. The chapter also provides review of the previous reported research studies regarding the performance improvement of MEMS accelerometers used for general applications, and in the field of vibration-based condition monitoring.

2.1 Accelerometers

Acceleration sensors or accelerometers are used to measure acceleration, vibration and mechanical shock. Acceleration is the first derivative of velocity and second derivative of displacement. The relationships between velocity and displacement for translational and rotational system can be expressed as:

$$a = \frac{dv}{dt} = \frac{d^2x}{dt^2} = \ddot{x} \quad (2.1)$$

$$\alpha_{\theta} = \frac{d\omega}{dt} = \frac{d^2\theta}{dt^2} = \ddot{\theta} \quad (2.2)$$

Although it is possible to compute the acceleration of an object from the output of a displacement or velocity, most accelerometers use a sensing method in which a proof

mass displacement with respect to the accelerometer housing is detected [25]. The basic sensing arrangement of an accelerometer is shown Figure 2.1.

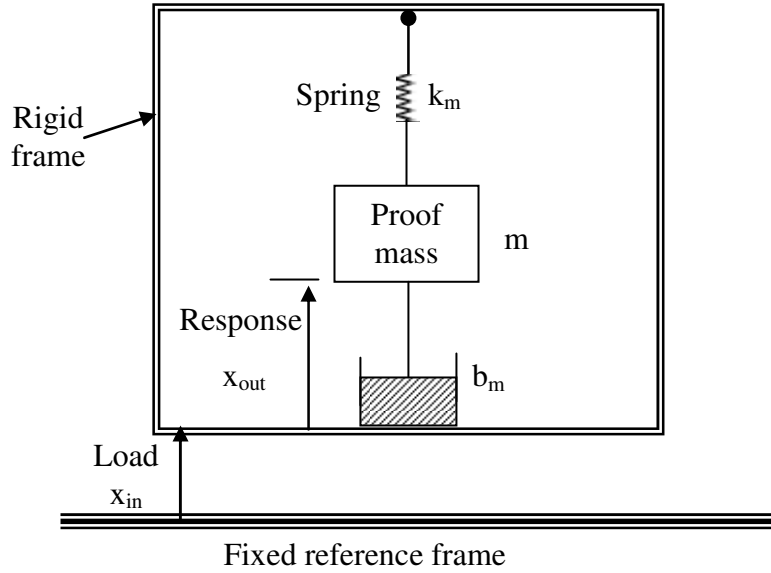


Figure 2.1 General layout of an accelerometer

The accelerometer is essentially a mass-spring –damper system in which the loading force $-m\ddot{x}_{in}$ drives a second order damped harmonic oscillator. The equation of motion of this system can be expressed as:

$$m\ddot{x}_{out} + b_m\dot{x}_{out} + k_m x_{out} = -m\ddot{x}_{in} \quad (2.3)$$

Where, x_{out} is the displacement of the proof mass (m) relative to the rigid frame. Under constant acceleration conditions, the displacement x_{out} is directly proportional to the input acceleration \ddot{x}_{in} where [26],

$$x_{out} = \left(\frac{m}{k_m} \right) \ddot{x}_{in} \quad (2.4)$$

The behaviour of this dynamic system is determined by two parameters; the natural frequency ω_o and the damping factor ζ where,

$$\omega_o = \sqrt{\frac{k_m}{m}} \quad (2.5)$$

$$\zeta = \frac{b_m}{2\sqrt{k_m m}} \quad (2.6)$$

There are different types of accelerometers and each has unique characteristics, advantages and disadvantages. The accelerometers can be classified according to the physical effect used in the sensing mechanism such as piezoelectric accelerometers, piezoresistive accelerometers, and strain gage accelerometers. These types can also be classified based on their operating mode such as compression mode, shear mode, and flexural mode.

2.1.1 Piezoelectric Accelerometers

Description

Accelerometers are sensing transducers that produce an electrical output signal proportional to the acceleration aspect of motion, vibration and shock. Most

accelerometers generate an electrical output signal that is proportional to an induced force. Piezoelectric accelerometers rely on the self-generating piezoelectric effect of either ceramic or quartz crystals to produce an electrical output proportional to acceleration. Some of them contain built-in conditioning circuitry and are known as Integrated Circuit Piezoelectric (ICP) while those that do not contain any additional circuit are called the charge mode or high impedance type. They are capable of measuring very high acceleration transients such as those encountered in machinery vibration and high frequency shock measurements.

Principle of Operation

A typical design of a conventional piezoelectric accelerometer is shown in Figure 2.2. It consists of a small mass, a spring made of piezoelectric crystal and a damping of around 0.7. For this configuration, if the natural frequency of the accelerometer is f_n then the linear frequency range of measurement is approximately 20% of the natural frequency, f_n . The input acceleration of a vibrating object causes the vibration of the accelerometer mass, m which results in the relative motion, $\Delta x(t)$, between the mass and the object in the piezoelectric spring generates the proportional electric charge, $\Delta Q(t)$.

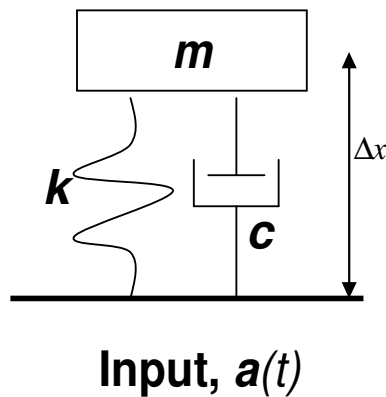


Figure 2.2 The conventional piezoelectric accelerometer

Mathematically it can be written as

$$\Delta x(t) \approx \frac{a(t)}{\omega_n^2} \propto \Delta Q(t) \quad (2.7)$$

where, $\omega_n = 2\pi f_n$. Hence the charge, $\Delta Q(t)$, is proportional to the acceleration of the vibrating object which is then converted into a voltage as the output for the accelerometer.

Charge mode accelerometers

Charge mode accelerometers output a high-impedance, electrical charge signal that is generated directly by the sensing element. A charge amplifier is needed to condition this high-impedance to a low-impedance voltage before it can be input into a readout or recording device. The use of a special low noise cable is employed to reduce the influence of cable noise and other environmental influences. Charge mode accelerometers are used in areas where expected temperatures are very high [27].

Integrated Circuit Piezoelectric (ICP) Accelerometers

These accelerometers incorporate built in signal conditioning electronics that have the function of converting the high-impedance charge signal generated by the piezoelectric sensing element into a usable low impedance voltage signal that can be easily transmitted over ordinary two-wire or coaxial cables, to any voltage read-out or recording device. The low impedance signal can be transmitted over long cable distances with little degradation. The simplicity of use, high accuracy, and broad frequency range make them the recommended type for use in most condition monitoring applications. A major disadvantage however lies in the fact that the

maximum operating temperature is limited to what is permissible for the built in circuitry [27].

2.1.2 Capacitive type Accelerometers

The simplest capacitor or condenser consists of two parallel metal plates separated by a dielectric or insulating material as shown in Figure 2.3. The capacitance of this parallel capacitor is given by:

$$C = \frac{\epsilon_o \epsilon A}{d} \quad (2.8)$$

Where, ϵ_o is the permittivity of free space (vacuum) of magnitude $8.85 \text{ (pf m}^{-1}\text{)}$, ϵ is the relative permittivity or dielectric constant of the insulating material, $A \text{ (m}^2\text{)}$ is the area of overlap of the plates, and $d \text{ (m)}$ is their separation [28]. Consequently, any phenomenon that changes area, the dielectric constant, or the separation of the capacitor plates will cause a change in the capacitance δC . This variation can be defined by the total differential formula:

$$\delta C = \left. \frac{dC}{dA} \right|_{\epsilon, d} \delta A + \left. \frac{dC}{d\epsilon} \right|_{A, d} \delta \epsilon + \left. \frac{dC}{dd} \right|_{\epsilon, A} \delta d \quad (2.9)$$

From Equations (2.8) and (2.9) C can be changed by changing either A , ϵ , or d ; for example, the mechanical displacement of one plate relative to the other could cause the

separation between the two plates to change by δd resulting in change in the capacitance C . This principle is exploited in a variety of capacitive type micro sensors [26]. Figure 2.3 shows the basic arrangements for capacitive sensor using each of these methods. In the variable area type, the displacement x causes the overlap area to decrease by $\Delta A = wx$, where w is the width of the plates, giving:

$$C = \frac{\epsilon_0 \epsilon}{d} (A - wx) \quad (2.10)$$

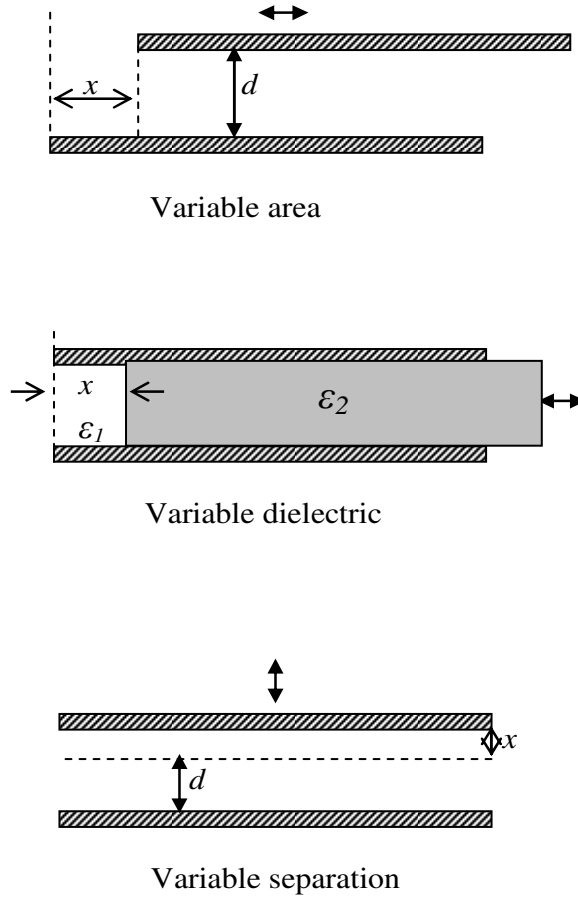


Figure 2.3 Capacitive sensing methods

In the variable dielectric type, the displacement x changes the amount of dielectric material ϵ_2 ($\epsilon_2 > \epsilon_1$) inserted between the plates. The total capacitance of the sensor is

the sum of two capacitances, one with area A_1 , dielectric constant ϵ_1 , and one with area A_2 , dielectric constant ϵ_2 ;

$$C = \frac{\epsilon_o \epsilon_1 A_1}{d} + \frac{\epsilon_o \epsilon_2 A_2}{d} \quad (2.11)$$

Since $A_1 = wx$, $A_2 = w(l-x)$, when w is the width of the plates,

$$C = \frac{\epsilon_o \epsilon}{d} [\epsilon_2 l - (\epsilon_2 - \epsilon_1)x] \quad (2.12)$$

If the displacement x causes the plate separation to increase to $d+x$, the capacitance of the sensor is:

$$C = \frac{\epsilon_o \epsilon A}{d+x} \quad (2.13)$$

This is a variable separation displacement sensor which has the disadvantage of being non-linear. This problem is overcome by using three-plate differential or push-pull displacement sensor as shown in Figure 2.4. This sensor consists of a plate M moving between two fixed plates P_1 and P_2 ; if x is the displacement of M from the centre line AB , then the capacitances C_1 and C_2 formed by MP_1 and MP_2 respectively, are:

$$C_1 = \frac{\epsilon_o \epsilon A}{d+x}, \quad (2.14)$$

$$C_2 = \frac{\epsilon_o \epsilon A}{d-x} \quad (2.15)$$

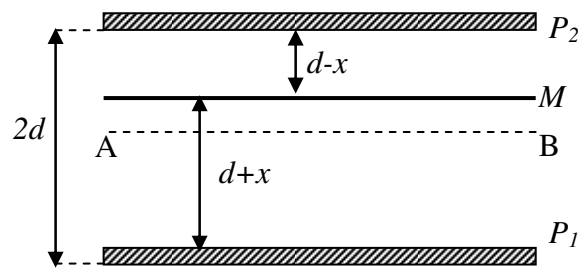


Figure 2.4 Differential or Push-pull displacement sensor

2.2 MEMS Accelerometers

The successful application of a sensor is determined by its performance, cost and reliability. Nevertheless a large sensor may have excellent operating characteristics but its marketability is severely limited simply by its size. A reduction in the size of a sensor often leads to an increase in the applicability through less weight (greater portability), lower manufacturing cost (less materials), and wider range of applications.

The cost of a sensor is often the single most important factor. Clearly, less material is needed to manufacture a small sensor but the cost of materials' processing is often a

more significant factor. Silicon technology has facilitated the production of small, reliable processors in the form of Integrated Circuits (ICs) using the microelectronic technology. The micromechanical components are fabricated using compatible "micromachining" processes that selectively etch away parts of the silicon wafer or add new structural layers to form the mechanical and electromechanical devices. Using silicon-based microelectronics with micromachining technology, micro sensors, micro actuators and signal conditioning electronic circuits can be integrated in one single chip and the acronym MEMS which stands for Micro-Electro-Mechanical Systems is used for the resulting device [29].

2.2.1 Sensing Mechanisms in MEMS Accelerometers

Many physical effects have been used for acceleration sensing in MEMS accelerometers. The first micromachined accelerometer commercialized by NovaSensor was piezoresistive [30]. The main advantages of piezoresistive accelerometers are the simplicity of their structures and fabrication processes as well as the read-out circuits. However, piezoresistive devices have some critical drawbacks such as low sensitivity and large temperature dependence. Complex temperature compensation circuits are often needed and a very large proof mass is essential for an acceptable sensitivity.

The capacitive sensing mechanism is dominant in MEMS accelerometers for several reasons. Both surface and bulk micromachining can be used to fabricate a variety of capacitive accelerometers with performance ranging from the low-end automotive application grade to the high-precision inertial navigation grade. Compared to

piezoresistive accelerometers, capacitive accelerometers have high sensitivity, low power consumption, low noise level, stable DC characteristics and less temperature dependence. Their simple structures and fabrication processes make the integration of conditioning circuits with sensing elements more straightforward.

While capacitive and piezoresistive sensing are two of the most common sensing mechanisms, other physical mechanisms such as resonant frequency shift, thermal transfer and quantum electron tunnelling have also been exploited acceleration and motion sensing. A micromachined vibrating beam accelerometer and a vacuum packaged resonant accelerometer have been reported for acceleration and motion sensing respectively [31, 32]. In both resonant accelerometers, the force generated by the external acceleration on the specially designed proof mass changes its resonant frequency. Therefore, the acceleration is measured in terms of a shifted resonant frequency of the resonant device. The apparent advantage of the resonant accelerometer is its direct digital output. Thermal accelerometers have also been developed based on the principle of convection heat transfer [33, 34]. Since there are no movable elements in this thermal accelerometer and the manufacturing variations do not influence the thermal performance of the device, these thermal accelerometers demonstrate very good robustness and good batch reproducibility. To achieve high sensitivity, current tunnelling effects have also been exploited for sensing acceleration [35-37]. These accelerometers measure the displacement operating on the principle of quantum electron tunnelling, which has very high position sensitivity. A resolution of $20 \text{ ng} / \sqrt{\text{Hz}}$ has been accomplished by the reported micromachined tunnelling accelerometer [38]. This particular accelerometer requires very specific technological processes. The complexity

of the fabrication and strict conditioning circuit design make it very difficult for this tunnelling accelerometer to be commercialized. Other accelerometers using optical, piezoelectric and electromagnetic sensing mechanisms have been demonstrated [39-42]. However, the integration of these accelerometers with CMOS technology is a challenge.

2.2.2 Capacitive Micro-accelerometer

The deflection of the proof mass can be measured by change in capacitance. Figure 2.5 shows a cross sectional diagram of a capacitive micro-accelerometer where the entire sensor is micromachined from silicon and the proof mass is sandwiched between metal plates. The plates form two capacitors, so that the differential method which is mentioned previously can be employed.

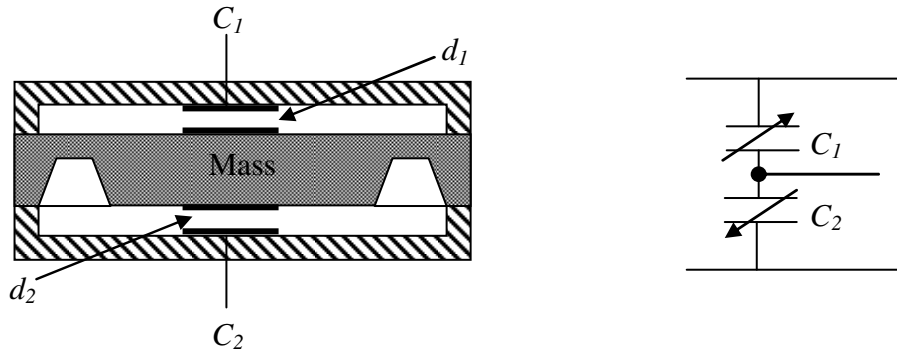


Figure 2.5 Capacitive Micro-accelerometer with differential capacitor

As the displacement x_{out} is proportional to acceleration (Equation 2.4), the inverse capacitance of each capacitor is proportional to the acceleration,

$$\frac{\delta C}{C} = \frac{x_{out}}{d} \propto \ddot{x} \quad (2.16)$$

And the ratio of capacitances is,

$$\frac{C_1}{C_2} = \frac{d_2}{d_1} \quad (2.17)$$

For a small displacement of x_{out} , $d_1 = d_1 - x_{out}$, and $d_2 = d_2 + x_{out}$, and the ratio of capacitances can be expressed as:

$$\frac{C_1}{C_2} = \frac{d_2 + x_{out}}{d_1 - x_{out}} \quad (2.18)$$

As the two capacitors are identical, $d_1 = d_2$ we can rewrite equation (2.18) as:

$$\frac{C_1}{C_2} = \frac{d_1 + x_{out}}{d_1 - x_{out}} \quad (2.19)$$

And it can be approximated as [26]:

$$\frac{C_1}{C_2} = \frac{d_2}{d_1} \approx \frac{1 + (x_{out} / d_1)}{1 - (x_{out} / d_1)} \approx 1 + \frac{2x_{out}}{d_1} \quad (2.20)$$

From Equation (2.20), the ratio of capacitances is independent from the dielectric constant and plate area, so it can be stated that measuring the ratio of the capacitances eliminates the temperature dependence of the dielectric constant and area.

In other configuration which is called *lateral comb capacitance*, the change of the capacitance is formed by change of the overlap area [43]. The moving plates translate along the long axis of plates as shown in Figure 2.6.

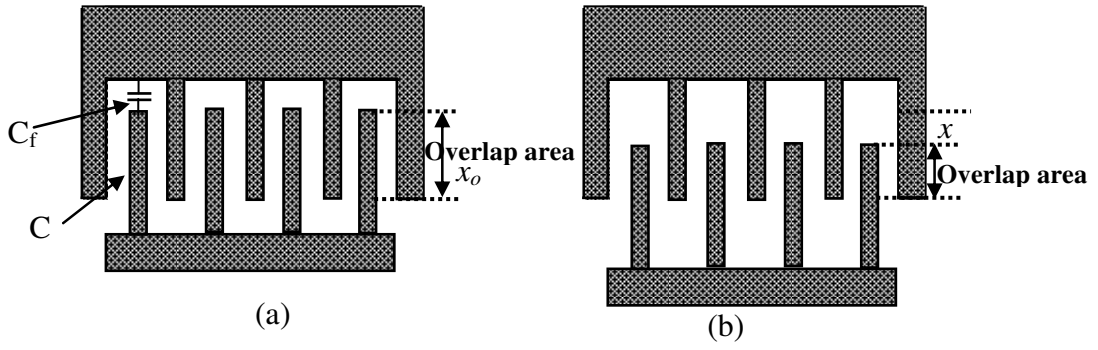


Figure 2.6 Lateral comb configurations: (a) before and (b) after movement

The total capacitance (C_{total}) of this configuration is,

$$C_{total} = N \left[\frac{\epsilon t (x - x_o)}{d} + C_f \right] \quad (2.21)$$

Where, t is the plate thickness, and C_f is the fringe capacitance.

Generally, the capacitive type MEMS accelerometer consists of a spring and a mass both made of a material commonly poly-silicon. Numbers of plates (fingers) are attached to the mass which are generally called as the “Moving fingers” and number of fingers attached to the fixed frame of the accelerometer, called “Fixed fingers”. The arrangement is such that a pair the fixed and moving fingers constitutes a parallel capacitor.

2.2.3 Design Parameters for Capacitive MEMS Accelerometers

The most common MEMS accelerometer design parameters; or sometimes called performance parameters; are resolution, sensitivity (scale-factor), bandwidth,

nonlinearity, acquisition time, and bias drift [44]. The process limitations directly affect the performance of the accelerometer. Moreover, some parameters like nonlinearity, bias drift and scale factor asymmetry cannot be estimated theoretically, because they are almost totally process dependent. Hence, the choice of the process is an important design issue. After choosing the process, the performance of the accelerometer can be optimized with a proper mechanical design and with using a proper readout circuit.

The performance parameters are directly affected by variables called design variables, these variables are varied during design to obtain optimal solution. The main design variables for accelerometer layout synthesis are: length and width of the central plate-mass, sizes and number of beams used in the serpentine spring, number of the fixed fingers, the gap between the fixed and moving fingers, and the length and width of the moving fingers. The sensing mass M_s of the accelerometer, which includes the seismic mass and all the movable fingers attached to it, can be expressed as:

$$M_s = \rho h (W_m L_m + N_f W_f L_f) \quad (2.22)$$

Where, ρ is the density of ploy-silicon material, h is the device thickness, W_m is mass width, L_m is mass length, N_f is the number of moving fingers, W_f is the width of moving finger, and L_f is its length.

The displacement of this sensing mass due to the applied acceleration can be expressed as [45]:

$$x = \frac{M_s g}{k} = \frac{\rho g (W_m L_m + N_f W_f L_f) L_b^3}{E W_b^3} \quad (2.23)$$

Where, E is the Young's modulus of poly-Silicon, and k is the mechanical spring constant which is defined (for one beam) as:

$$k = \frac{E h W_b^3}{L_b^3} \quad (2.24)$$

Where, L_b and W_b are the beam length and width respectively.

Sensitivity is defined as the ratio of a change in the output to a change in the input intended to be measured [46, 47]. The sensitivity of a capacitive type accelerometer is determined by its capacitive sensitivity ($pF/\mu m$) and mechanical sensitivity ($\mu m/g$).

$$S(pF/g) = \frac{\Delta C}{\Delta x} \cdot \frac{\Delta x}{g} \quad (2.25)$$

The unit of the sensitivity is V/g if mechanical part and readout circuitry is considered together. In order to obtain a high sensitivity and low mechanical noise, the proof mass should be as large as possible, reducing the air gap between the sensing electrodes and increasing the overlap area between the electrode fingers [46, 47]. Large proof mass can be achieved by increasing the thickness and/or increasing the surface area which will increase the capacitance value. However, the thickness of the proof mass can only be increased up to the limitation of the capability of the fabrication equipments. Therefore,

the design of the accelerometer needs to be optimized to achieve high sensitivity and minimum mechanical noise based on the allowable fabrication process parameters. The voltage sensitivity is not an indicator of the performance of the accelerometer because with external amplifiers this sensitivity value can be arranged to any value. However, the capacitance sensitivity mainly shows the performance of the accelerometer mechanical part.

Spring constants play an important role in determining the performances of the accelerometer. The performance is related with the easiness in the movement of the proof mass in certain directions and also with the difficulty in the movement of the proof mass in some other directions. For the parallel plate configuration, the total spring constant is the sum of electrical spring constant and mechanical spring constant [48].

$$K_T = k + k_{elec} \quad (2.26)$$

$$\text{where, } k_{elec} = -\frac{\epsilon A}{d_o^3} V^2 \quad (2.27)$$

This electrical spring, which known as a non-linear electrostatic force, acts as mechanical spring with negative spring constant. Hence, this spring constant may cause electromechanical instability (Pull-in) if it is greater than the mechanical spring constant. Analyses show that pull-in occurs when the distance of the two electrodes become 2/3 of the original distance ($x=d/3$). The voltage difference applied to the electrodes that causes pull-in is called pull-in voltage and can be calculated as [49]:

$$V_{pull-in} = \sqrt{\frac{8d^3k}{27\epsilon A}} \quad (2.28)$$

This voltage is important as for the voltage biased accelerometer the device becomes unstable if the bias voltage exceeds $V_{pull-in}$.

The resolution is defined as the smallest signal change that needs to be detected; and it is governed by the sensitivity, i.e. the magnitude of the response for a given input and the noise. It can be improved by either increasing sensitivity, or by lowering the noise [50]. Resolution can be defined as the noise floor of the accelerometer system. The sources of noise in accelerometer system come from both mechanical and electrical parts of the system. The mechanical noise source is the vibration of the polysilicon springs while the electrical noise source is the signal conditioning circuitry [51]. In today's accelerometers, due to high proof mass values, the mechanical noise floor is nearly neglected compared to electrical noise, but with a proper electrical circuitry design, electrical noise floor can be reduced significantly [51].

Bandwidth is the length of the frequency range that input signal frequency can vary. While calculating the bandwidth of the accelerometer 3dB concept may not be used. Instead, the maximum accelerometer response deviation with input acceleration frequency change defines the bandwidth of the system. The bandwidth values are directly related to resonance frequency of the accelerometer.

Nonlinearity of the accelerometer is defined as the deviation of the accelerometer response from the best fit curve for different magnitudes of acceleration signal in its working range. Although the capacitive sensing topology may introduce nonlinearity, especially parallel plate configuration, this nonlinearity is almost insignificant compared to nonlinearity due to fabrication. The fabrication of the sense capacitances does not yield perfectly matched capacitances and this mismatch causes nonlinearity.

Bias drift is defined as the maximum deviation of the accelerometer system output with time for a fixed input acceleration signal. The exact reasons of bias drift are believed to be the fabrication mismatches, the hysterical behaviours of the springs, the change of the mechanical properties of the material with different environment conditions, cross-axis effects, and the change of the performance of the readout circuit with different environment conditions [52].

Other design parameters, which also affect the performance of the accelerometers, are temperature dependence of some parameters, axis misalignment, and cross-axis nonlinearities. However, there are some variables which do not affect the device performance directly, like the width of fixed fingers. They are always chosen by the optimisation to have some constant value in order to maximize performance; these variables are called style variables.

Considering the design parameters, the fabrication process is one of the main issues for high performance accelerometers. A proper fabrication will significantly reduce undesired nonlinearities. Next important issue is the readout circuitry because readout

circuit plays an important role in the overall performance of the accelerometer as it converts the detected acceleration into voltage signal.

2.3 MEMS Fabrication Technology

MEMS fabrication technologies are classified into three categories; bulk micromachining, surface micromachining and LIGA technologies [53].

2.3.1 Bulk Micromachining

In this fabrication process, the complete wafer is etched to create the masses and spring suspensions. As a result, the formed mass-spring system is usually has high quality factor which needs to be damped. Therefore, the device is encapsulated and gas or sometimes liquid is used between mass and the encapsulation to provide damping [54]. This technique also protects the mass from break-out by providing an over range protection [53, 54].

2.3.2 Surface Micromachining

Selective etching of sacrificial layers, which have a thickness of typically several microns, forms the masses and spring suspension. The main advantage of this approach is the low cost in case of high-volume fabrication. The basic steps of the surface micromachining are [53]:

- Lithography;
- Deposition of thin films and materials (electroplating, chemical vapour deposition, plasma enhanced chemical vapour deposition, evaporation, etc.);
- Removal of materials (patterning) by wet or dry techniques;
- Etching (plasma etching, reactive ion etching, laser etching, etc.);
- Doping;
- Bonding (fusion, anodic, and other);
- Planarisation.

2.3.3 LIGA

The LIGA process, which denotes Lithography-Galvanoforming-Molding (in German Lithografie Galvanik Abformung) is used to fabricate micro structures with high aspect ratios and high precision [53, 55]. Etching of a sacrificial layer is carried out by synchrotron x-ray radiation through a mask which partly covered with a strong X-ray absorbing material. This forms a mould that electroplating fills and then the remaining resist can be etched leaving the electroplated parts attached to the substrate. This process is expensive and not well suited to mass production.

2.4 MEMS Packing

Packaging operations may consist of some post fabrication processes required for a device to function properly as well as assembly of the MEMS device into a next level

assembly or final product that provides a function for the end user. The package containing the MEMS device needs to provide the following functions:

- *Mechanical support:* The package must mechanically support or contain the MEMS device so that it can function alone or within another system. The package will physically protect the MEMS device.
- *Interconnection:* The package must provide for communication between the microscale connection of a MEMS device and the macroscale connection that will be used to function or interface with the device. The connections may encompass a variety of physical phenomena such as electrical, optical, fluidic, biologic, etc.
- *Environment control:* The package must control the environment necessary for the MEMS device to function properly throughout its lifetime. The necessary environmental controls may include thermal management, particulate contamination, or ambient atmosphere control (i.e., humidity, atmosphere, and atmospheric pressure).

2.5 Previous Works

The existing MEMS accelerometers are generally less accurate than conventional accelerometers but they represent a low-cost, small size, and less weight solution with potential advantages in many applications. Therefore, various works on the improvement of these accelerometers have been reported in literature and research studies which also present more detail of the measurement principles, construction, and fabrication processes of MEMS accelerometers [56-78]. However, very few research

studies have been reported concerning the application of these accelerometers in the field of vibration based condition monitoring. The following sections present some of these research studies on the performance evaluation and improvement for general applications and condition monitoring respectively.

2.5.1 General Applications

Bell et al [79] compared the performance of MEMS sensors and actuators as a function of operating principles. The performance of MEMS sharing common operating principles is compared with each other and with equivalent macroscopic devices. It is stated that the performance of MEMS sensors is superior to macro sensors in terms of resolution and maximum frequency. The comparison was based on data obtained from the literature for the mechanical performance characteristics of actuators, force sensors and displacement sensors. *Yasin et al* [51] stated that there are three primary noise sources in typical MEMS accelerometer measurement that influence the performance of the accelerometer especially when operating at lower g conditions. They [51] presented design and built of a measurement system to measure noise characteristics of MEMS accelerometers. The system was used to measure the noise characteristics of three MEMS accelerometers operating at 0 g, +1g and -1g. The results showed that MEMS accelerometers noise sources have $1/f$ –type noise characteristics at low frequencies and white Gaussian noise at higher frequencies. The magnitude of the noise power spectral density is acceleration dependant. The results also showed spectral peaks originating from the oscillators inside the accelerometers.

Pereira et al [80] presented a solution to improve the performance of MEMS accelerometer exploring oversampling and sensor fusion techniques. The proposed solution seems to be sufficient for any measurement application that requires sensor fusion of two quantities, acceleration and temperature where two different waveform parameters: duty-cycle and period are provided by a single MEMS integrated circuit. However, this work was carried out to improve the performance of the measurement by multiplexing both measurements in a single signal rather than improving the MEMS accelerometer measurement. *Alsaleem et al* [81] presented a theoretical and experimental investigation into the effect of the motion of a printed circuit board (PCB) on the response of MEMS devices to shock loading. It was found that neglecting the PCB effect on the modelling of a microstructure of a MEMS device could underestimate the microstructure motion. For MEMS devices actuated electrostatically, it is found that a poor design of the PCB can lead to an early dynamic instability (dynamic pull-in) under shock load which is shown by comparing the relative mass deflection with and without PCB as shown in Figure 2.7.

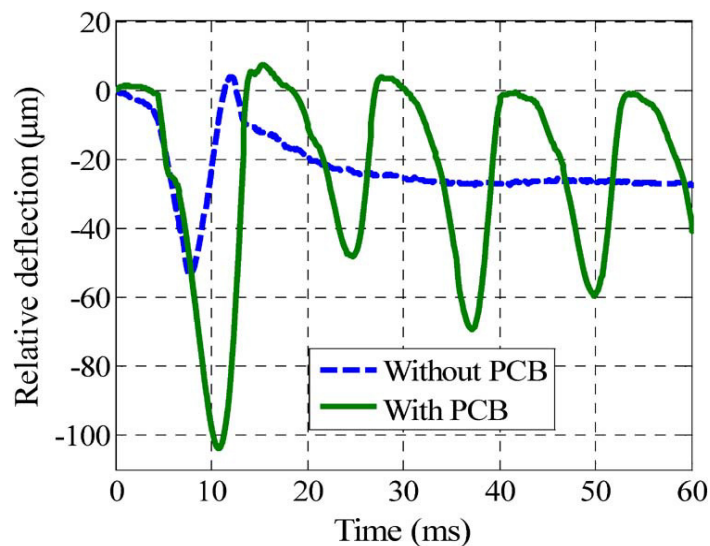


Figure 2.7 Transient response of the proof mass with and without PCB when subject to a mechanical shock [81]

Trusov and Shkel [82] reported a capacitive detection method, called sideband-ratio (SBR) detection. The approach constructively utilizes the inherent nonlinearity of parallel-plate sense capacitors in order to measure only the amplitude of sinusoidal motion. *Kajita et al* [83] proposed third-order noise-shaping accelerometer interface circuit to enhance the signal-to-noise ratio. The presented interface circuit is separately implemented; hence a fully-differential cross-coupled integrator with cross-coupled correlated double sampling is proposed to solve the problems arising from stray capacitance due to the wiring between sensors and circuits.

Liu et al [84] presented a CMOS closed-loop readout circuit which can be integrated with micro-machined accelerometer to improve the bandwidth, linearity and dynamic range. The performance of the mathematical model, which uses electrostatic force as a negative feedback, was compared with an open loop accelerometer. Also, the result of the circuit simulation (using Hspice) showed good sensitivity and low power consumption, and the circuit structure was optimised to reduce the noise effect. *Liu et al* [85] also performed system damping ratio analysis and optimization of a capacitive MEMS accelerometer. The results indicate that when the accelerometer works without damping it is easily damaged because of resonance. However, when it works with damping, its dynamics characteristics will be improved and its bandwidth will be widened. Analysis of harmonic response to a sinusoidal load is performed to verify the results using the FEM software ANSYS. A damping coefficient formula is used to optimize the system dynamic characteristics by adjusting system-damping ratio to 0.678 through changing the parameters of the proof mass. *Zhu et al* [86] addressed the MEMS accelerometer two modelling errors; fringing field effect and deformations, which may

lead to performance degradation. Hence, they presented a modelling approach to handle such errors. They showed, by FEM-based simulations, that these errors can be compensated by a variable serial capacitor.

2.5.2 MEMS Accelerometers in Condition Monitoring

The use of the MEMS accelerometers in machine condition monitoring is still limited to literature or testing stage in the laboratory experiments. For example, *Marinov et al* [87] proposed a combination of MEMS accelerometers and microcontrollers to form an intelligent system for remote vibration-based machine condition monitoring. The measurement system shown in Figure 2.8 is based on Labview software which checks the accelerometers, in case they are not calibrated, the system goes into calibrating mode, and then starts the vibration measurement. The measured values are then sent through a parallel port, either to a memory for storing or to a personal computer.

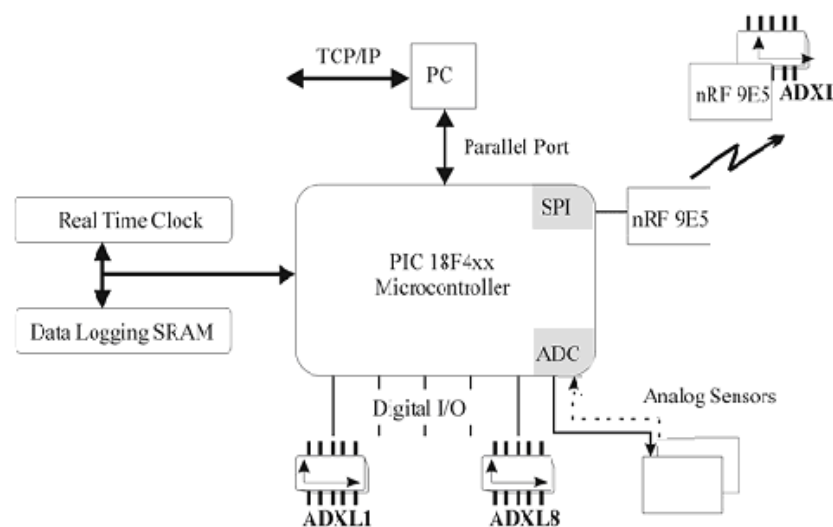


Figure 2.8 Functional layout of the measurement system [87]

Pandiyan et al [88] presented over all design of an industrial vibration transmitter using MEMS capacitive accelerometer. The output of the acceleration sensing transmitter is a current signal (4-20mA) which is proportional to input acceleration (0-10g RMS). The block diagram of this transmitter is shown in Figure 2.9. The accelerometer sensor interfacing circuit, RMS-to-DC converter and voltage to current loop converter circuit design, calibration procedure and mounting methods have been discussed. However, the testing and calibration procedure was only carried out for the interfacing circuit. Similar work has been carried out by *Abd. Rahim et al* [89] as they used MEMS accelerometer to develop a vibration measuring unit for machine condition monitoring. The MEMS accelerometer was used as a detection sensor for the measuring unit which also included an interface circuit, an RMS-to-DC circuit and alarming circuit. The experimental tests were carried out to measure the output DC voltage for applied acceleration with range of up to 5g at only one frequency of 100 Hz.

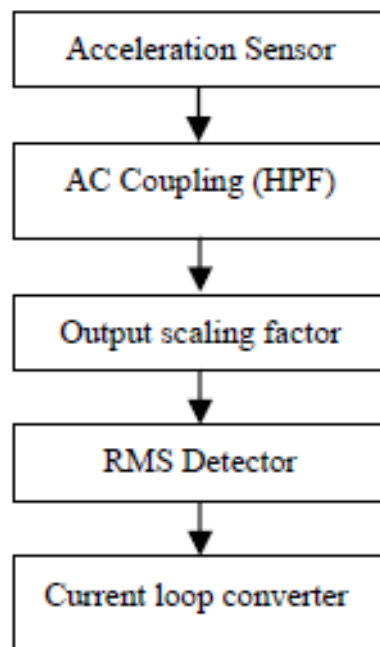


Figure 2.9 Block diagram of acceleration sensor transmitter [88]

Ratclif et al [90] investigated the possibility of changing the data acquisition for non destructive inspection test from a roving hammer method, to a procedure that employs an array of capacitive type MEMS accelerometers. The roving hammer and MEMS array methods are compared by testing a composite vertical stabilizer from an airbus A320 aircraft. The quality of data which was monitored using coherence functions showed average coherence more than 98% for ICP type accelerometer while the coherence for MEMS accelerometers showed a slight degradation as shown in Figure 2.10.

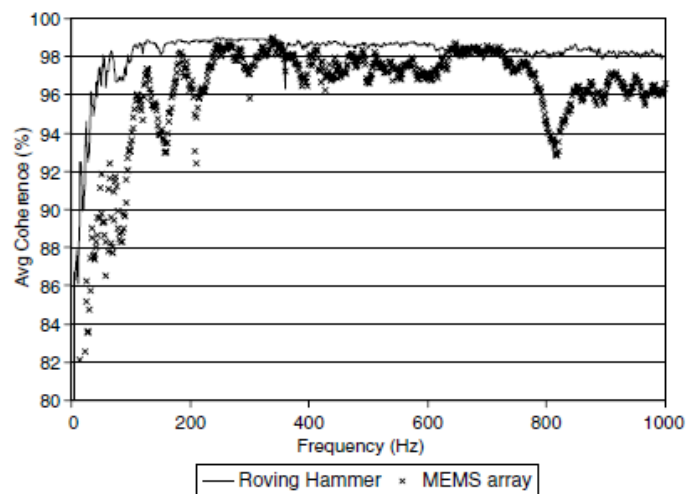


Figure 2.10 Average coherence for all data acquired during the tests [90]

Tjiu et al [91] presented the design and demonstration of tire condition monitoring system which include three MEMS sensors; pressure sensor, temperature sensor and accelerometer. The accelerometer is a capacitive type MEMS accelerometer used for measuring the vibration of the tires while traversing, especially on rough road surface. The characteristics of the accelerometer were only examined by recording its output voltage when applying certain motion. *Thanagasundram and Schlindwein* [21] have used the MEMS accelerometer together with a conventional accelerometer for

measuring the vibration of a pump during its normal operation. They [21] found that the frequency content from both sensors were in agreement.

Peiner [92] investigated the application of piezoresistive type MEMS accelerometer designed for low-frequency resonant operation. The accelerometer used for vibration monitoring of to detect incipient fatigue damage on the cups of axle box bearings. The accelerometer can be only used for this application as it is designed with a resonance frequency close to the frequency of this fault. Another piezoresistive type MEMS accelerometer shown in Figure 2.11 has been developed by *Vogl et al* [93]. The accelerometer is intended for wireless vibration measurements on AC motors for condition monitoring. However, the frequency response tests show some changes in the sensitivity with frequency. Moreover, the accelerometer has no built in signal conditioning circuit as external circuits have been used in the testing.

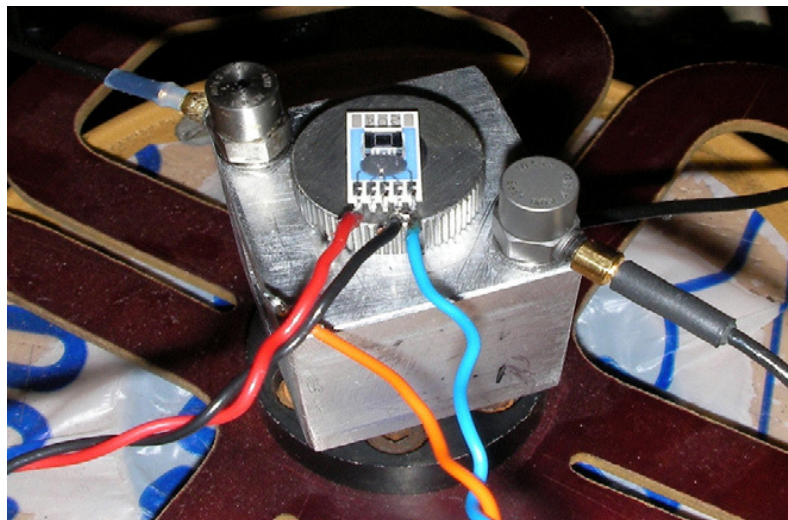


Figure 2.11 Sensor device mounted on a shaker for frequency testing [93]

Wright et al [94] studied the overall potential of wireless sensor nodes and networking in manufacturing environments. In the experimental work, a wireless sensor platform which includes MEMS accelerometer was used to monitor the vibration of a 3-axis milling machine. The case study's focus is not on vibration analysis itself. Rather, experiments have been carried out to show the capability of wireless sensor networks, to provide new tools for research in predictive maintenance and condition-based monitoring. Also, *Huang et al* [95] evaluated a wireless sensor node-based MEMS accelerometer for condition monitoring of milling machine as shown in Figure 2.12. However, only the statistical results of time domain data processing such as RMS and peak values are transferred to the server.

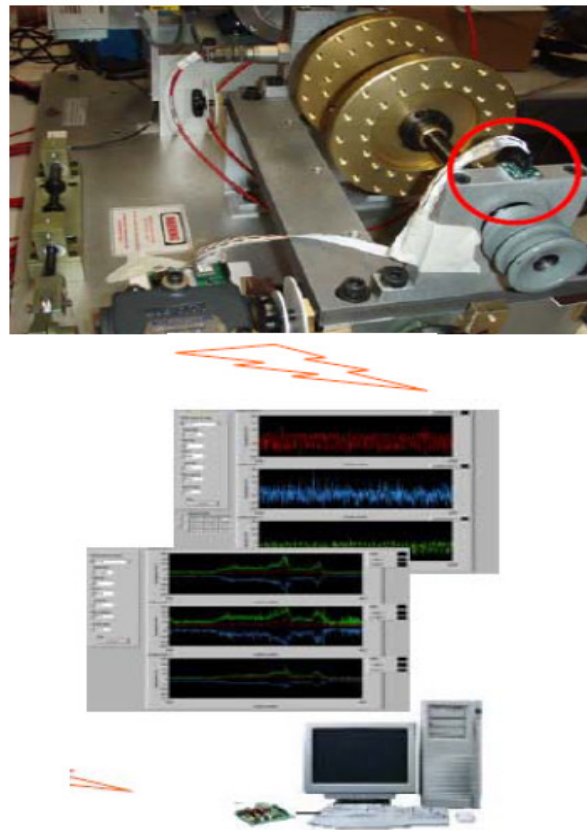


Figure 2.12 Wireless sensor node for vibration monitoring [95]

As mentioned in Chapter 1, the accelerometers are intended to measure the different kinds of signals; sinusoidal, random, and impulsive signals and from the review carried out it can be concluded that only few works done on performance evaluation and these works did not consider all these kinds of signals. Moreover, most of works on MEMS accelerometers were focused on presenting the possibility of using these accelerometers in different fields of applications. However, *Albarbar et al* [22] have investigated all these requirements on a laboratory experiments. They found that the frequencies in the acceleration responses measured by both MEMS and a conventional accelerometer were same but their amplitudes and phases were generally different.

2.6 Summary

MEMS accelerometers are currently designed and used to detect the event of vibration or impact in many applications and not particularly for conventional vibration measurement. Several sensing mechanisms have been used for acceleration sensing in these accelerometers but the change in capacitance is the most widely used. The performance parameters of these accelerometers are affected by design variables and manufacturing process. Many research studies have been presented regarding the performance improvement of these accelerometers. However, the performance of these accelerometers in the field of vibration-based condition monitoring is not yet well evaluated.

CHAPTER 3

TEST SETUP

This chapter describes the experimental set up that has been used to carry out different tests, mainly to make the comparison between the responses of MEMS accelerometers and a reference accelerometer. Test equipments that have been used will be listed and briefly described and the testing methodology will also be explained. The MEMS accelerometers, their specifications, theory of operation and electrical connections are also described.

3.1 Introduction

In this section, general accelerometer specifications and calibration procedures have been briefly discussed.

3.1.1 Accelerometer Specifications

The following technical specifications are usually considered for selecting the accelerometer for any application;

- (a) *Sensitivity* which relates the electrical signal to the amplitude of vibration in acceleration.
- (b) *Frequency range* in which vibration measurement is useful.

(c) *Amplitude limit* that specifies the maximum range of acceleration that can be measured accurately.

(d) *Shock limit* is maximum level of acceleration that the accelerometer can withstand without any damage.

(e) *Linearity* is the accuracy of the measured acceleration amplitude in the measuring Frequency range.

(f) *Natural frequency* which is indirectly indicative of the measuring *Frequency range*. Higher the natural frequency of an accelerometer, larger the measuring frequency range in general.

(d) *Phase linearity* which is the direct proportionality of phase shift to frequency over the frequency range of interest. Perfect accelerometer expected to give zero degree phase shift over its entire operating frequency range.

3.1.2 Calibration Procedures

The International code ISO 5347-0 [96] gave the guidelines for the calibration of vibration pickups, which is generally followed by the manufacturers. The calibration procedure adopted generally uses the sinusoidal vibration generator (shaker) with varying frequency and amplitude to characterise the accelerometer to be calibrated by comparing its measured responses with other well-calibrated accelerometer. Accuracy in sinusoidal response measurement satisfies the calibration procedure adopted. However, accelerometers are in general used for following types of signal measurements:

- (a) Periodic signal—Sinusoidal or/and swept-sine,
- (b) Random,
- (c) Impulsive.

It has been observed that the performance of such calibrated accelerometer may not be useful for measuring the random and impulsive behaviour of structures [97]. Hence the random and the impulsive loading test should also be included in the calibration along with the standard calibration procedure for the accelerometer. Hence the accuracy of all above measurements is important.

3.2 Test Setup

The test setup shown in Figure 3.1 was used to carry out the comparison between MEMS accelerometers and a calibrated conventional accelerometer (Reference accelerometer). The test setup consists of the following equipments:

1. Electro-dynamic shaker,
2. Power amplifier for the shaker,
3. Signal generator, which is able to generate sine, sweep-sine, and random signals,
4. Sensor signal conditioner,
5. NI 6009 Data acquisition card,
6. A computer with Labview and Matlab softwares in it,
7. DC power supply for the MEMS accelerometers.
8. Reference accelerometer.



Figure 3.1 Test Setup

The Electro-dynamic shaker, model V406, has a wide frequency band of operation from 5 Hz – 9 KHz, velocity sine peak of 1.78 m/s and maximum acceleration sine peak of 981 m/s^2 . Its peak to peak displacement is 17.6 mm. The Power amplifier PA30VA is a linear amplifier used to drive the electro-dynamic shaker. It accepts any type of input wave shape and is able to oscillate over a frequency range of 0.2 Hz – 20 KHz in 5 selectable decades with frequency indication provided by a graduated scale. It exhibits low distortion over its frequency range and operates with a wide variety of load impedances. Dual channel FFT analyzer model CF-350 has been used as the signal generator. Different output waveforms can be generated using this equipment such as sine wave, sweep-sine, random, and impulse.

The sensor signal conditioner, Model 442B104, is Four-Channel ICP amplifier with x1, x10 and x100 gain, its excitation voltage is 25.5VDC and frequency response from 0.05 to 100 KHz with output range ± 10 Volt.

The data acquisition module (USB-6221 BNC) from The National Instruments is a USB high-performance M Series multifunction data acquisition module optimized for superior accuracy at fast sampling rates. The module is ideal for applications such as data-logging and bench top sensor measurements. It provides 8 analogue inputs, 2 analogue outputs, 8 DIO and 2 user defined BNC terminals, and includes a certified power supply. The National Instruments USB-6221 BNC is designed specifically for mobile or space-constrained applications. Plug-and-play installation minimizes configuration and setup time; while direct screw-terminal connectivity helps keep costs down and simplifies signal connections.

3.2.1 Test Rig Configuration

The test setup configuration is illustrated in Figure 3.2; which shows how the equipments are connected. The selected excitation type which is generated by the signal generator is fed into the power amplifier where it is amplified and applied on the shaker. The shaker will vibrate according to the selected excitation. The accelerometers were mounted back to back on the especially designed shaker armature using petro wax. The outputs from MEMS accelerometers are connected directly to the data acquisition card while the output from the standard accelerometer is connected through the signal conditioning unit where the accelerometer output is amplified. Finally, the voltage

signals from the accelerometers were processed through a data acquisition card. Then the generation of the time domain and the frequency domain of the signals were processed in a personal computer with a Labview and MATLAB signal processing packages installed in it.

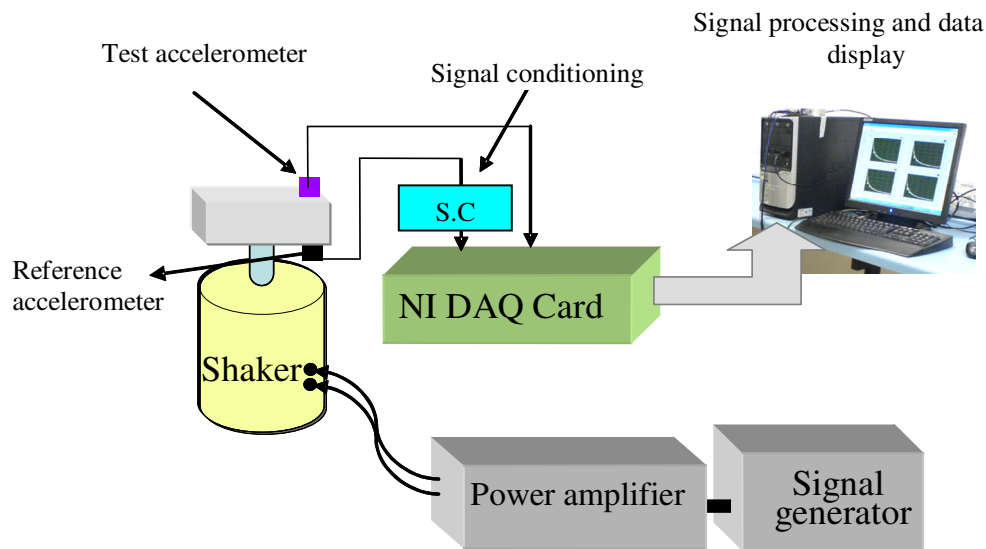
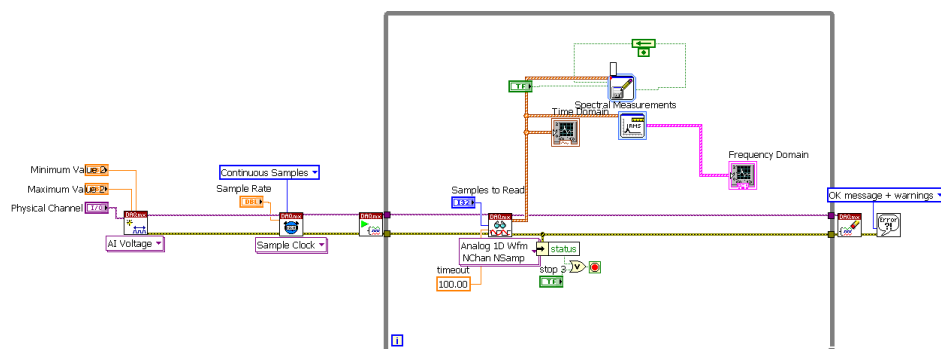


Figure 3.2 Test rig Configuration

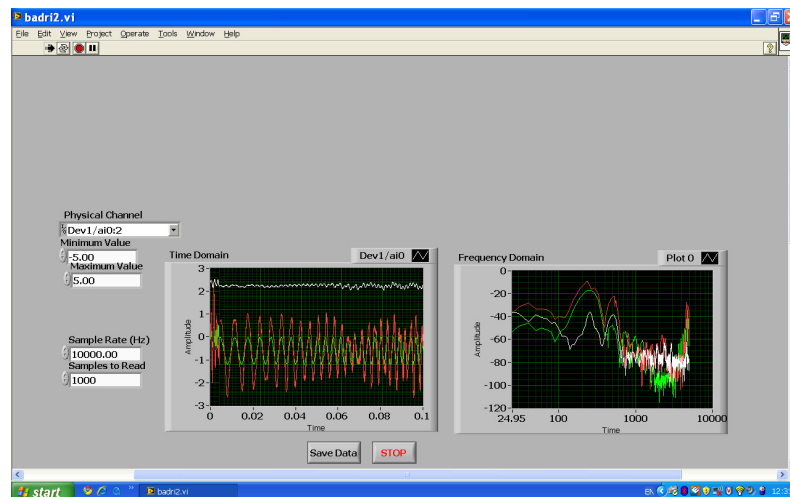
3.2.2 Methodology of Testing

The methodology is based on applying the same input excitation to the MEMS accelerometer and the reference accelerometer so that they experience identical motion on the shaker. The input vibration is simulated by sinusoidal, sweep-sine, random, and impulsive excitations. Sinusoidal excitation for example, was given to the shaker through a power amplifier at different frequencies and different amplitudes. The response was measured from both of the accelerometers and the signal from the standard accelerometer was used as a reference for frequency and amplitude levels. The analogue voltage output of the accelerometers is converted into digital signals by the

data acquisition card which is connected into the PC where the acquired signals are displayed using data acquisition programme created in Labview software. Figure 3.3 (a) shows the connections diagram of this programme and its front panel. The programme is also used to convert the vibration signals from time domain to frequency domain using Fast Fourier Transformation (FFT) technique, so the acquired signals are displayed on the front panel in time domain and frequency domain as shown in Figure 3.3 (b).



(a)



(b)

Figure 3.3 (a) Diagram connections of data acquisition programme, (b) Display front panel

3.3 The MEMS Accelerometers

Number of MEMS accelerometers has been used in the experimental work but due to similarity of the results, only three MEMS accelerometers of different specifications will be presented.

3.3.1 MEMS 1 Accelerometer

MEMS 1 is a complete dual-axis accelerometer with signal conditioned voltage outputs, all on a single monolithic integrated circuit. It can measure both dynamic acceleration (e.g., vibration) and static acceleration (e.g., gravity) with a full-scale range of ± 2 g. The outputs are analogue voltages proportional to acceleration. The sensor is a surface micromachined polysilicon structure built on top of the silicon wafer. Polysilicon springs suspend the structure over the surface of the wafer and provide a resistance against acceleration-induced forces. Deflection of the structure is measured with a differential capacitor structure that consists of two independent fixed plates and a central plate attached to the moving mass. A 180° out-of-phase square wave drives the fixed plates. An acceleration causing the beam to deflect will unbalance the differential capacitor resulting in an output square wave whose amplitude is proportional to acceleration. Phase sensitive demodulation techniques are then used to rectify the signal and determine the direction of the acceleration. The output of the demodulator is amplified and brought off-chip through a built-in $32\text{ k}\Omega$ resistor. To improve the measurement resolution and prevent aliasing, the user can set the signal bandwidth of the device by adding capacitors C_X and C_Y at X_{FILT} and Y_{FILT} output pins. Bandwidths

of 1 Hz to 2 kHz may be selected to suit the application. The equation for the 3 dB bandwidth is:

$$F_{-3dB} = \frac{1}{2\pi(32k\Omega) \times C_{(X,Y)}} \quad (3.1)$$

A minimum capacitance of 1000 pF for C_X and C_Y is required in all cases. Another capacitor of 0.1 μ F is suggested to decouple the accelerometer from noise on the power supply. Some of technical specifications of this accelerometer are presented in Table 3.1, and picture for this accelerometer with its wiring is shown in Figure 3.4.

Table 3.1 MEMS 1 Specifications

Accelerometer property	Value
Acceleration Range	$\pm 2g$
Frequency range	0- 2 kHz
Sensitivity	170 mV/g
Temperature range	0-70 °C



Figure 3.4 MEMS 1 accelerometer

3.3.2 MEMS 2 Accelerometer

MEMS 2 accelerometer is a single axis capacitive type and similar to MEMS 1 accelerometer in the theory of operation, but its specifications such as sensitivity, resonance frequency, and measurement range are different. The sensitivity is 250mv/g, the frequency range is 1.5 kHz, measurement range is $\pm 1.7g$, and the operating temperature range is -55 to 125°C.

3.3.3 MEMS 3 Accelerometer

MEMS 3 accelerometer, is also a complete single axis acceleration measurement system on a single integrated chip. The theory of operation of this accelerometer is similar to MEMS 1, but has different architecture for the built in electronic circuit. Moreover, this accelerometer features an on-board temperature sensor with an output of 8mV/°C for optional temperature compensation of offset vs. temperature for high accuracy application. The main specifications for this accelerometer are listed in Table 3.2.

Table 3.2 MEMS 3 Specifications

Accelerometer property	Value
Acceleration Range	$\pm 5g$
Frequency range	0- 10 kHz
Sensitivity	250 mV/g
Temperature range	-40-85 °C

3.3.3.1 Packing MEMS 3 Accelerometer

In order to prepare the MEMS accelerometer it should be connected to other electrical parts such as power supply, capacitor and resistors which is suggested by the manufacturer. The accelerometer was firstly connected to a special printed circuit board and then all the other parts were added. Much care was taken when soldering the accelerometer chip and also it was essential to make the design as small as possible. Figure 3.5 shows a picture of the accelerometer with all parts attached.



Figure 3.5 MEMS 3 accelerometer

It was impractical to mount the accelerometer with its PCB and all the components attached to it, therefore it was decided to pack the accelerometer in a metal case filled with an epoxy potting compound. The packing structure and final packing of MEMS 3 accelerometer are shown in Figure 3.6.

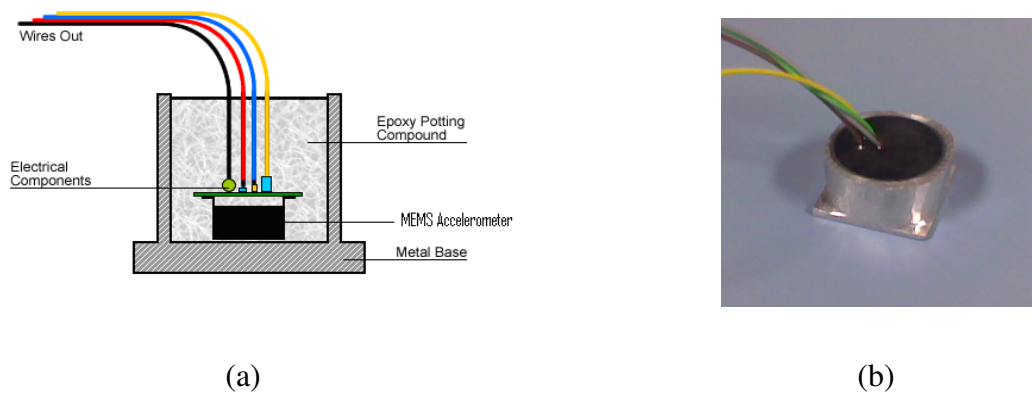


Figure 3.6 (a) MEMS 3 packing structure, (b) final packing

3.4 The Reference Accelerometer

It is calibrated ICP type conventional accelerometer which structured with a ceramic crystal sensing element operating in flexural mode, and a built-in microelectronic charge-to-voltage convertor housed in a lightweight composite-structured housing. Some important specifications of this accelerometer are summarised in Table 3.3.

Table 3.3 Reference accelerometer Specifications

Accelerometer property	PCB
Acceleration Range	$\pm 50g$
Sensitivity	100 mV/g
Frequency Range	1-2000 Hz
Temperature range	-40 – 120 °C

CHAPTER 4

PERFORMANCE EVALUATION OF MEMS ACCELEROMETERS

Reformatted version of the following papers:

1. Performance evaluation of MEMS accelerometers

Authors: A. Albarbar, A. Badri, Jyoti K. Sinha and A. Starr

Published in: Measurement, Volume 42, Issue 5, June 2009, Pages 790-795

2. Improvement in measured signals of MEMS accelerometer

Authors: Abdellatef Badri and Jyoti K. Sinha

Published in: The third International Conference on Integrity, Reliability and Failure, Porto/Portugal, 20-24 July 2009, Paper Ref: S1146_P0507.

Abstract

Researchers have been looking for alternatives of expensive conventional accelerometers in vibration measurements. Micro-ElectroMechanical Systems (MEMS) accelerometer is one of the available options. Here the performance of one of these MEMS accelerometers compared with that of a well known commercial accelerometer.

4.1 Introduction

Condition based monitoring is now accepted practice for critical machines and structures for Industries to enhance availability, low maintenance costs and plant safety. Often, the decisions regarding the repair or replacement of a machine part, overhauls,

and standard maintenance are made on the basis of the measured condition of the machine. One such monitoring technique is vibration based condition monitoring. Measuring vibration is very essential in detecting and diagnosing any deviation from normal conditions. The use of conventional piezoelectric accelerometers in vibration measurements is well known and accepted, but is high cost, especially if simultaneous multiple data collection points are required; this is mainly because of their cost and the price of the associated electronic signal conditioning circuits.

The recent advances in embedded system technologies such as Micro-Electro-Mechanical Systems (MEMS) sensors hold a great promise for the future of vibration measurement based condition monitoring, which is a much cheaper alternative. It has built-in signal conditioning unit as well. The cost of a MEMS accelerometer may be just 10% or less compared to the commercially available cheapest conventional accelerometer together with the signal condition unit. There are number of research studies in the literature [32, 56-61, 98] about the MEMS accelerometers construction and the measurement principle. The use of the MEMS accelerometers is still limited to testing stage in the laboratory experiments. Thanagasundram and Schlindwein [21] have used the MEMS accelerometer together with a conventional accelerometer for measuring the vibration of a pump during its normal operation. They [21] found the frequency content from both sensors were in agreement. However no rigorous investigation has been done to compare the performance of this MEMS accelerometer which is required to measure the different kinds of signals – sinusoidal, random, and impulsive signals [97]. Hence the performance of one of these MEMS accelerometers compared with a well known and calibrated commercial accelerometer.

4.2 MEMS Accelerometers

MEMS accelerometers are divided into two main types: piezoresistive and capacitive based accelerometers [61]. The conventional piezoelectric accelerometers generally consist of a single-degree of freedom system of a mass suspended by a spring. Here in piezoresistive MEMS accelerometer also, it has a cantilever beam having a proof mass at the beam tip and a piezoresistive patch on the beam web. The schematic of a piezoresistive MEMS accelerometer is shown in Figure 4.1(a). The movement of the proof mass when subjected to vibration changes the resistance of the embedded piezoresistor. The electric signal generated from the piezoresistive patch due to change in resistance is proportional to the acceleration of the vibrating object. The capacitive based MEMS accelerometers measure changes of the capacitance between a proof mass and a fixed conductive electrode separated by a narrow gap [61]. The schematic of a capacitive MEMS accelerometer is shown in Figure 4.1(b). The papers [32, 56-61, 98] gave the details of the working principle and so not discussed here.

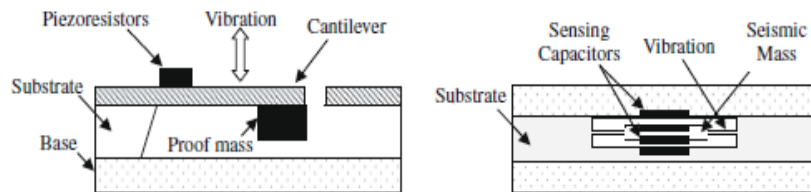


Figure 4.1 A typical MEMS accelerometer construction: (a) piezoresistive using cantilever design, (b) capacitive based on membrane design [61]

4.3 Test Setup

A schematic of the Test setup is shown in Figure 4.2. The setup consists of a small shaker (M/s GW make) together with a shaker power amplifier, signal generator and a

PC based data acquisition for data collection and storage for further signal processing in MatLab. Two accelerometers (one PCB accelerometer and other capacitive type MEMS accelerometer) were attached back to back on the armature attached to the shaker as shown in Figure 4.2. The PCB accelerometer used for this experiment is an ICP (Integrated Circuit Piezoelectric) type with the technical specifications – 100 mV/g, linear frequency range up to 2 kHz, 50 g level. This type of accelerometer has been calibrated as per the ISO/IEC 17025 standard and they are well accepted in practice because of their performance. A typical MEMS accelerometer of technical specifications – 250 mV/g, frequency range 10 kHz, 5 g level is used for comparison [99] which is relatively new technology for the accelerometer.

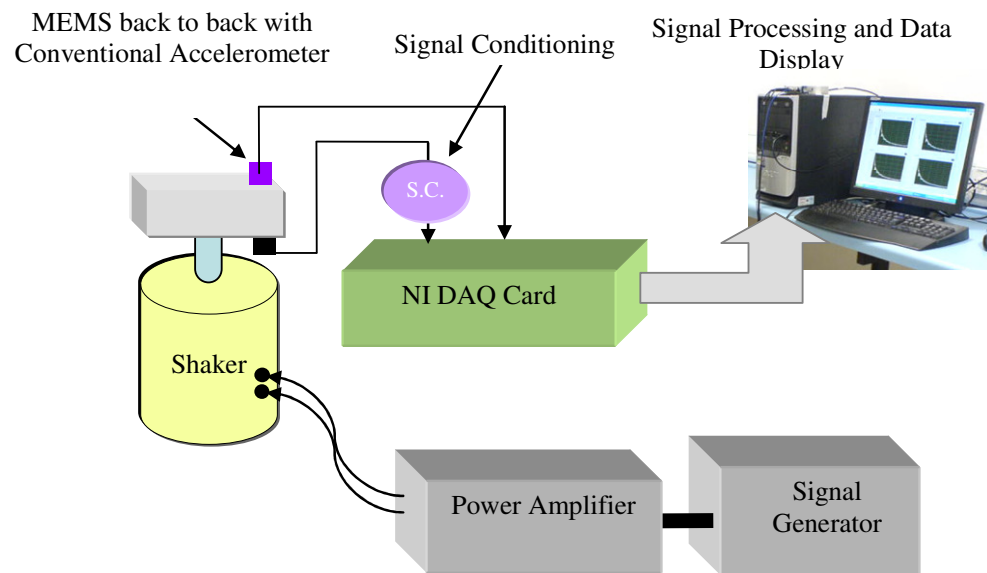


Figure 4.2 Test setup

4.4 Testing and Results

As it is well known that the accelerometers are used for measuring the periodic (sinusoidal, step-sine, multi-sine, etc.), random and impulsive signals [97], hence these tests were carried out on the Test setup and results were compared.

4.4.1 Periodic Excitation

Sinusoidal signals were given to the shaker at two frequencies - 66 Hz and 157 Hz deliberately away from the line frequency of 50 Hz and its harmonics. A number of experiments were performed at these two frequencies with different amplitude levels of shaker excitation and simultaneously responses were measured from the accelerometers.

A few typical measured responses both in time and frequency domain are shown in Figures 4.3 to 4.5. No distortion is seen in the measured responses by the MEMS accelerometer as well. However there are significant shift in phase and sensitivity compared to the reference accelerometer. In fact the estimated sensitivity based on the reference accelerometer seems to be varying from 38 mV/g to 69 mV/g and phase shift is also not constant with respect to the reference accelerometer responses, which are clearly seen in the time response plots in Figures 4.3 to 4.5.

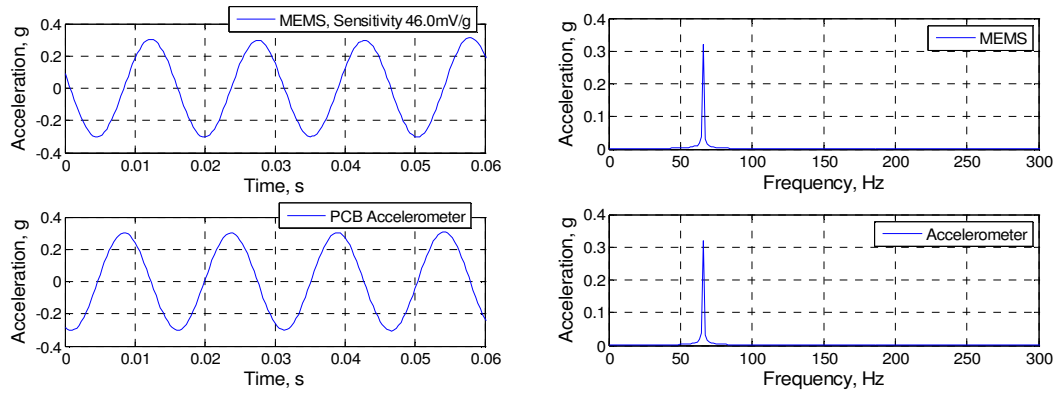


Figure 4.3 Measured acceleration responses by MEMS 3 accelerometer and the reference (PCB) accelerometer at 66Hz for the excitation level 0.3g

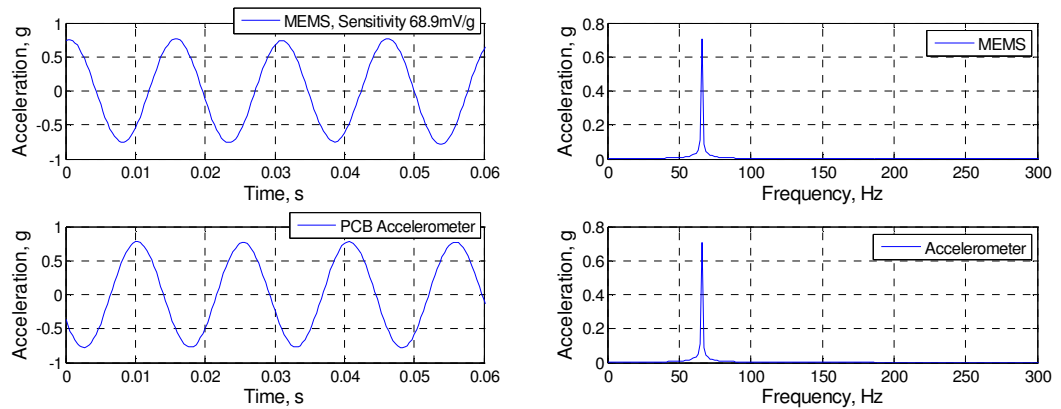


Figure 4.4 Measured acceleration responses by MEMS 3 accelerometer and the reference (PCB) accelerometer at 66Hz for the excitation level 0.75g

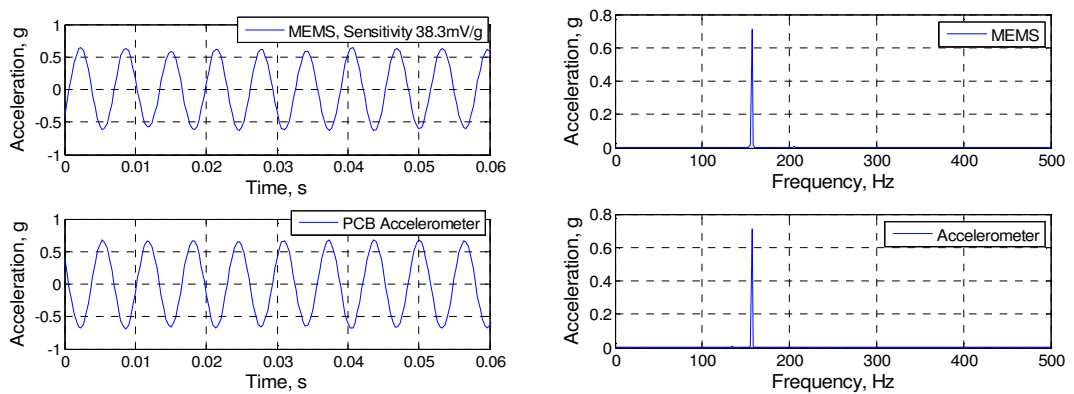


Figure 4.5 Measured acceleration responses by MEMS 3 accelerometer and the reference (PCB) accelerometer at 157Hz for the excitation level 0.65g

4.4.2 Random Excitation

Similar to the sinusoidal tests; the shaker was excited with random excitation in a frequency band from 10 Hz to 1.5 kHz with different amplitudes. Typical responses of both accelerometers in time and frequency domains are shown in Figure 4.6. Both accelerometers responses look to be identical in time and frequency domains, but here again the estimated sensitivity found to be 225 mV/g though it is close to the design value of the sensitivity for this MEMS accelerometer but much different than the estimated sensitivity during the sinusoidal tests. To determine the linearity in the measurement over the frequency band of excitation and phase shift, the frequency response function (FRF-the transfer function in frequency domain) has also been calculated assuming the responses of the MEMS accelerometer as the output and the reference accelerometer responses as the input. Both the amplitude and phase FRF plots are shown in Figure 4.7. The response spectra shown in Figure 4.6 look to be identical, but the amplitude deviation between two accelerometers is found to be up to approximately 20 dB at some frequencies and the phase shift of 180 degrees up to around 100 Hz and then the shift is approximately linear from 180 degrees at 100 Hz to 0 degree at 1.5 kHz.

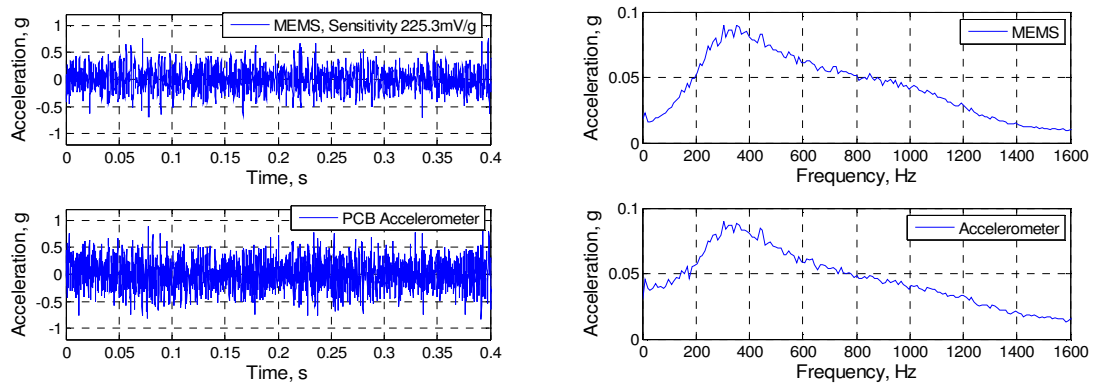


Figure 4.6 Measured acceleration responses by MEMS 3 accelerometer and the reference (PCB) accelerometer at 157Hz for random excitation

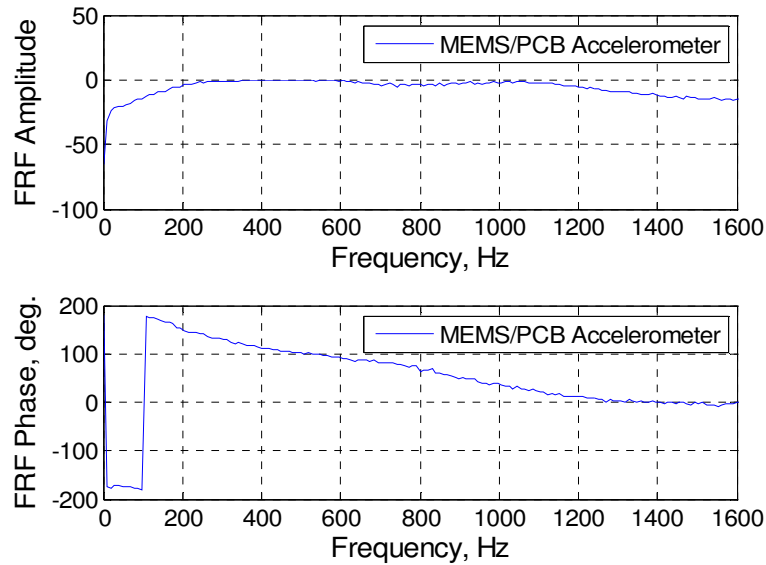


Figure 4.7 A typical measured FRF for the random excitation

4.4.3 Impulse Excitation

In the same experimental setup, the impact excitation was given at the centre of the armature using a soft tip hammer within the frequency band of excitation up to 400–500 Hz. Typical time domain responses of both accelerometers are shown in Figure 4.8. The measured responses are typically decay type responses as expected for the impact excitation by both accelerometers with maximum amplitude level of 0.6 g. However the estimated sensitivity was found to be 155.9 mV/g, which is different than earlier estimated value and the fast decay in the response seen in the MEMS accelerometer compared to the reference accelerometer. To understand this typical behaviour of the MEMS accelerometer, the averaged spectra of the 3 decay responses were computed for both accelerometers and compared which is shown in Figure 4.8. The presence of the frequency peaks is consistent in both responses; however the peaks amplitudes are much different. Since the MEMS accelerometer introduces the phase shift known from

previous tests, so these phase shift at different frequencies might be resulted into the fast decay in the measured responses compared to the reference accelerometer.

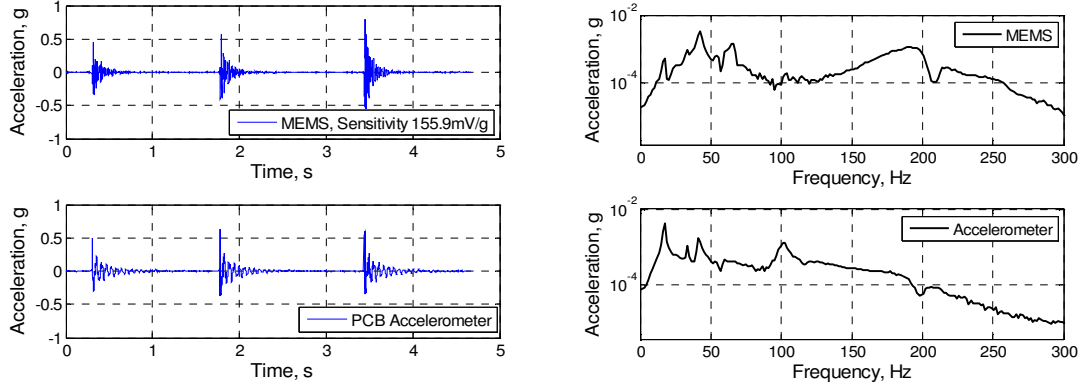


Figure 4.8 A comparison of measured responses by MEMS 3 accelerometer and the PCB accelerometer when the shaker armature excited by impacts from a hammer

4.4.4 Further Analysis

In vibration analysis, the ordinary coherence between two vibration signals is defined as [100]:

$$Coh(\gamma^2) = \frac{|S_{xy}(\omega)|^2}{S_{yy}(\omega)S_{xx}(\omega)} \quad (4.1)$$

where $S_{xx}(x)$ and $S_{yy}(y)$ are the power spectral densities of two signals, $x(t)$ and $y(t)$, and $S_{xy}(x)$ is their cross-power spectrum at an angular frequency (ω) . The coherence between two signals indicates the degree to which two signals are linearly correlated at a given frequency. A coherence (**Coh**) close to unity means the signal $x(t)$ is linearly correlated to the signal $y(t)$. Reduction in the coherence from 1 indicates that the two signals are either noisy or having nonlinear relation. Hence the coherence was computed

between two responses measured by the MEMS and the reference accelerometers. Figure 5.9 shows the coherence plots for the random and impact tests. Generally coherences are above 0.8 at many frequencies indicating good relation between two signals, but also low at several other frequencies. Hence this indicates the measurements by the MEMS accelerometer used in the present study deviate compared to the reference accelerometer.

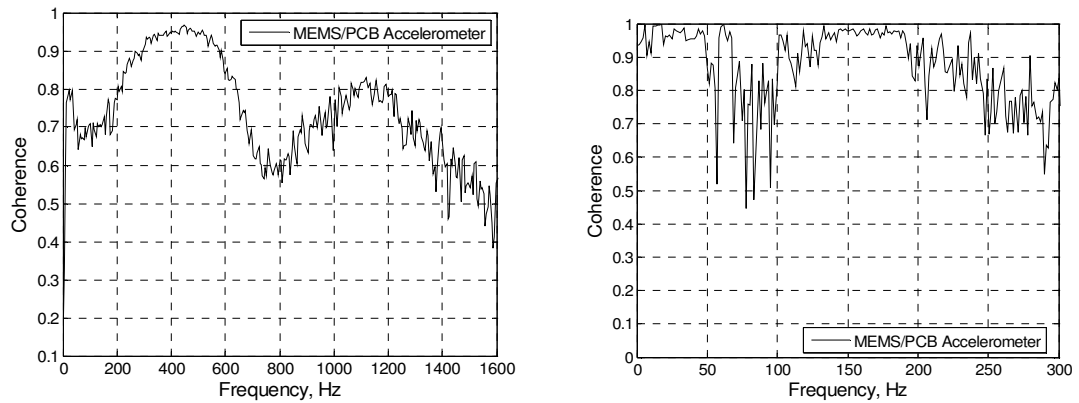


Figure 4.9 Coherence plots between the measured responses by MEMS 3 accelerometer and the reference accelerometer (a) Random test; (b) Impact test

4.5 Comments

The performance tests of a typical capacitive type MEMS accelerometer are carried out for different excitations – sinusoidal, random and impulse. The measured responses of the MEMS accelerometer were compared with a well accepted ICP type accelerometer. All tests were conducted well within the technical specifications of both accelerometers. The MEMS accelerometer seems to be performing well for the sinusoidal measurements though shift in phase is observed and sensitivity changes with the excitation level. This can be related to the packing, which presented in the previous chapter, as the

accelerometer is not directly mounted. However, a significant deviation has been observed in the MEMS responses to random and impact excitations though the frequency peaks content is also found to be same in comparison with the conventional accelerometer for the impact excitation. Therefore, lots of improvement needed before use in practice. It is being planned to carry out more investigation with several numbers of the MEMS accelerometers without packing to understand the future direction for improvements. The following sections present the test results for MEMS 1 and MEMS 2 accelerometers.

4.6 MEMS 1 Accelerometer

The performance of this MEMS accelerometer is compared with the reference accelerometer when they are simultaneously excited by sinusoidal, sweep-sine and random signals. The comparison for sinusoidal excitation will be presented at only two frequencies (145Hz and 376Hz).

4.6.1 MEMS 1 Sinusoidal Excitation

The frequency domain for measured responses by both accelerometers when excited at 145 is shown in Figure 4.10. The amplitude of MEMS 1 accelerometer spectrum is much lower than the amplitude of the reference accelerometer spectrum. This can be seen in the FRF plot shown in Figure 4.11 where the amplitude is approximately 0.16 and phase difference is about -7 degrees.

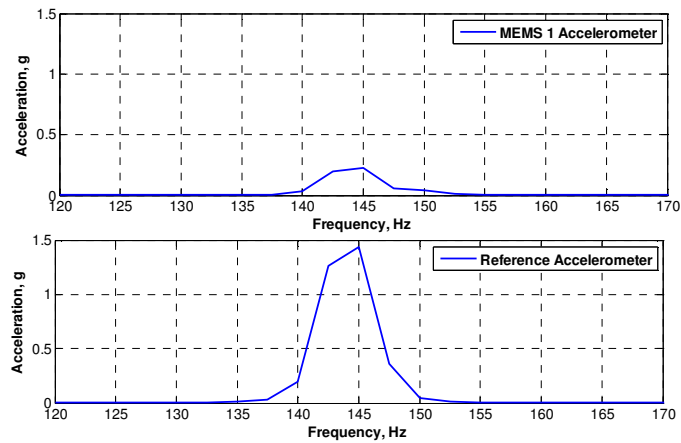


Figure 4.10 MEMS 1 spectrum at 145Hz

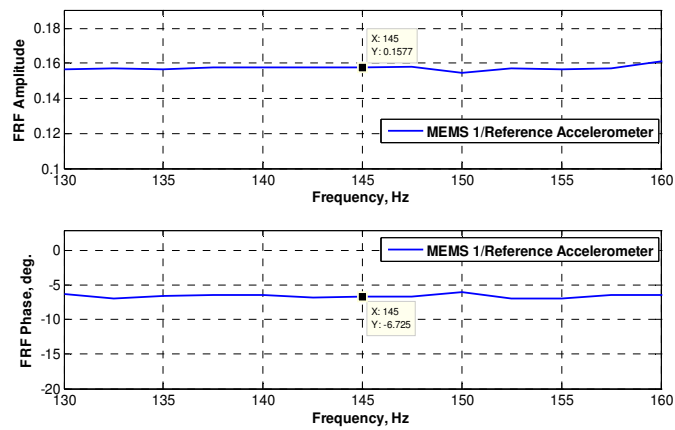


Figure 4.11 FRF for MEMS 1 at 145 Hz

Measured responses in frequency domain for excitation at 376 Hz are shown in Figure 4.12 and FRF plots are shown in Figure 4.13. Again, MEMS 1 response is deviated in both amplitude and phase as the FRF amplitude at this excitation frequency is approximately 0.1355 and phase is 8.5 degrees.

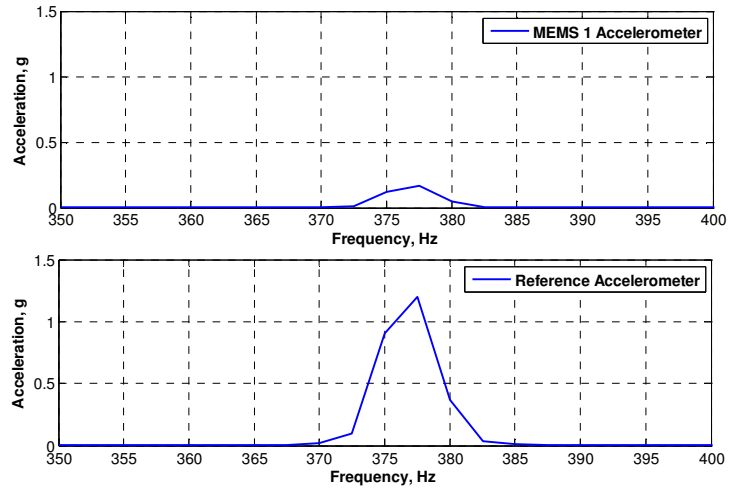


Figure 4.12 MEMS 1 spectrum at 375Hz

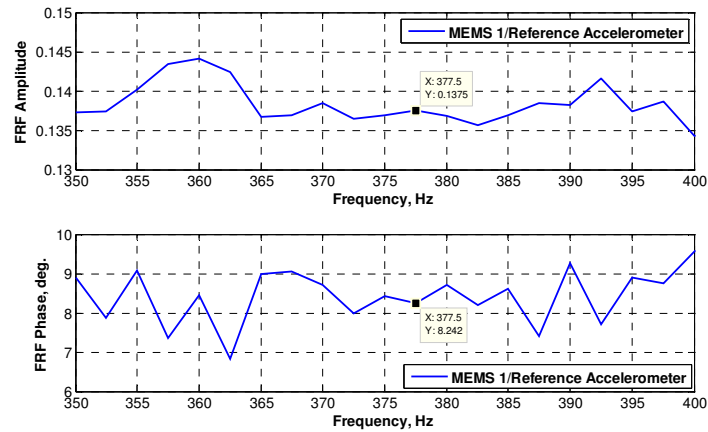
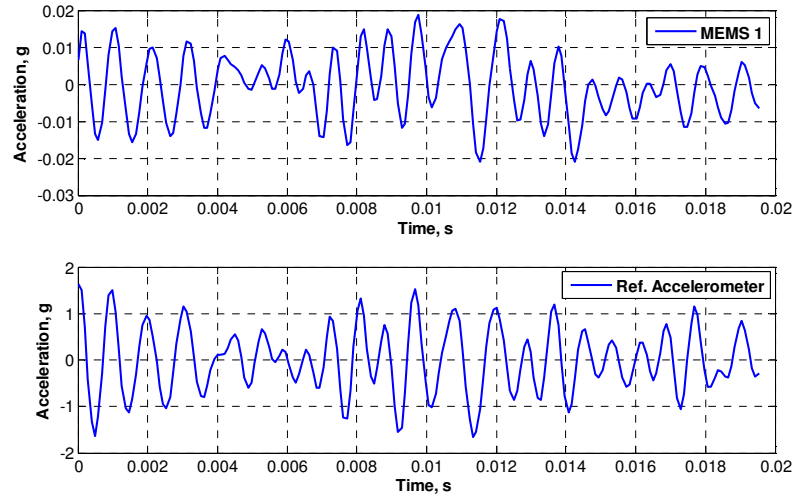


Figure 4.13 MEMS 1 FRF at 375Hz

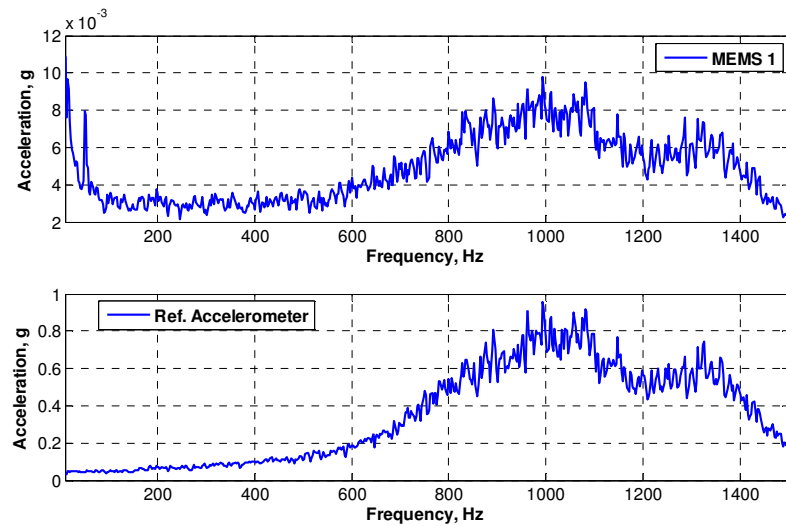
4.6.2 MEMS 1 Random Excitation

Typical measured responses of MEMS 1 and reference accelerometers in time domain and frequency domain for the random excitation in a frequency band of 10 Hz to 1.5 KHz are shown in Figure 4.14. The amplitude of MEMS 1 accelerometer output is very low compared with the reference accelerometer also there is a significant phase shift

between the two accelerometers and this shift is changing with frequency as shown in FRF plots of Figure 4.15.



(a) Time domain



(b) Spectra

Figure 4.14 MEMS 1 time domain signals and their spectra for random excitation

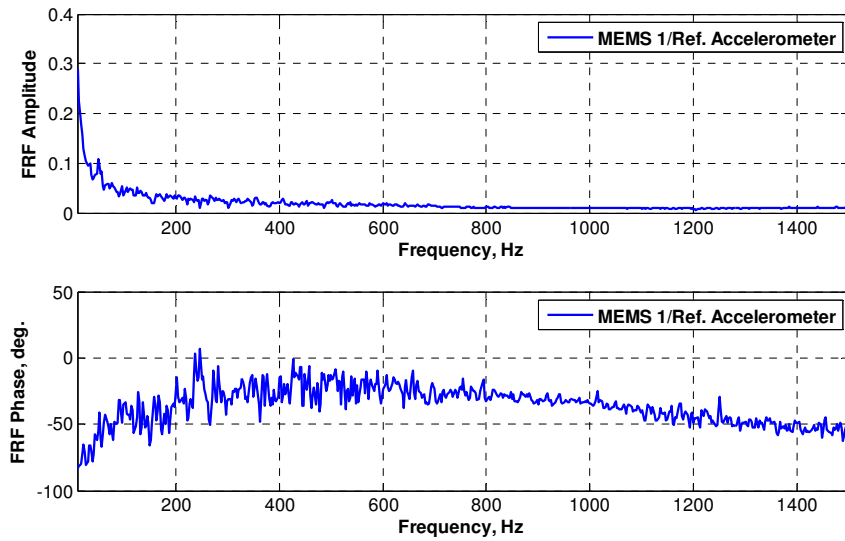
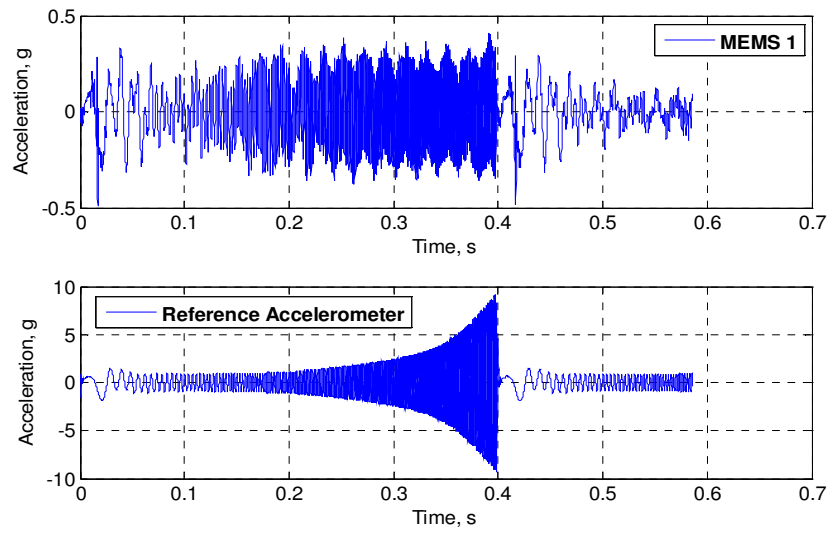


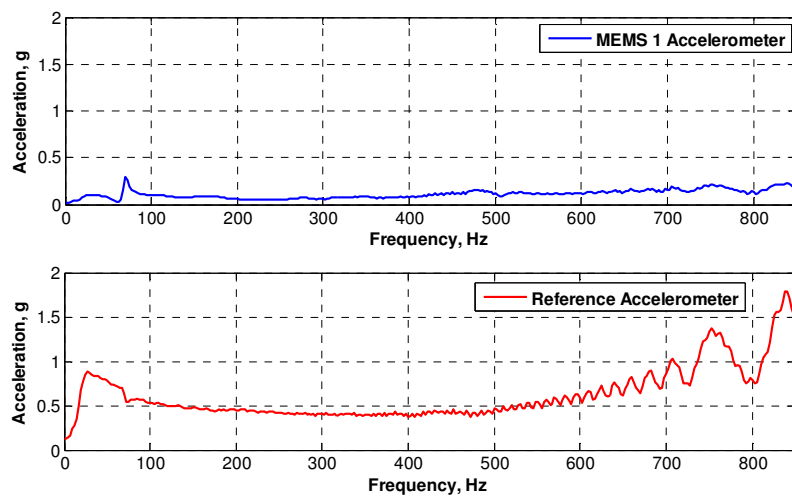
Figure 4.15 MEMS 1 FRF for random excitation

4.6.3 MEMS 1 Sweep-sine Excitation

Typical measured responses of the MEMS 1 and reference accelerometer in time domain are shown in Figure 4.16 for sweep-sine excitation. This figure shows that the response of the reference accelerometer follows the sweep-sine pattern of the input excitation given to the shaker from 0 to 1 kHz, but the measurement by the MEMS 1 accelerometer is much different and noisy. The measured time domain signal itself indicates the MEMS 1 performance is not good enough. Both spectra and FRF quantify the error in the measurement by MEMS 1 accelerometer. It is because the amplitude at each frequency of excitation for MEMS 1 is significantly different from the reference accelerometer. In fact, the FRF plot shown in Figure 4.17 indicates the amplitude ratio and phase between the MEMS 1 and the reference accelerometer is not just a constant value over the frequency range of excitation but is different at each frequency.



(a) Time domain



(b) Spectra

Figure 4.16 MEMS 1 time domain signals and their spectra for the sweep-sine excitation

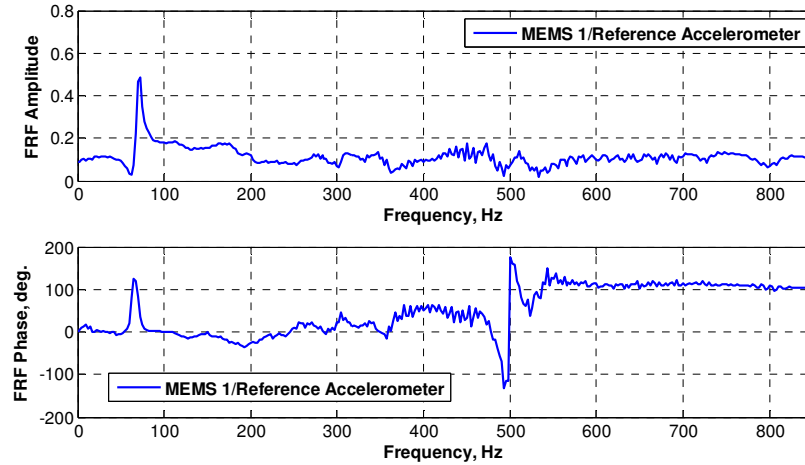


Figure 4.17 MEMS 1 FRF for sweep-sine excitation

4.7 MEMS 2 Accelerometer

The performance of this MEMS accelerometer is also compared with the reference accelerometer when they are simultaneously excited by sinusoidal, sweep-sine and random signals. The comparison for sinusoidal excitation will be presented at only two frequencies (237Hz and 376Hz).

4.7.1 MEMS 2 Sinusoidal Excitation

The frequency domain for measured responses by both accelerometers when excited at 237 Hz is shown in Figure 4.18. The amplitude of MEMS 2 accelerometer spectrum is approximately half of the amplitude of the reference accelerometer spectrum. This can be seen in the FRF plot shown in Figure 4.19 where the amplitude ratio is approximately 0.5 and MEMS 2 response has phase shift of 107 degree from the response of the reference accelerometer. The measured responses and the FRF for the

other excitation at 377.5 Hz are shown in Figures 4.20 and 4.21 respectively which again indicate deviation in MEMS 2 accelerometer response compared with the reference accelerometer.

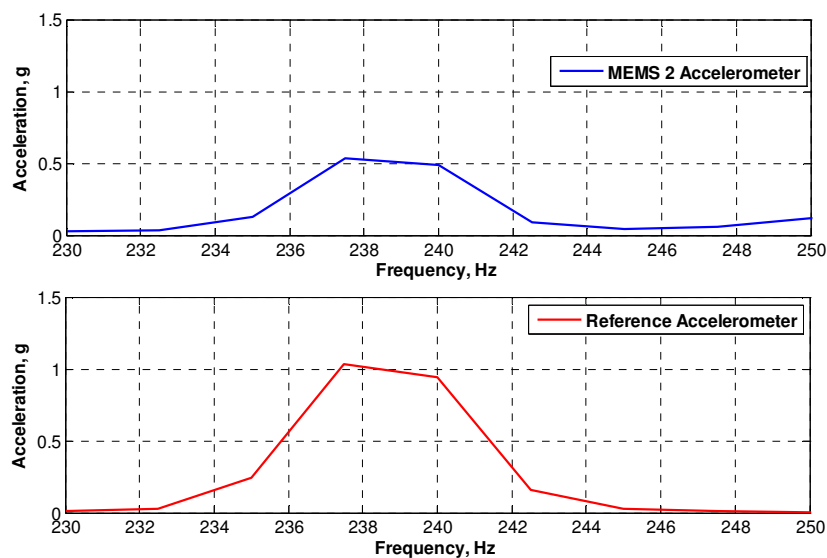


Figure 4.18 MEMS 2 spectrum at 237Hz

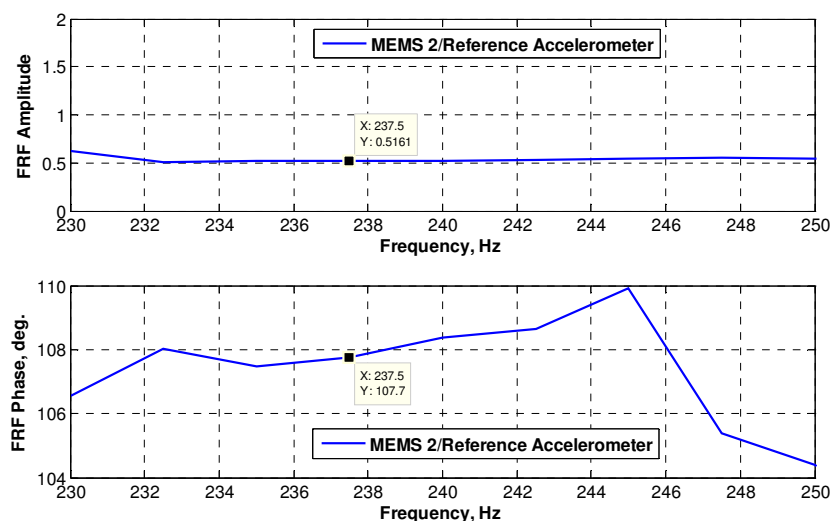


Figure 4.19 MEMS 2 FRF at 237Hz

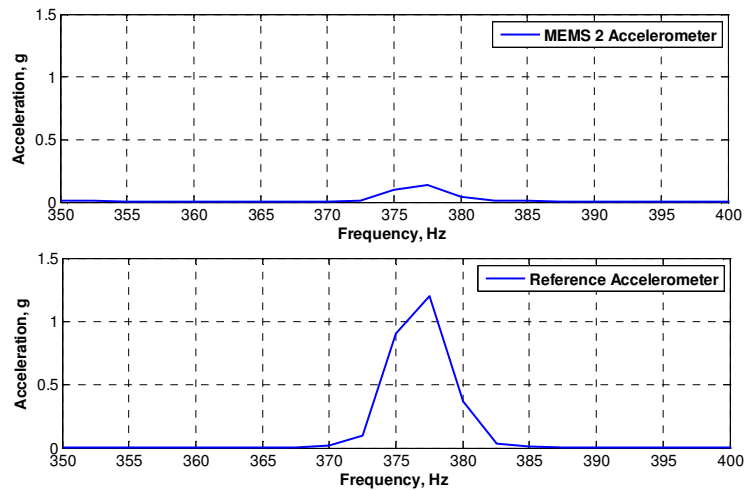


Figure 4.20 MEMS 2 spectrum at 377.5Hz

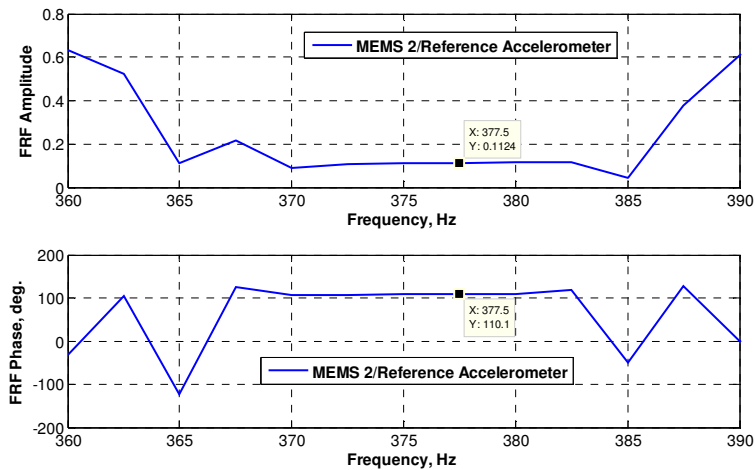
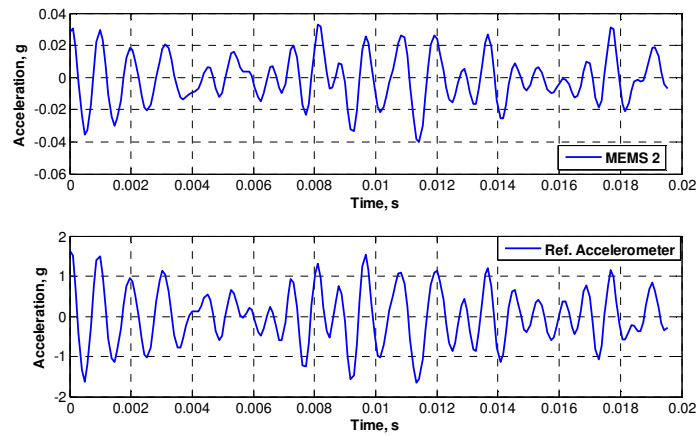


Figure 4.21 MEMS 2 FRF at 377.5Hz

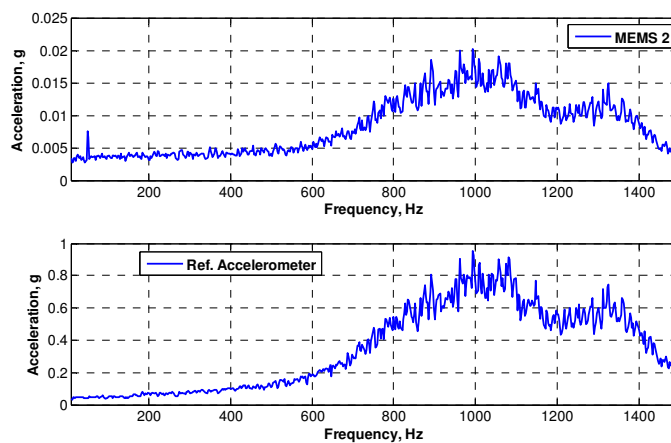
4.7.2 MEMS 2 Random Excitation

Typical measured responses of both accelerometers in the time domain and the frequency domain for the random excitation in a frequency band of 10 Hz to 1.5 KHz are shown in Figure 4.22. Both accelerometers responses look to be identical in the time domain as MEMS 2 accelerometer generally follows the pattern of applied excitation. However, its amplitude is very low compared with the reference accelerometer. This

can be seen in the FRF amplitude which shows very low amplitude ratios at all frequencies. Moreover, FRF for phase shows that there is a phase shift at every frequency starting from about -57 degree at 10 Hz and then changing from negative to positive values till frequency of about 400 Hz. Thereafter phase is changing only in negative values as show in Figure 4.23. Therefore, it can be stated that this accelerometer also shows significant deviation in both amplitude and phase compared with the reference accelerometer.



(a) Time domain



(b) Spectra

Figure 4.22 MEMS 2 time domain signals and their spectra for the random excitation

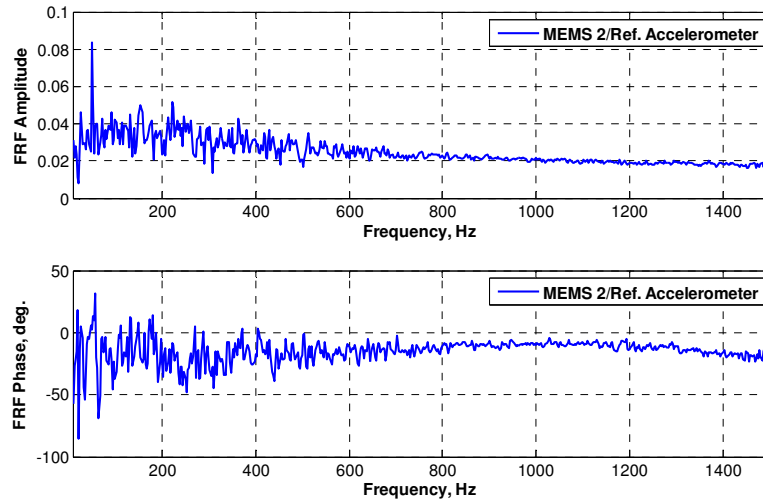
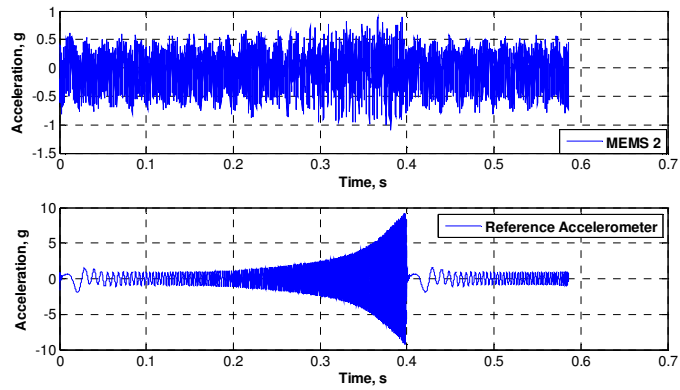


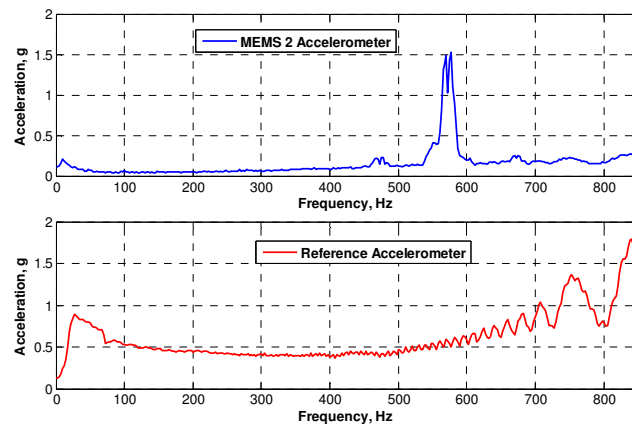
Figure 4.23 MEMS 2 FRF for random excitation

4.7.3 MEMS 2 Sweep-sine Excitation

Typical measured responses of the MEMS 2 and reference accelerometers in time domain and frequency domain for sweep-sine excitation are shown in Figure 4.24. This figure shows that the response of the MEMS 2 accelerometer does not follow the sweep-sine pattern of the input excitation given to the shaker from 0 to 1 kHz, also the measurement by the MEMS 2 accelerometer is much different and noisy. The measured time domain signal itself indicates the MEMS 2 performance is not good enough. In addition, FRF plots shown in Figure 4.25 show significant deviation in both amplitude and phase responses of this accelerometer compared with the reference accelerometer.



(a) Time domain



(b) Spectra

Figure 4.24 MEMS 2 time domain signals and their spectra for the sweep-sine excitation

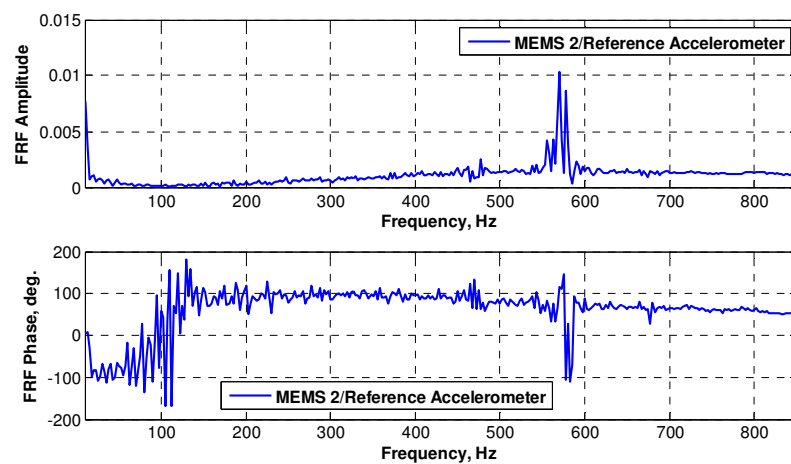


Figure 4.25 MEMS 2 FRF for sweep-sine excitation

4.8 Comparison between Random and Sweep-sine Measurements

As previously presented, all MEMS accelerometers were tested to measure sine, random and sweep-sine excitations. The responses of MEMS 1 and MEMS 2 accelerometers to random and sweep sine excitations were compared. It has been observed that the FRF between these accelerometers and the reference accelerometer for the random excitation was significantly different when compared with the FRF for the sweep-sine excitation. Typical FRF plots comparing the two kinds of tests for MEMS 1 are shown in Figure 4.26. They are significantly different. This simply indicates that the random vibration measurement by the MEMS accelerometers may not be useful for the practical purpose which needs further investigation.

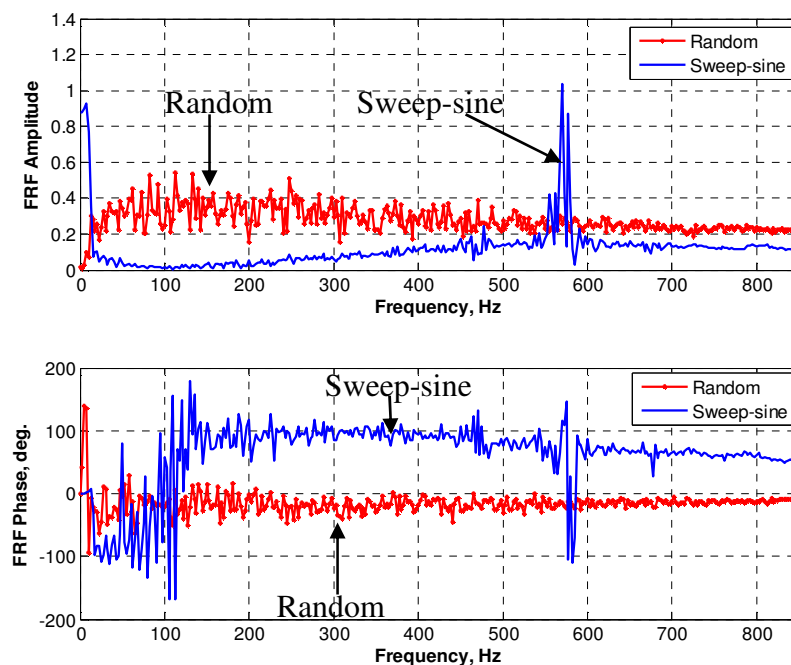


Figure 4.26 Comparison of the FRF plots between MEMS 1 accelerometer and the reference accelerometer due to sweep-sine and random excitations

The FRF between each MEMS accelerometer and the reference accelerometer for sine excitations were also compared with the FRF for the sweep-sine excitation. The results for these comparisons will be presented in Chapter 6.

4.9 Conclusion

The performance tests of typical capacitive type MEMS accelerometers are carried out for different excitations – sinusoidal, sweep-sine, random and impulse. All tests were conducted well within the technical specifications of the accelerometers. The measured responses of the MEMS accelerometers were compared with a calibrated ICP type accelerometer. The tests performed here clearly show lots of improvement needed before their use in practice. It is being planned to carry out more investigation with several numbers of MEMS accelerometers to understand the future direction for improvements.

CHAPTER 5

CORRECTION IN TIME DOMAIN

Reformatted version of paper:

A Typical Filter Design to Improve the Measured Signals from MEMS Accelerometer

Authors: Abdellatef Badri, Jyoti K. Sinha and A. Albarbar

Paper published in Measurement 43 (2010) 1425-1430

Abstract

The MEMS type accelerometers have been receiving attention due to their low cost and small size. But the accurate vibration measurements of both amplitude and phase at all frequencies in the measurement frequency range are important for the reliable vibration analysis for any type of accelerometers. However, it has been observed that such accelerometers show some deviation, both in amplitude and phase, based on the controlled vibration measurements in the Laboratory using a number of the MEMS accelerometers. Hence, a characteristic function (CF) of a typical MEMS accelerometer has been generated by the laboratory experiments when compared with a reference accelerometer and then a new filter has been designed matching the CF (both amplitude and phase). This filter has then been used to correct the measured signals from the MEMS accelerometer.

Keywords: MEMS Accelerometer; Vibration test, Characteristic Function.

5.1 Introduction

Vibration measurement and analysis has traditionally been used to provide condition monitoring of machinery, dynamic qualification in design of novel components, fault prediction, defects within aging structures and the diagnosis of structural dynamic effects. Recently *Sinha* [101] gave an overview of the vibration measurement and analysis in different roles. Using several piezoelectric and/or ICP (integrated circuit piezoelectric) accelerometers in a particular application/structure is expensive, and it would be advantageous to replace these by low cost and small size MEMS accelerometers. MEMS accelerometers are a new integrated circuit technology; and confidence in their performance needs to be established, particularly in comparison to conventional accelerometers. The main comparison between MEMS and conventional accelerometers has been in their signal frequencies, and it appears that their frequency content have similar spectrums [56–58]. However, comparison of their amplitudes shows significant deviation. *Albarbar et al.* [22] have recently compared the performance of three different types of these MEMS accelerometers and used them for vibration based machinery condition monitoring. Two of the used MEMS accelerometers were found reliable in measuring a CNC machine vibration signals.

Amplitude correction, either in the frequency or time domain, would allow the reliable use of the MEMS accelerometer. Vibration based diagnosis of machines and structures have generally used the frequency domain data, this is presented earlier in the literature [21, 99]. However a significant deviation has been noticed in the amplitude and phase [23]. This need to be corrected for the reliable vibration based diagnosis using the MEMS accelerometers. This can be done either in frequency domain or in time domain. In practice, many vibration based diagnosis for machines and structures have been

utilizing the frequency domain data for the system and fault identifications. Hence a correction method for signals in the frequency domain has been presented earlier in the literature [24, 102]. This study attempts to correct the raw MEMS signal in the time domain, and this paper describes the proposed method and its results.

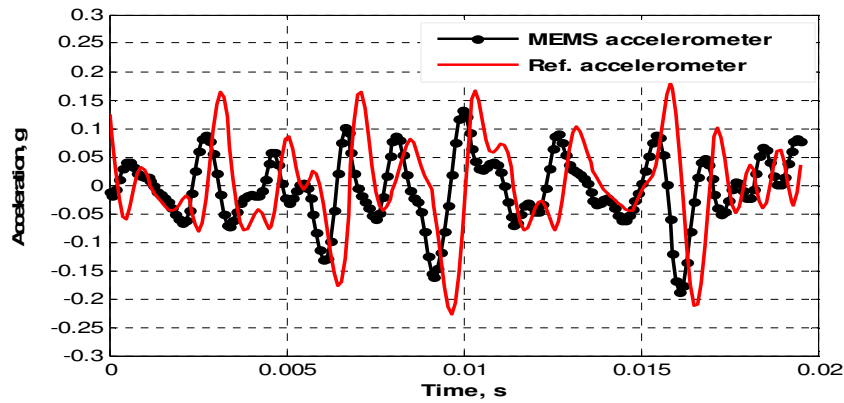
5.2 The Experiment Arrangement

The arrangement consists of a small size payload shaker (M/s GW make), a shaker power amplifier, signal generator and a PC based data acquisition system. A schematic of the arrangement is shown in Figure 4.2. The MEMS and reference accelerometers are attached back to back on the shaker's armature; this to ensure that the accelerometers are subjected to identical vibrations. The reference accelerometer is a conventional and well known ICP type conventional accelerometer having a specification of 100 mV/g, linear frequency range up to 2 kHz, 50 g level. The MEMS accelerometer is 250 mV/g, frequency range 1.5 kHz, ± 2 g level. In the experiment, the shaker's armature was randomly energized producing vibration frequencies up to 1.5 kHz, and the data was collected at the sampling rate of 5000 samples/s.

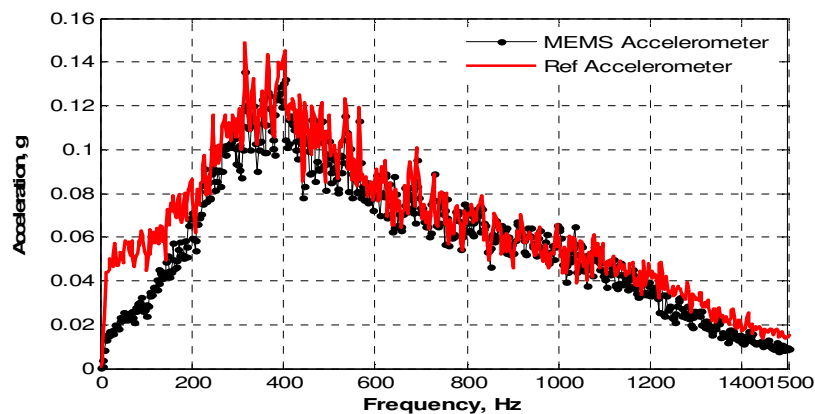
5.3 The Experimental Results

The MEMS and reference accelerometer responses are significantly different, when subjected to the same vibrations; graphs of their responses are shown below in Figure 5.1a and 5.1b. The graphs show that, above a shaker frequency of approximately 400 Hz, their signal amplitudes decrease; this is owing to the randomness of the shaker frequencies.

The frequency response function (FRF) between the MEMS and reference accelerometers is shown in Figure 5.2; the MEMS accelerometer is used as the output and the reference accelerometer as the input. The graphs show significant deviations in the amplitude ratio and phase relation of the accelerometers; ideally within the frequency range, the amplitude ratio should be unity and the phase difference should be zero. Analysis of the data indicates that, without correction, the output of the MEMS accelerometer is unreliable for vibration measurement as a means of vibration measuring.



(a) Time domain



(b): Frequency domain

Figure 5.1 Measured responses of the MEMS and reference accelerometers

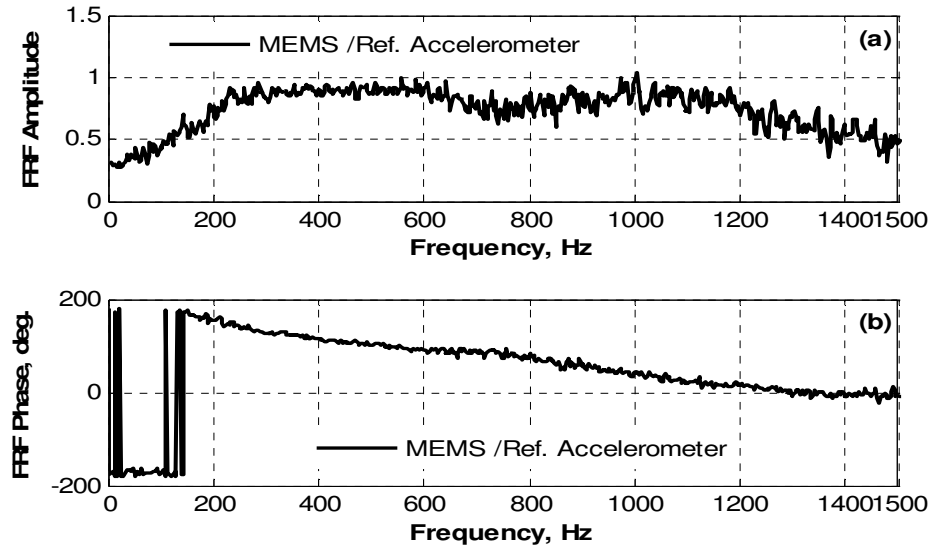


Figure 5.2 FRF plot between MEMS and reference accelerometers, (a) Amplitude, (b) Phase

It is expected that the MEMS accelerometer will show same deviation at different frequencies when used at the plant site. Hence the measured signals need to be corrected such that the corrected time domain MEMS signals should produce a FRF plot with amplitude and phase equal to 1 and 0 degree respectively. Therefore, it is required to design a special filter that filters amplitude and phase which must be the inverse of the FRF shown in Figure 5.2 so that the signal can be corrected for both amplitude and phase at all frequencies in the measured frequency band. The inverse of the FRF, which is computed as, $1/FRF(\omega)$ is shown in Figure 5.3. The curve of the measured inverse FRF plot was not smooth, so it was smoothen by curve fitting. The amplitude and phase are fitted separately to the frequency range using polynomial curve fitting. To achieve the best fitting, different orders have been tested and the best fitted curves are also shown in Figure 5.3 for comparison. The fitted curves shown in Figure 5.4 have now

been referred to as the Filter Characteristic Function (FCF) of the MEMS accelerometer.

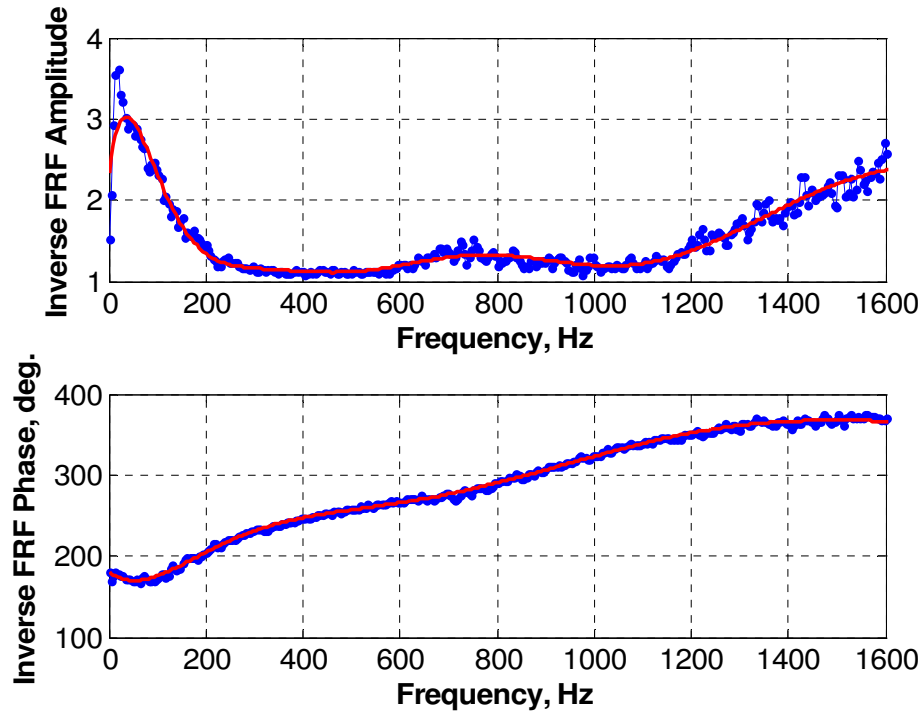


Figure 5.3 Inverse FRF (the FCF curve) plot- Comparison of original and fitted curves,
Line with dots - Original, solid line- Fitted

5.4 Proposed Correction Method

Generally, digital and analogue filters have a specified frequency range over which they operate. The filters may be low pass, high pass or band pass and the appropriate frequencies are attenuated or removed [103, 104]. Most filters exclusively modify either the amplitude or phase of a particular signal, however, the MEMS response requires both amplitude and phase modification as indicated in Figure 5.3. The transfer function (TF) of a linear time-invariant discrete- time filter is defined as [103]

$$H(\omega) = \frac{Y(z)}{X(z)} \quad (5.1)$$

where $Y(z)$ and $X(z)$ are the z transform of the filter output signal $y(n)$ and the input signal $x(n)$ respectively, and $z = e^{j\omega}$, where ω is angular frequency (rad/s) and n is the function of time, $t(n) = (n-1)dt$, $n=1, 2, 3, \dots, n$ and dt is the time interval between two samples. Here, the signals, $x(n)$, are the MEMS accelerometer measured signals (input signals) and the output signals, $y(n)$, are the corrected MEMS signals.

This transfer function (TF) can further be written as,

$$H(\omega) = \frac{b_0 + b_1 z^{-1} + \dots + b_N z^{-N}}{1 + a_1 z^{-1} + \dots + a_M z^{-M}} \quad (5.2)$$

where b_0, b_1, \dots, b_N and a_1, a_2, \dots, a_M are the polynomial coefficients. N and M denote the orders of these polynomials.

The amplitude and phase data of the CF (the fitted curves in Figure 5.3) have been converted into the transfer function (TF), $H(\omega)$, using Equation (5.3) and then coefficients for the filter transfer function in Equation (5.2) have been obtained.

$$H(\omega) = A_{CF}(\omega) e^{j\theta_{CF}(\omega)} \quad (5.3)$$

where $A_{CF}(\omega)$ is the amplitude and $\theta_{CF}(\omega)$ is the phase angle at the angular frequency ω , for the CF shown in Figure 5.3. The coefficients, a and b , have then been calculated using the discrete filter least squares fit to the TF, $H(\omega)$, function in the MatLab code [105]. Once the coefficients have been computed the corrected signals for the MEMS accelerometer can be computed as:

$$\begin{aligned}
 y(n) &= b_0 x(n) + b_1 x(n-1) + \dots + b_M x(n-M) - a_1 y(n-1) - \dots - a_N y(n-N) \\
 &= \sum_{i=0}^M b_i x(n-i) - \sum_{j=1}^N a_j y(n-j)
 \end{aligned} \tag{5.4}$$

It is important to note that the coefficients, a and b , related to the TF, $H(\omega)$, must be stored for the MEMS accelerometer so that the correction in the measured signals can be done using Equation (5.4).

5.5 Application of the Proposed Method

Initially different number of coefficients orders, N and M , in Equation (5.2) have been attempted to obtain the best fit and stable filter. The stability of the filter can be evaluated by pole-zero Maps for the filter TF. The filter stability for each fitting order was checked. Figure 5.4 shows the poles and zeros of the filter transfer function when the fitting order $N = M = 21$ was used. As the radius of all poles (measured from the origin) has been observed as less than unity they denote a stable filter [106]. The designed filter TF has also been computed from the stable filter coefficients to confirm whether this is close to the required CF curves (the inverse of FRF) shown in Figure

5.3. This is shown in Figure 5.5 which is definitely same as Figure 5.3 except in the lower frequency range. Hence the designed filter can be considered as acceptable.

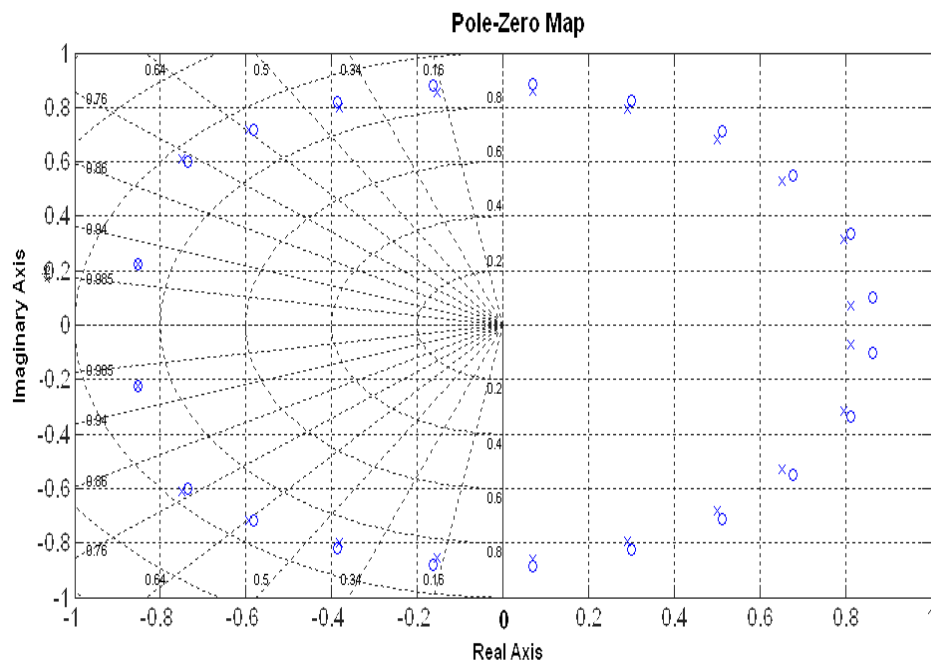


Figure 5.4 Poles and Zeros Map

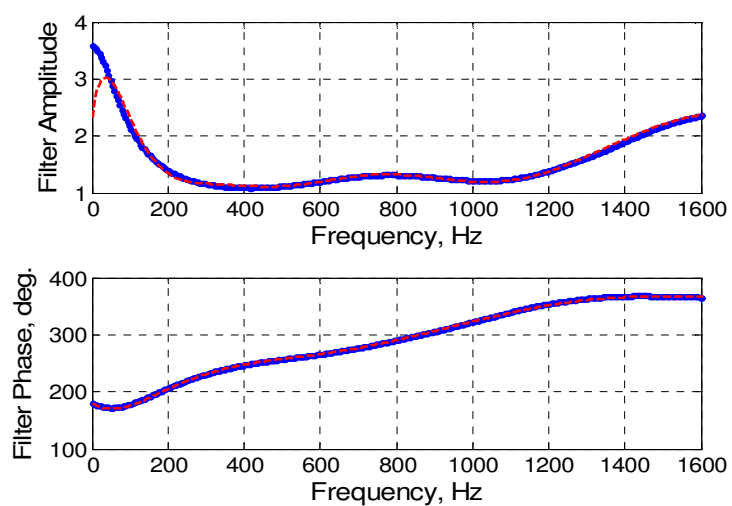


Figure 5.5 The designed filter transfer function (TF) for phase and amplitude (dash line) and comparison with the CF (solid line with dots)

Once the stable filter coefficients are known, the input signals were corrected using Equation (5.4). The output of the filter delays the response which depends on the number of coefficients. Hence, the delay error has been removed. The filtered MEMS accelerometer signals compare reasonably well with the reference accelerometer signals. A typical signal is shown in Figure 5.6.

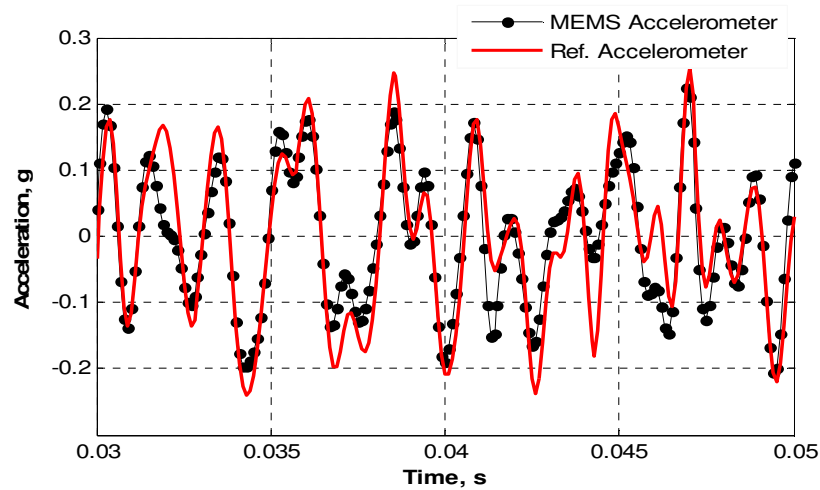


Figure 5.6 The corrected MEMS measured response (line with dots) compared with the reference accelerometer (solid line)

The spectrum of the corrected MEMS response compared with the reference accelerometer is shown in Figure 5.7. Both spectra are nearly identical. The FRF between the corrected MEMS and the reference accelerometer signals has also been computed and shown in Figure 5.8. Both amplitude and phase show improvement compared to Figure 5.2 before correction because they are close 1 and 0 degree respectively, however the correction in the phase seems more promising compared to the amplitude. Hence the proposed method is able to correct measured signals.

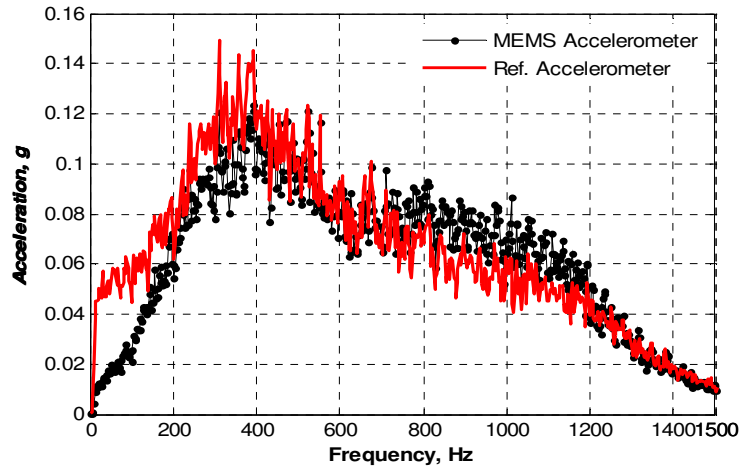


Figure 5.7 Amplitude spectrum of corrected MEMS response (line with dots) compared with reference accelerometer (solid line)

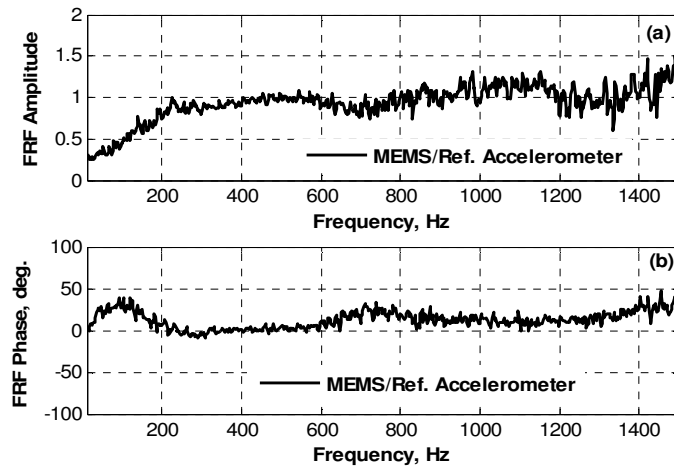


Figure 5.8 FRF plot of the MEMS accelerometer (after correction) with respect to the reference accelerometer, (a) Amplitude, (b) Phase

5.6 Conclusion

The measured signals from a typical MEMS accelerometer show significant deviation in both amplitude and phase when compared with a well known conventional signal. A correction method has been proposed by developing a filter based on the Characteristic Function (CF) obtained experimentally in the Laboratory experiments. This proposed technique appears to be a successful, in the time domain, in correcting the measured

signal of an MEMS accelerometer. An appropriate filter, tuned during calibration, could be incorporated in a practical accelerometer unit, for applications where reliable and practical signals are required.

CHAPTER 6

CORRECTION IN FREQUENCY DOMAIN

Reformatted version of papers:

1. Correcting Amplitude and Phase measurement of accelerometer in Frequency Domain.

Authors: Abdellatef Badri and Jyoti K. Sinha

The Fifth International Conference on Condition Monitoring & Machinery Failure Prevention Technologies, Heriot-Watt University, Edinburgh, July 2008, pp. 94-100

2. Enhancing the Frequency Range of Measurement for an Accelerometer.

Authors:

Abdellatef Badri, Jyoti K. Sinha and A. Albarbar

Paper published in: Noise & Vibration Worldwide, Volume 40, Number 6 / June 2009

3. Improvement in measured signals of MEMS accelerometer.

Authors:

Abdellatef Badri and Jyoti K. Sinha

Paper published in: The third International Conference on Integrity, Reliability and Failure, Porto/Portugal, 20-24 July 2009, Paper Ref: S1146_P0507.

4. A Method to Calibrate the Measured Responses by MEMS Accelerometers.

Authors:

Abdellatef Badri, Jyoti K. Sinha, and A. Albarbar

Paper published in: Strain Journal, DOI: 10.1111/j.1475-1305.2010.00764.x

Keywords: MEMS Accelerometer; Vibration Measurement; Spectrum; Frequency Response Function; Characteristic Function.

Abstract:

MEMS (Micro Electro-Mechanical System) accelerometers have been receiving attention due to their low cost and small size. Accurate vibration measurements of both amplitude and phase at all frequencies in the measurement frequency range are important for the reliable vibration analysis. However, it has been observed that such accelerometers show some deviation. Hence, a simple calibration method in the frequency domain has been used for correcting both amplitude and phase for the measured signals by the MEMS accelerometers. The paper presents the calibration procedure and results of the present study applied on two different types of the MEMS accelerometers.

6.1 Introduction

Vibration measurement and analysis is one of the accepted methods in machinery condition monitoring techniques; it plays a significant role in the dynamic qualification of newly designed structural components, prediction of faults and structural aging-related problems, and several other structural dynamics studies and diagnosis [101]. However, multiple data

collection points are generally required in most of the condition monitoring systems which makes the system costly if conventional accelerometers are used. Hence, there is a need for a cheaper and reliable alternative to conventional accelerometers. The MEMS accelerometers are one such options recently receiving attention due to their low cost and small size [90]. It is a new technology for an accelerometer and produced in a similar fashion as an integrated circuit manufacturing [88]. However, the use of MEMS accelerometers is still limited in the field of condition monitoring because of lack of confidence level in their performance. A few earlier researches gave comparison of the performance between the MEMS and conventional accelerometers, mainly related to the frequency content in the spectrum of the measured signals.

It has been observed that the frequencies content in the spectrum of the measured signal from the MEMS accelerometer are same as the spectrum obtained from the conventional accelerometer; however the significant deviation has been noticed in the amplitude and phase [23]. This need to be corrected for the reliable vibration based diagnosis using the MEMS accelerometers. This can be done either in frequency domain or in time domain. In practice, many vibration based diagnosis for machines and structures have been utilising the frequency domain data for the system and fault identifications, hence this chapter presents a correction method for MEMS accelerometer response in the frequency domain.

6.2 The Proposed Correction Method

The accuracy of the measured signals by the MEMS accelerometers can be improved by

either modifying the MEMS accelerometer design or by a simple calibration of the measured signals of the existing MEMS accelerometers by comparing with a well-accepted reference accelerometer. However, the modification in the MEMS accelerometer design needs extensive effort so the later option has been used to correct the measured signals by the MEMS accelerometers. For this purpose a Characteristic Function (CF) for a MEMS accelerometer has been generated and stored for the MEMS accelerometer which has then been used for the correction of the measured signals by this MEMS accelerometer. The procedure for generation of the CF and then correction in measurements has been discussed here.

6.2.1 Generation of Characteristic Function (CF)

A schematic of the test setup is shown in Figure 6.1. The test setup consists of a small size shaker together with a shaker power amplifier, signal generator and a PC based data acquisition for data collection and storage for further signal processing. Two accelerometers (one reference accelerometer and the other the test MEMS accelerometer) were attached back to back on the armature of the shaker.

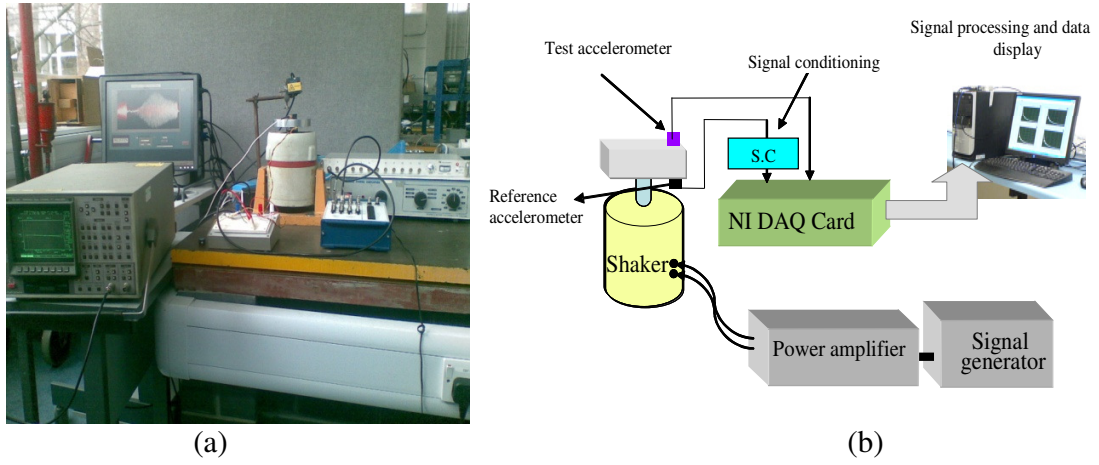


Figure 6.1 Test setup (a) picture, (b) schematic

The linear sweep-sine excitation up to the frequency measurement range for the test MEMS accelerometer has been used to drive the shaker for the vibration test. The measured signals from both the accelerometers have then been processed to compute the Frequency Response Function (FRF) using the test MEMS accelerometer as output and the reference accelerometer as input. The FRF, $H_{CF}(f)$ has been computed as:

$$H_{CF}(f) = \frac{S_{xy}(f)}{S_{xx}(f)} \quad (6.1)$$

where $S_{xy}(f)$ is the cross spectral density and $S_{xx}(f)$ is the Power Spectral Density (PSD) at frequency (f) . $y(t)$ is the test MEMS accelerometer signal and $x(t)$ is the reference accelerometer signal. The functions $S_{xy}(f)$ and $S_{xx}(f)$ have been computed as:

$$S_{xy}(f) = E \left(\sum_{r=1}^n X_r(f) \cdot Y_r^*(f) \right) \quad (6.2)$$

$$S_{xx}(\omega) = E \left(\sum_{r=1}^n X_r(f) \cdot X_r^*(f) \right) \quad (6.3)$$

where, $X_r(f)$ is the Fourier Transformation (FT) at the frequency, f , of the r th segment of $x(t)$, $X_r^*(f)$ is its complex conjugate, $Y_r(f)$ is the FT of the r th segment of $y(t)$, $Y_r^*(f)$ is its complex conjugate, and $E(\cdot)$ indicates the simple arithmetic mean operator. Since the sweep-sine excitation was used here so the total time for any segment used for the FT was kept equal to one complete cycle of the chirp excitation to ensure all exciting frequency components must be available in each segment and to reduce the affect of the non-stationary signals in the FT. It was averaged over a few sweep cycles to get a good representative FRF plot for the experiments. Otherwise use step-sine excitation to compute the FRF data at each frequency.

This FRF gives both the amplitude ratio and phase relation between two signals. Ideally the amplitude ratio should be 1 (or 0dB) and phase to be 0 degree at all frequencies between the two accelerometers. However, it may deviates if the MEMS accelerometer is not good enough. Hence, this FRF, $H_{CF}(f)$, has been referred as the CF for the test MEMS accelerometer.

6.2.2 Correction in Frequency Domain

Now it has been assumed that the test MEMS accelerometer has been used in the field, the measured data is $y_m(t)$ which has been divided into 'n' number of segment for the FT calculation. Let $Y_{m,r}(\omega)$ be the FT for the r th segment of $y_m(t)$, this $Y_{m,r}(f)$ will have error in both amplitude and phase. Hence, the corrected FT, $Y_{m,r}^c(f)$, for r th segment can be calculated as:

$$Y_{m,r}^c(f) = \frac{Y_{m,r}(f)}{H_{CF}(f)} = \frac{B_{Y_{m,r}}(f)e^{j\theta_{Y_{m,r}}(f)}}{A_{H_{CF}}(f)e^{j\theta_{H_{CF}}(f)}} = \frac{B_{Y_{m,r}}(f)}{A_{H_{CF}}(f)} e^{j(\theta_{Y_{m,r}}(f) - \theta_{H_{CF}}(f))} \quad (6.4)$$

where, $A_{H_{CF}}(f)$ and $B_{Y_{m,r}}(f)$ are the amplitude of the $H_{CF}(f)$ and $Y_{m,r}(f)$ respectively and their associated phase angles are $\theta_{H_{CF}}(f)$ and $\theta_{Y_{m,r}}(f)$ at the frequency, f . Finally the corrected PSD of the test MEMS accelerometer data can be computed as:

$$S_{yy}^c(f) = E \left(\sum_{r=1}^n Y_{m,r}^c(f) \cdot Y_{m,r}^{*c}(f) \right) \quad (6.5)$$

It is also important to note that the use of the suggested method in Equation (6.4) allows the correction, both in amplitude and phase, so that it can be reliably used with other signals measured by other vibration sensors to compute a number of parameters used in vibration

analysis, for example, FRF, Cross-power spectrum, coherences, etc.

6.3 Test Examples

Here a PCB accelerometer has been used as a Reference Accelerometer. The PCB accelerometer is an ICP type with the technical specifications – Sensitivity 100mV/g, Linear frequency range 2kHz, 50 g level, amplitude linearity within $\pm 5\%$ and phase deviation within $\pm 5^\circ$. Although the amplitude linearity and phase are slightly high for the Reference Accelerometer used for the calibration purpose but it has been considered to be acceptable for the present purpose to illustrate the calibration procedure for the existing MEMS Accelerometers. In the present study two typical MEMS Accelerometers, namely MEMS 1 and MEMS 2, were used. The technical specifications for MEMS 1 and MEMS 2 are given in section 3.3 of chapter 3. The experiments were conducted using the chirp-sine excitation up to 1 kHz with linear chip rate of 2.5 kHz/s to drive the shaker shown in Figure 6.1. Hence the time period for 1 cycle of the chirp sine excitation from 0 to 1kHz was 0.4s and the data were collected at 10240 Samples/s for 4s using the 16 bit Analogue to Digital, 8 channels data acquisition card into the computer for further signal processing. The CFs were then estimated for both the MEMS Accelerometers using Equation (6.1) when 0.4s (4096 FFT points) segment size was used to reduce the affect of the non-stationary signals in the FT. A total 10 averages in FRF computation without overlap were used to get a good representative CF with the frequency resolution of 2.5Hz for the MEMS 1 and MEMS 2 respectively. Now, the application and usefulness of this CF in the calibration/correction of the measured signals by the MEMS 1 and MEMS 2 Accelerometers has been discussed

here.

6.3.1 Case I: MEMS 1 Accelerometer

Typical measured responses of the MEMS 1 and reference accelerometers in time domain are shown Figure 6.2. This figure shows that the response of the MEMS 1 accelerometer is different from the response of the reference accelerometer and hence the measurement of this MEMS 1 accelerometer needs to be corrected for the reliable measurement and vibration analysis.

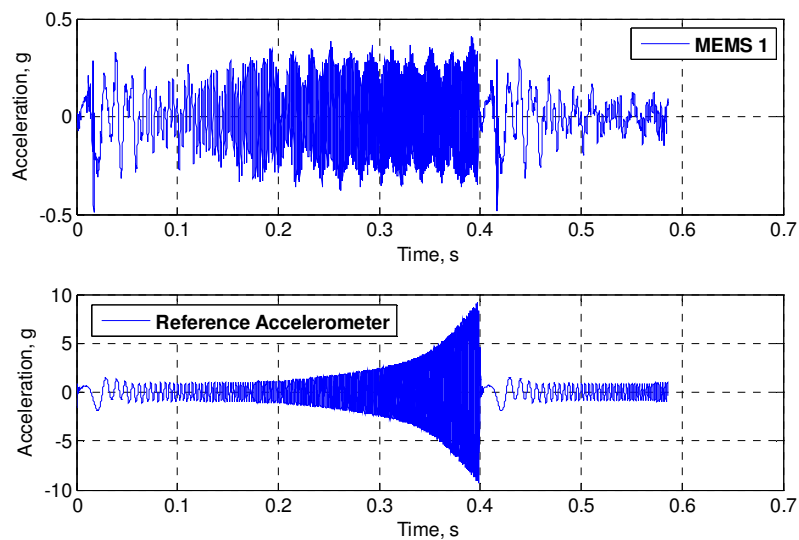


Figure 6.2 Measured acceleration responses of the MEMS 1 and reference accelerometer

The spectra and the FRF of the measured acceleration responses are shown in Figure 6.3. Both the spectrum and the FRF of the MEMS 1 are observed to be significantly different then the reference accelerometer. It has also been seen the deviation in the amplitude and phase of the MEMS 1 compared to the reference accelerometer are changing with

the frequency as shown in Figure 6.3(b). The experiments were also conducted using the sinusoidal excitation at the number of frequencies with different amplitudes. The amplitude and phase of the FRF between the MEMS 1 and the reference accelerometer for the sweep-sine excitation and the single sine excitation at number of frequencies are listed in Table 6.1 and shown graphically in Figure 6.4.

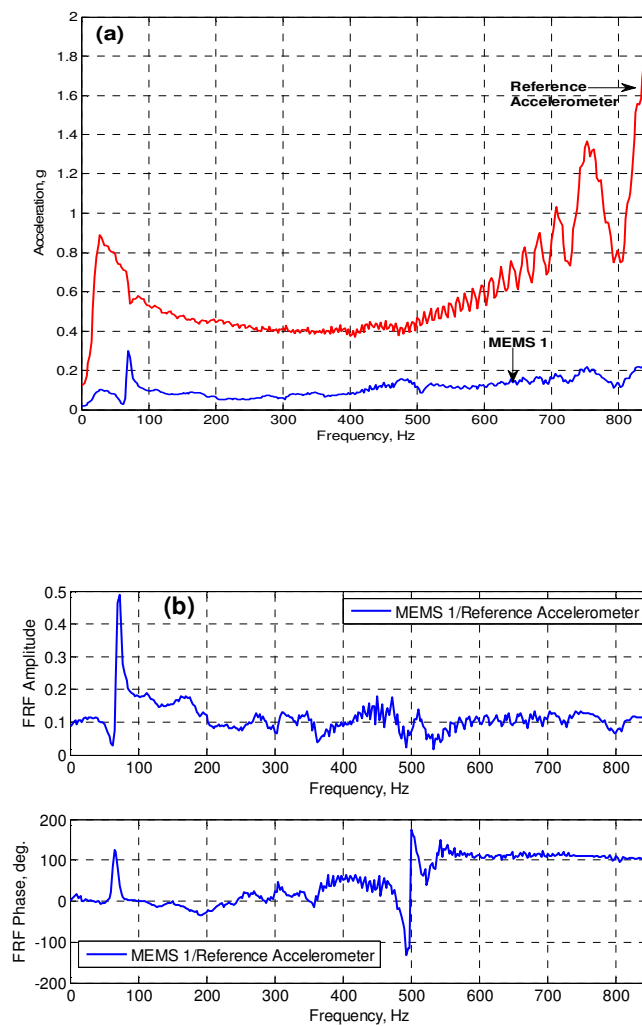


Figure 6.3 Acceleration responses in frequency domain for the MEMS 1 and reference accelerometer, (a) Amplitude Spectra, (b) FRF Amplitude and Phase

Table 6.1 Comparison of the FRF Amplitude and Phase for MEMS 1 due to Sine and Sweep-sine excitations with respect to the reference accelerometer

	Sweep-Sine Excitation		Single Sine Excitation	
Frequency (Hz)	Amplitude (ratio)	Phase (degree)	Amplitude (ratio)	Phase (degree)
20	0.11	1	0.10	1
95	0.183	2	0.19	-1
145	0.153	-5	0.157	-7
185	0.133	-26	0.142	-30
240	0.084	-6	0.098	-8
310	0.165	11	0.172	8
375	0.135	14	0.14	9
420	0.118	15	0.125	7
570	0.104	110	0.18	-43
690	0.112	107	0.25	-46
825	0.11	103	0.346	-95

It has been observed from Table 6.1 and Figure 6.4, that the behaviour of the MEMS 1 to the sweep-sine excitation approximately matches when compared with the single sine excitation up to the frequency of 400 Hz, but beyond this frequency it deviates significantly. It could be due to an acceleration level higher than 2g during sweep-sine excitation. Hence the frequency up to 400Hz can be considered here for further analysis. The amplitude and phase of the MEMS accelerometer with respect to the reference accelerometer at a frequency of the sine excitation remain unchanged with amplitude of the excitation up to 400Hz. Hence the FRF plot shown in Figure 6.3(b) up to 400 Hz has been

stored as the CF for the MEMS1 accelerometer which is shown in Figure 6.5. The CF function has now been used to correct the MEMS 1 measured signals in the frequency domain.

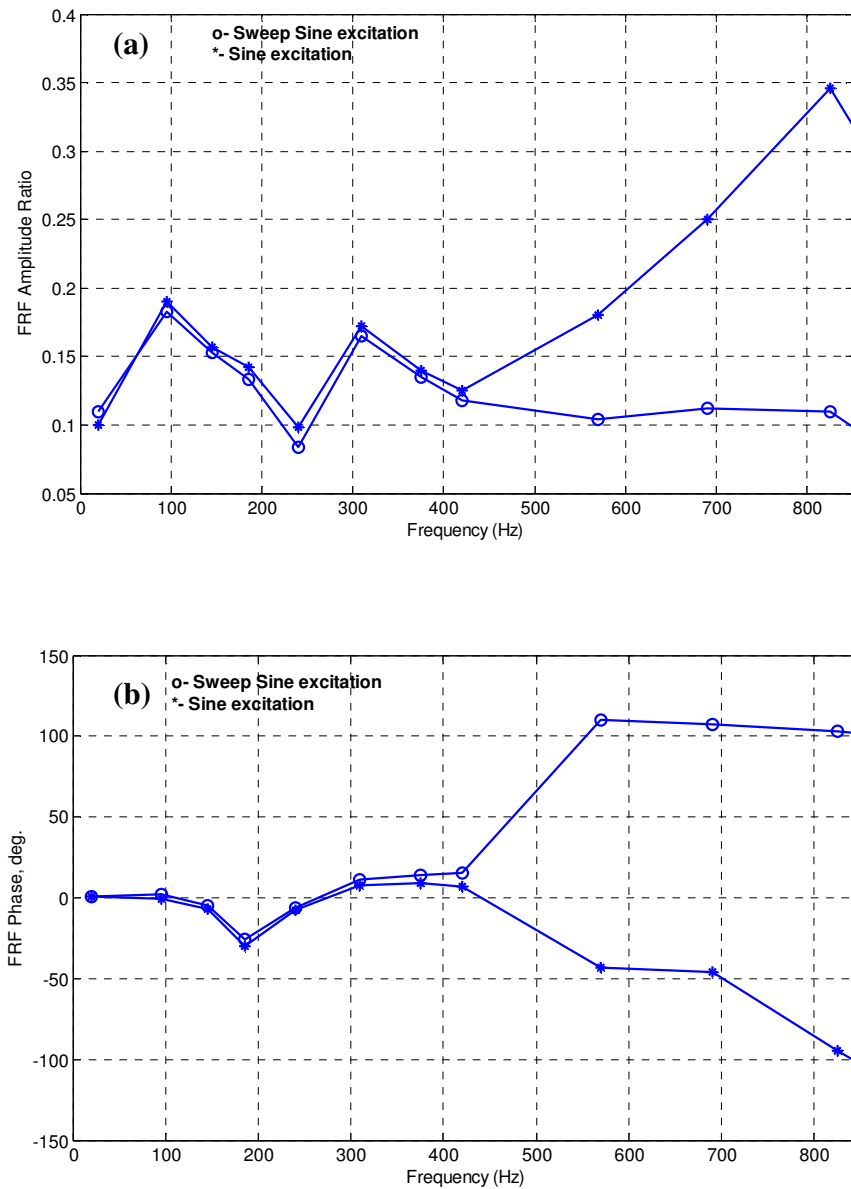


Figure 6.4 Comparison of the MEMS 1 responses due to Sine (line with dot) and Chirp-sine (line with circle) excitations, (a) FRF Amplitude, (b) FRF Phase

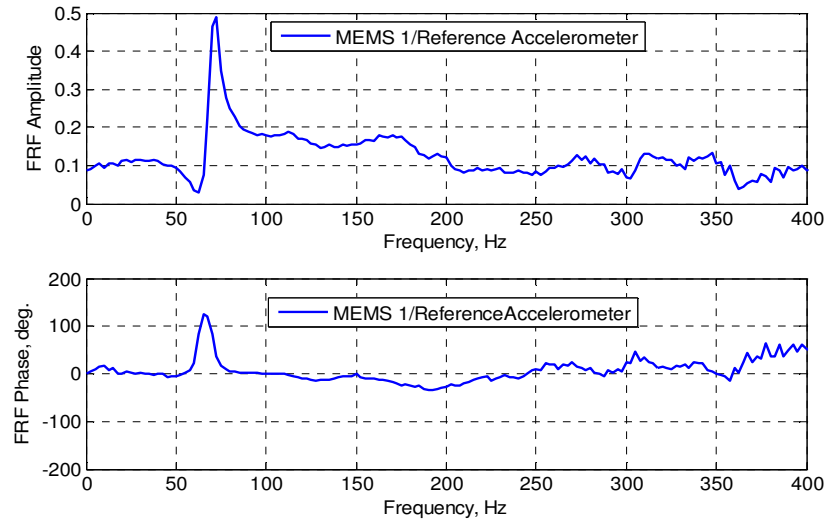


Figure 6.5 The CF in the frequency range (0-400 Hz) for the MEMS 1 accelerometer with respect to the reference accelerometer

6.3.1.1 The Sweep-sine Signal

The amplitude spectrum before correction of the MEMS 1 measured responses up to 400Hz is shown in Figure 6.6. The amplitude spectrum of the reference accelerometer is also shown in Figure 6.6 for comparison when shaker in Figure 6.1 subjected to the linear chirp-sine excitation. Now, the correction has been applied to the measured signals by the MEMS 1 accelerometer 1. The correction method discussed in Section 6.2.2 has been used. The corrected amplitude spectrum for the MEMS 1 accelerometer is shown in Figure 6.7, and it is also compared with the amplitude spectrum of the reference accelerometer. The FRF between the MEMS 1 accelerometer and the reference accelerometer after correction has also been computed which is shown in Figure 6.8. The amplitude ratio is now 1 with 0 degrees phase at all frequencies. The small scatter seen in the phase angle at different

frequencies in Figure 6.8 is almost negligible error. Hence, this example shows the advantages of the proposed method.

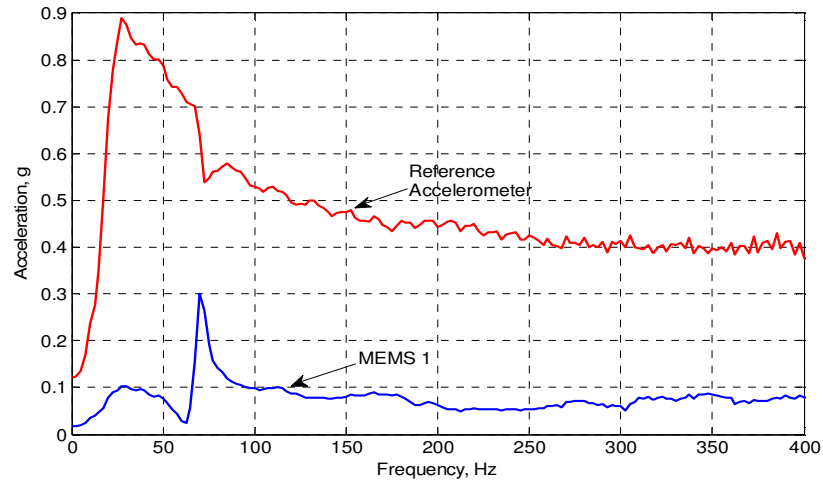


Figure 6.6 Amplitude spectra of the MEMS 1 (before correction) and the reference accelerometer for the linear sweep-sine excitation

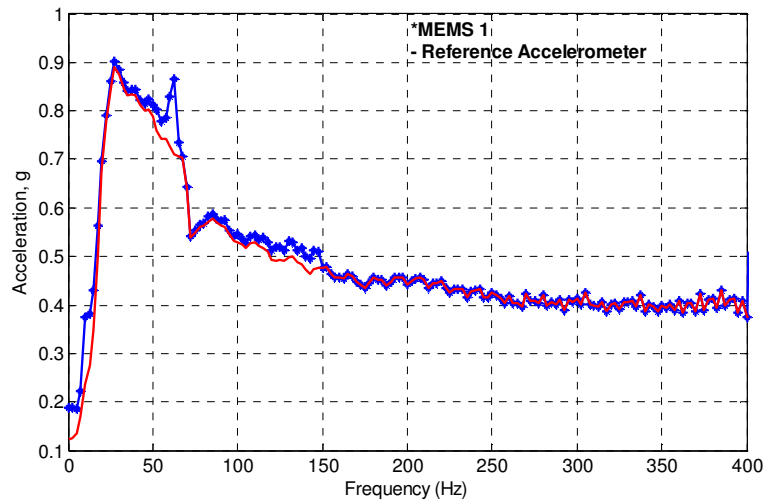


Figure 6.7 Comparison Amplitude spectra of the MEMS 1 (after correction, line with dot) and the reference accelerometer (solid line) for the linear sweep-sine excitation

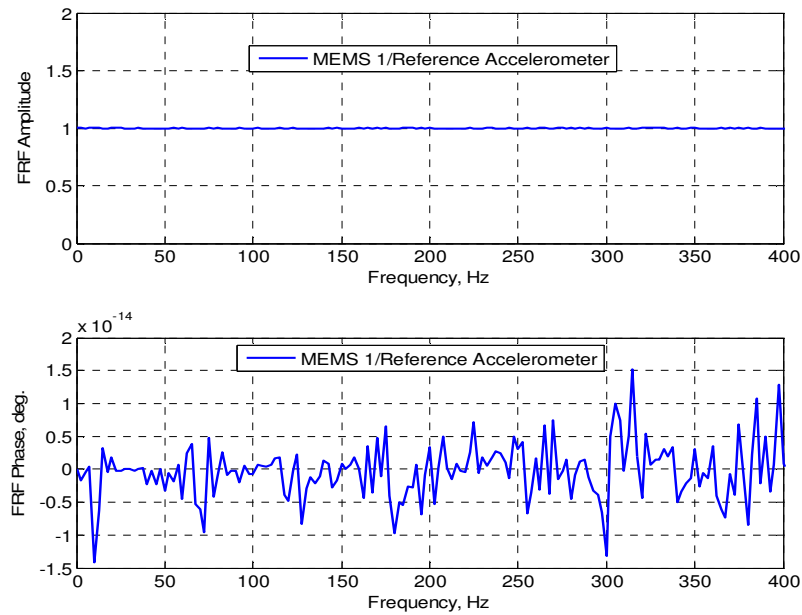


Figure 6.8 FRF plot between the MEMS 1 (after correction) and the reference accelerometer for the linear sweep-sine excitation

6.3.1.2 The Sinusoidal Signals

Number of test experiments was also conducted when the sine wave excitation at a number of frequencies was used to drive the shaker shown in Figure 6.1. The measured responses by both MEMS 1 accelerometer and reference accelerometer were collected at a sampling frequency of 10240 samples/s and stored for further signal processing. The correction procedure has then been applied to the measured responses by the MEMS 1 using the CF shown in Figure 6.5 to calculate the PSD and the FRF between the MEMS 1 and the reference accelerometer signals. The results were observed to be very encouraging. A few typical examples at 20Hz, 145Hz and 377Hz (before and after correction) are shown in Figures 6.9 to 6.14. As can be observed from these Figures, the amplitude spectra show

significant amplitude error and phase error up to 8 degrees when compared with the reference accelerometer before correction. However, when the correction method has been applied, insignificant error has been observed in the signals measured by the MEMS 1 accelerometer.

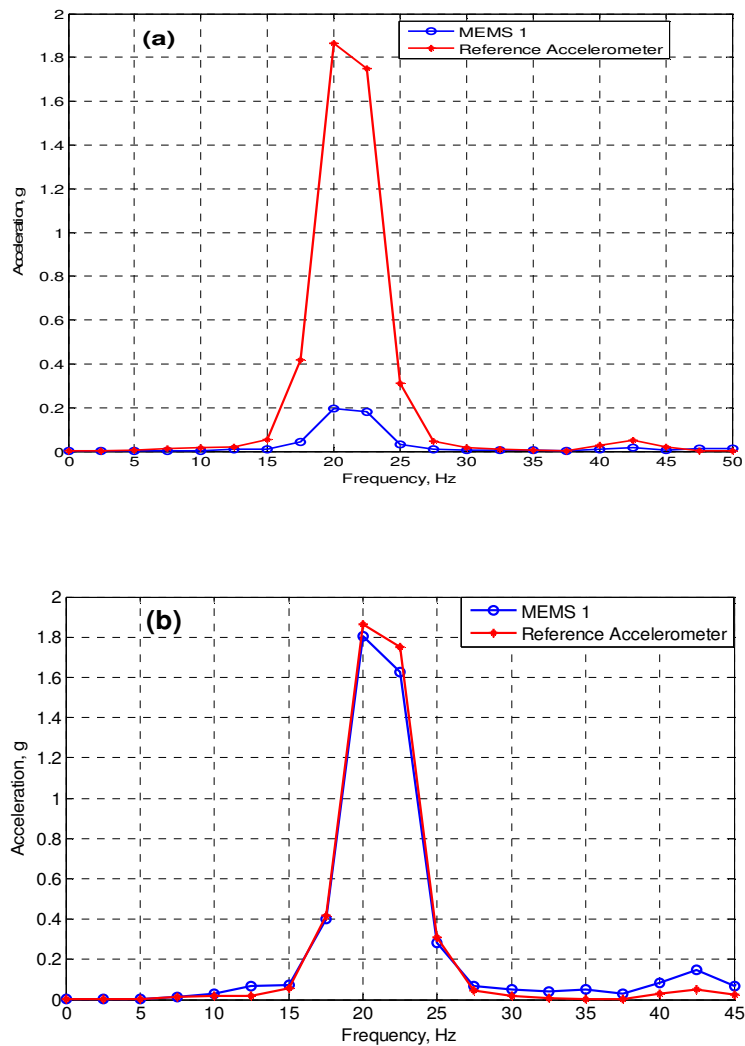


Figure 6.9 Comparison of the amplitude spectra of the MEMS 1 (line with circle) and the reference accelerometer (line with plus) for the sinusoidal signal at 20 Hz, (a) before correction, (b) after correction

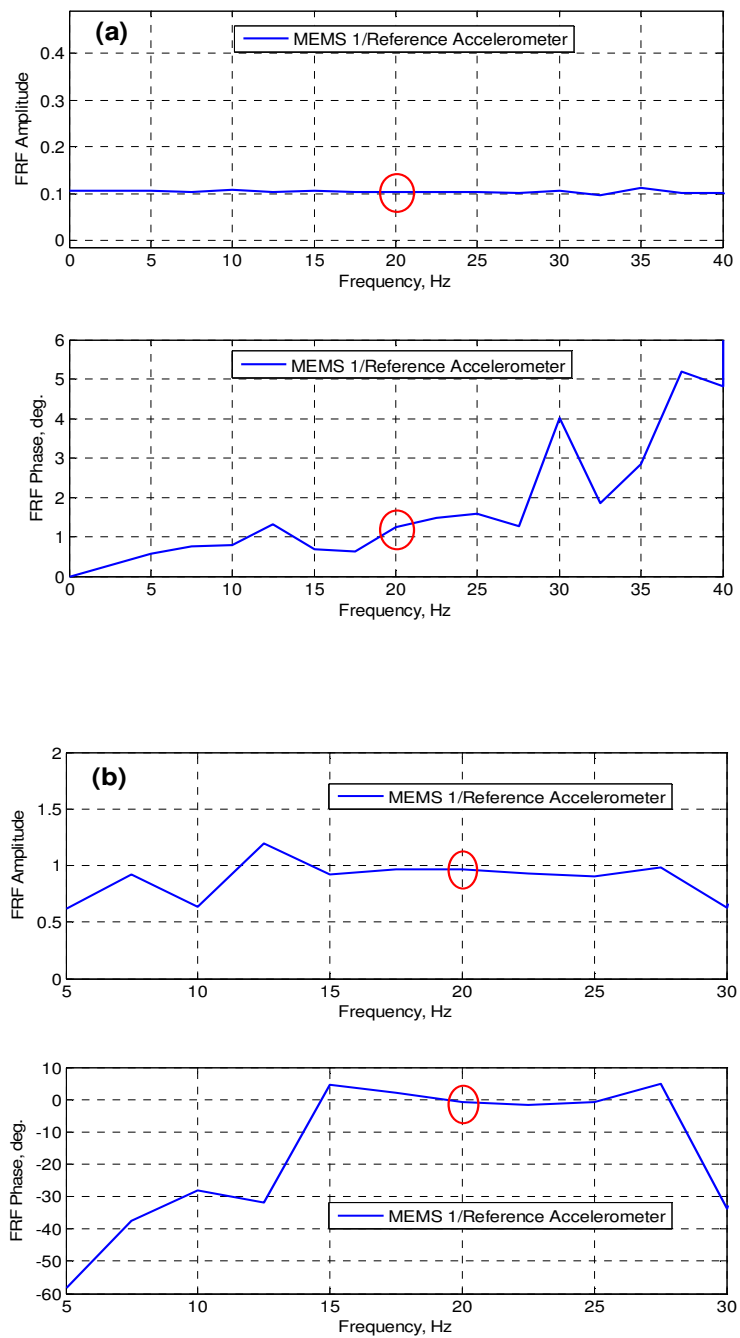


Figure 6.10 FRF plots the MEMS 1 with respect to the reference accelerometer for the sinusoidal signal at 20 Hz (indicated by circle), (a) before correction, (b) after correction

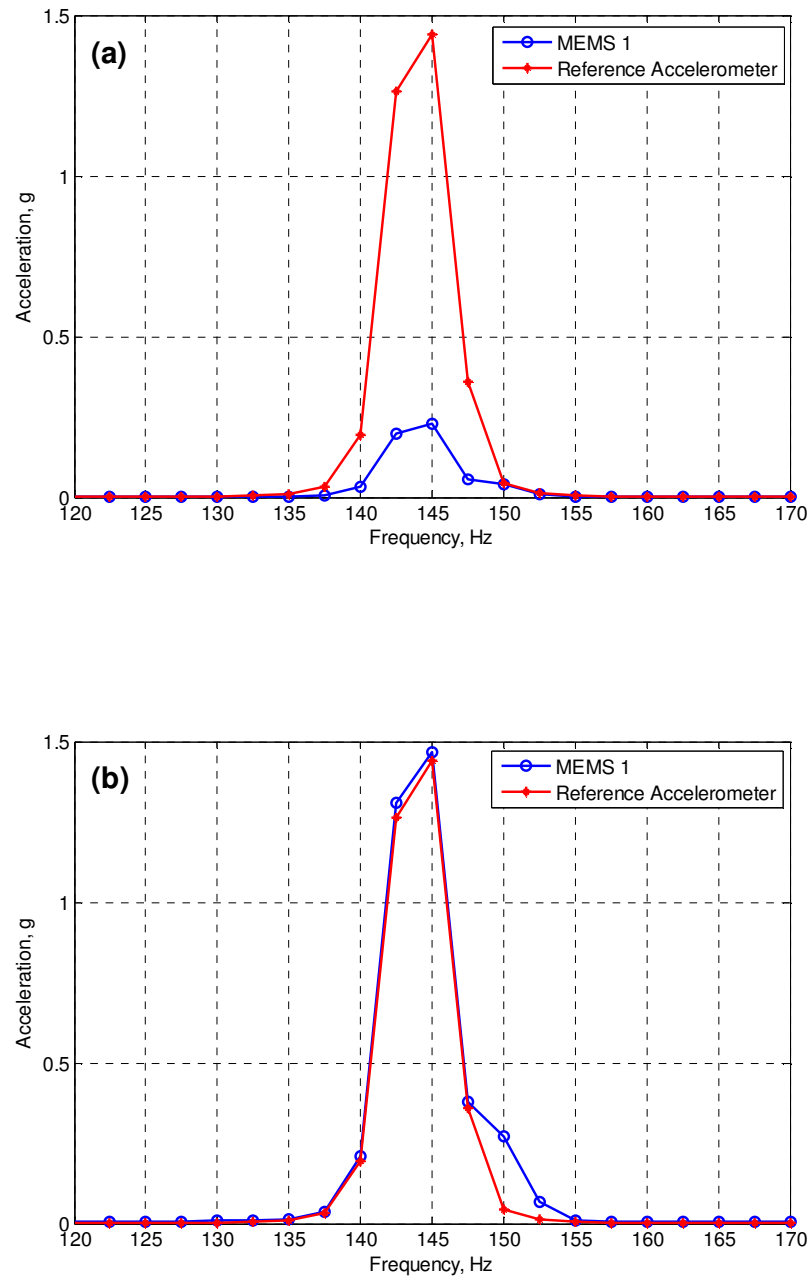


Figure 6.11 Comparison of the amplitude spectra of the MEMS 1 (line with circle) and the reference accelerometer (line with plus) for the sinusoidal signal at 145 Hz, (a) before correction, (b) after correction

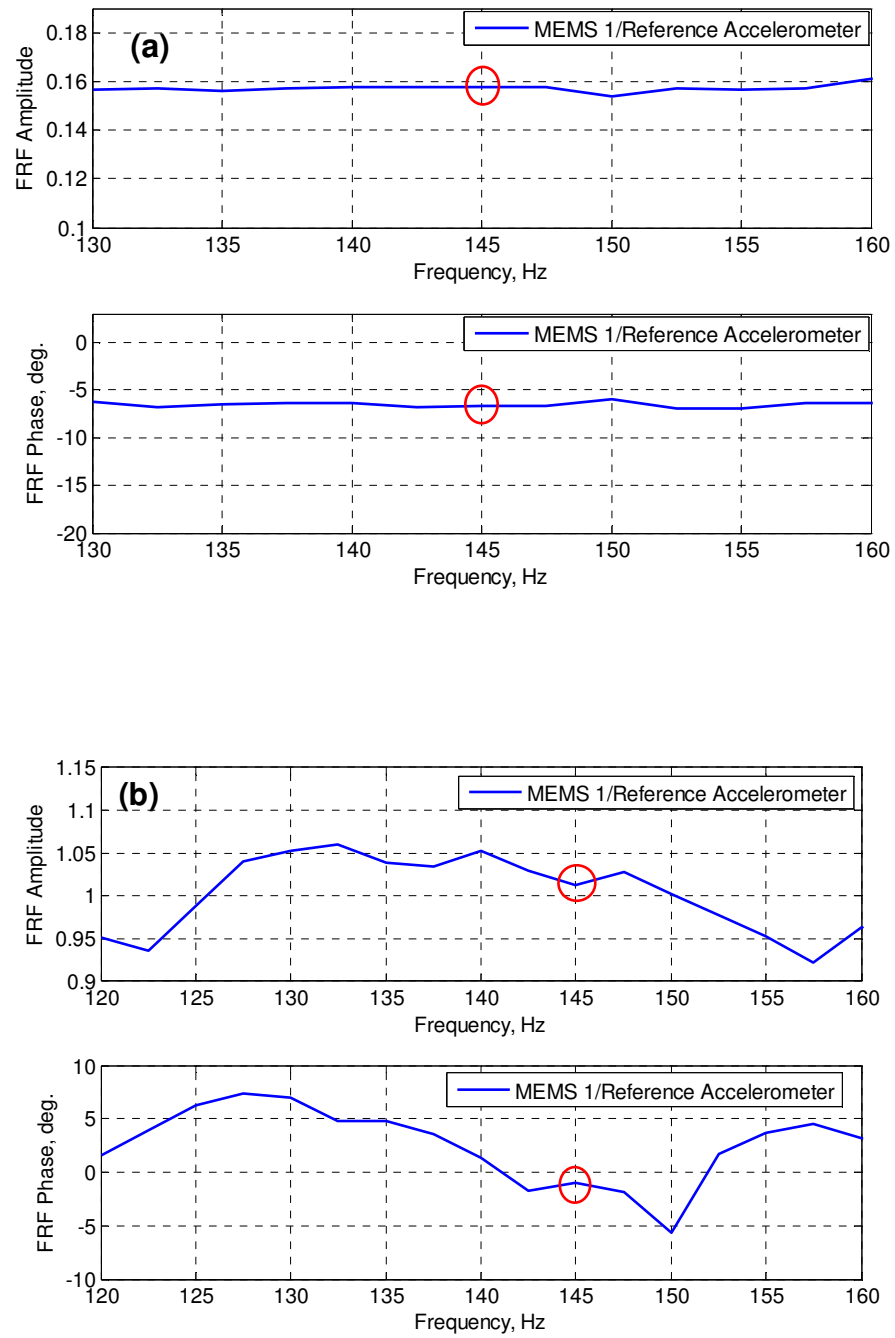


Figure 6.12 FRF plots the MEMS 1 with respect to the reference accelerometer for the sinusoidal signal at 145Hz (indicated by circle), (a) before correction, (b) after correction

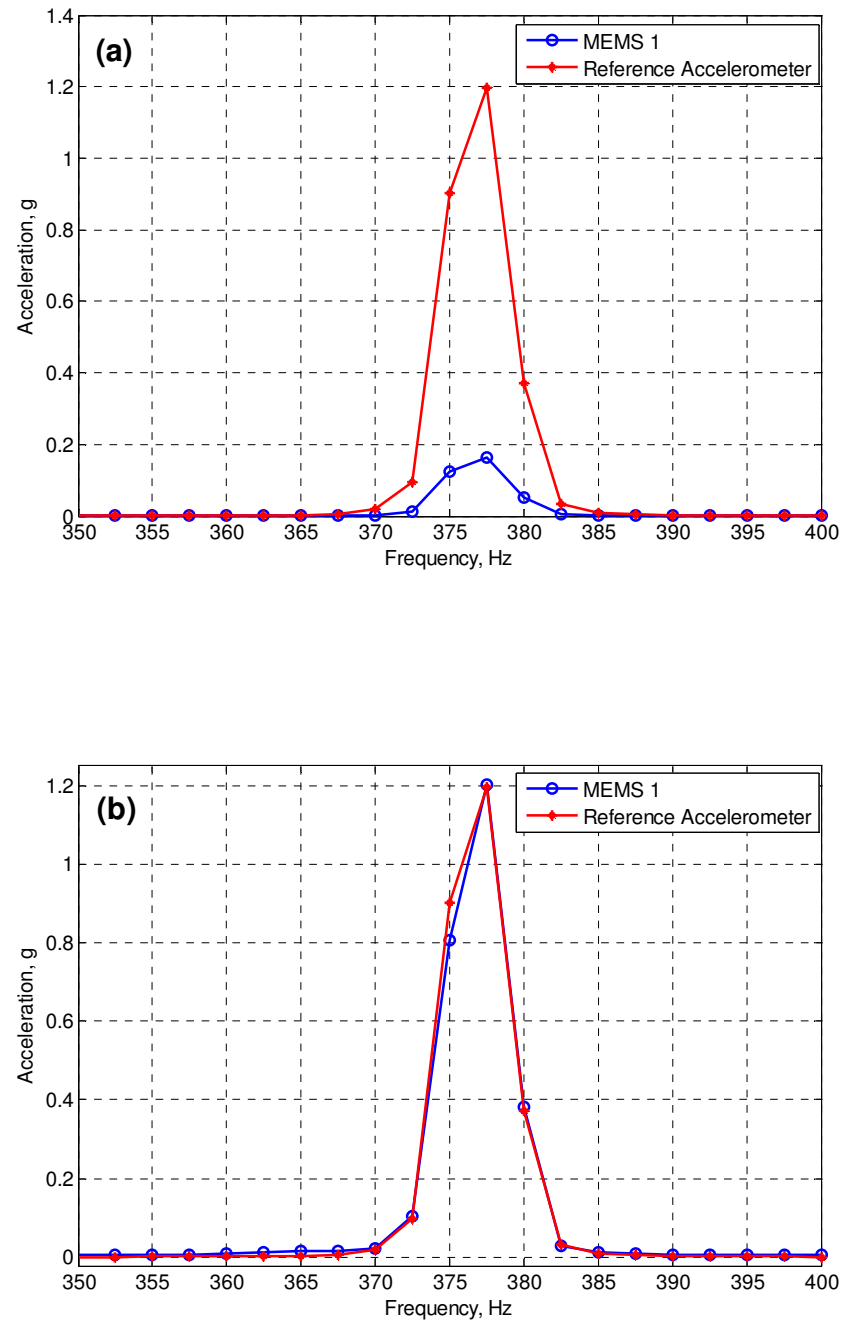


Figure 6.13 Comparison of the amplitude spectra of the MEMS 1 (line with circle) and the reference accelerometer (line with plus) for the sinusoidal signal at 377Hz, (a) before correction, (b) after correction

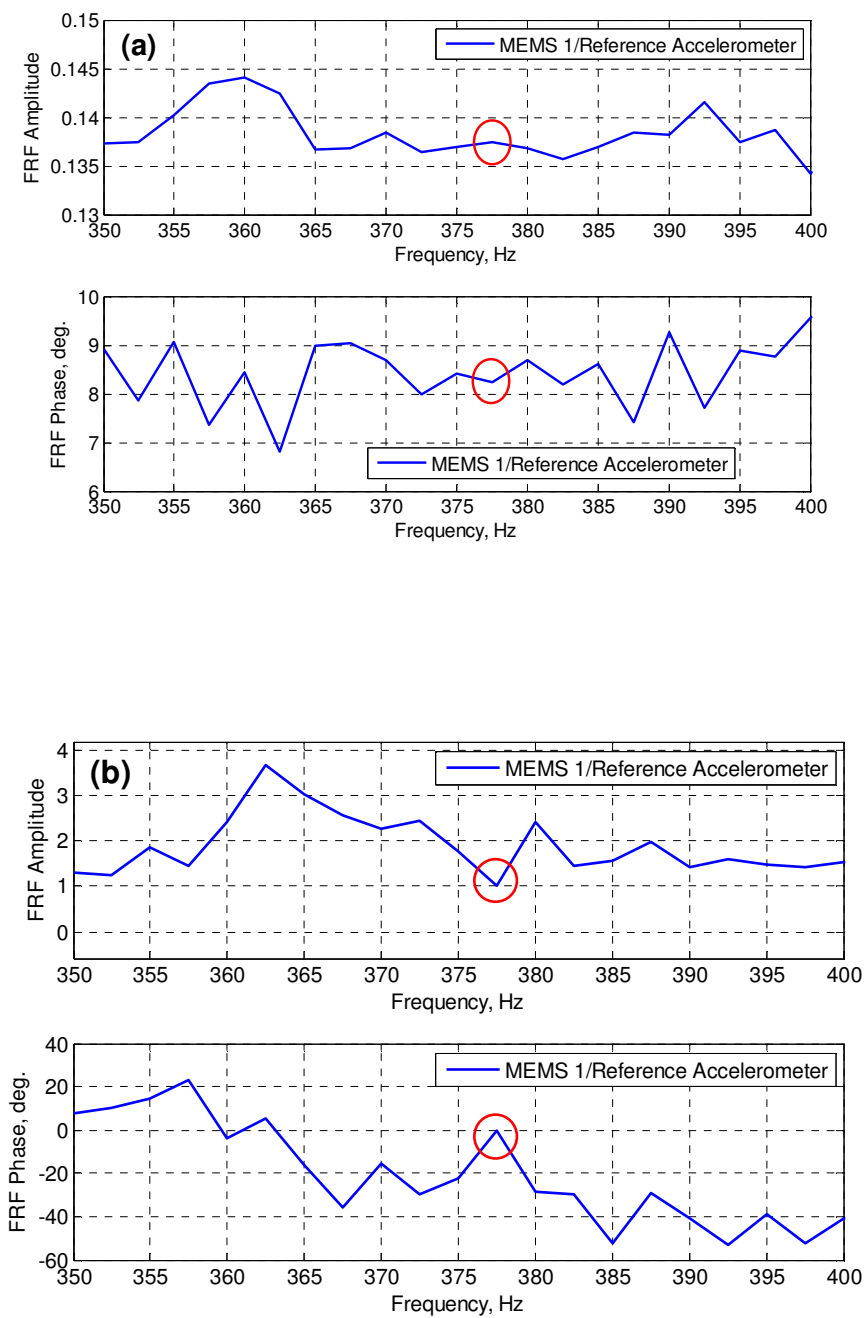


Figure 6.14 FRF plots the MEMS 1 with respect to the reference accelerometer for the sinusoidal signal at 377Hz (indicated by circle), (a) before correction, (b) after correction

6.3.2 Case II: MEMS 2 Accelerometer

Similar tests, both linear sweep-sine and sinusoidal, were conducted for the MEMS 2 accelerometer. The comparison of results between these tests were listed in Table 6.2 and also shown graphically in Figure 6.15. Here again, the results were observed to be consistent up to 420Hz, however the excitation level was less than 1.7g up to 800Hz as seen in Figure 6.16. Hence the FRF plot of the MEMS 2 (as output) and the reference accelerometer (as input) up to 400Hz was considered as the CF for the MEMS 2 accelerometer. As observed from Table 6.2 and Figure 6.17, the measured signals from the MEMS 2 accelerometer show significant error in both amplitude and phase, however these errors have been successfully reduced to negligible errors when the correction method discussed in Section 6.2 has been applied. Two typical examples for the sine wave excitation at 237.5Hz and 377Hz are shown in Figures 6.18 and 6.19 where large error in both amplitude and phase reduced significantly.

Table 6.2 Comparison of the FRF Amplitude and Phase for MEMS 2 due to sine and sweep-sine excitations with respect to the reference accelerometer

	Sweep-Sine 1KHz		Single Sine Excitation	
Frequency (Hz)	Amplitude (ratio)	Phase (degree)	Amplitude (ratio)	Phase (degree)
20	0.1	-105	0.09	-100
95	0.016	-31	0.004	-4
145	0.018	60	0.02	92

185	0.057	82	0.035	97
240	0.062	102	0.05	107
310	0.09	100	0.085	110
375	0.128	97	0.12	110
420	0.106	87	0.13	108
570	1.03	114	0.2	105
690	0.123	61	0.26	100
825	0.12	56	0.32	99

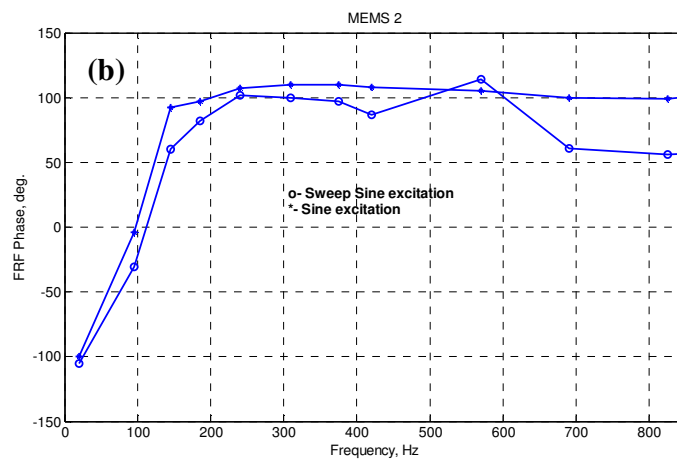
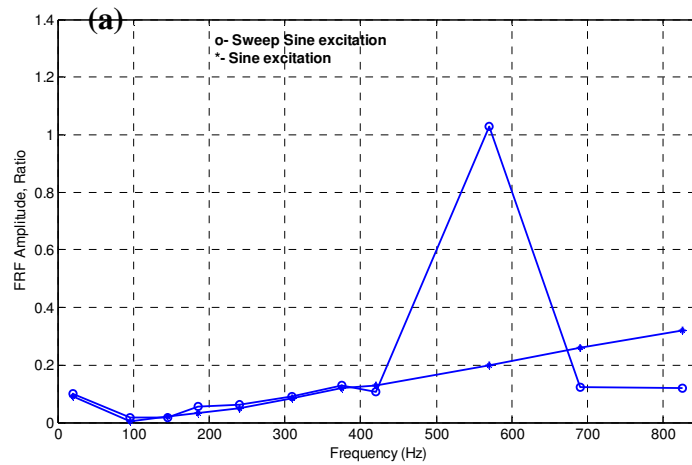


Figure 6.15 Comparison of the MEMS 2 responses due to Sine (line with dot) and Sweep-sine (line with circle) excitations, (a) FRF Amplitude, (b) FRF Phase

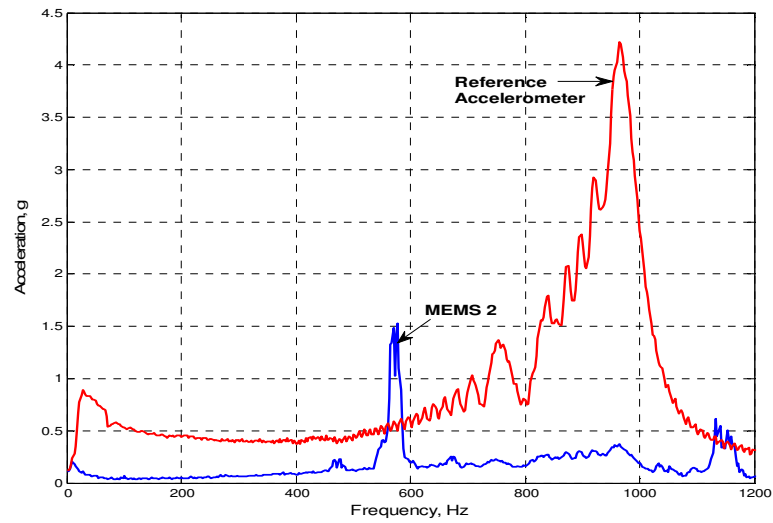


Figure 6.16 Amplitude spectra for the MEMS 2 and reference accelerometers for the linear sweep-sine excitation

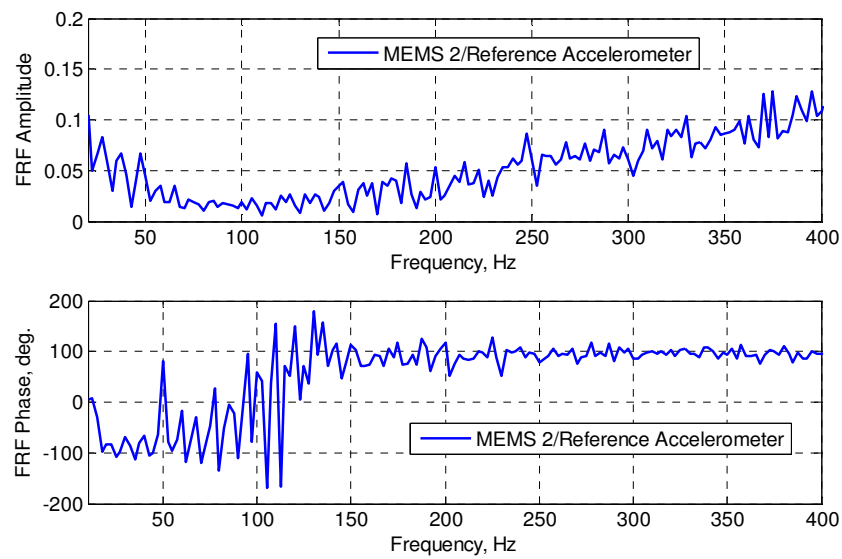


Figure 6.17 The CF in the frequency range (0-400 Hz) for the MEMS 2 accelerometer with respect to the reference accelerometer

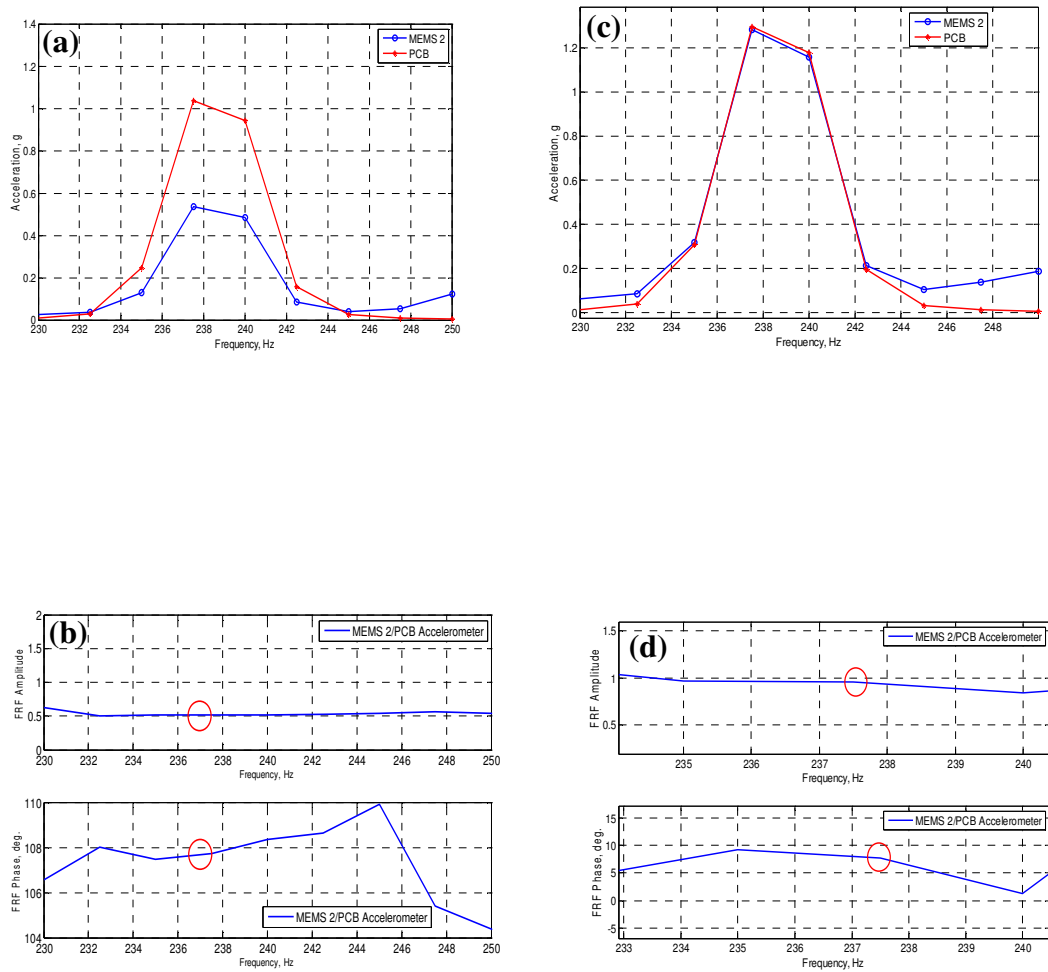


Figure 6.18 Comparison of the amplitude spectra and FRF of the MEMS 2 (line with circle) and the reference accelerometer (line with star) for the sinusoidal signal at 237.5 Hz, (a) & (b) before correction, (c) & (d) after correction

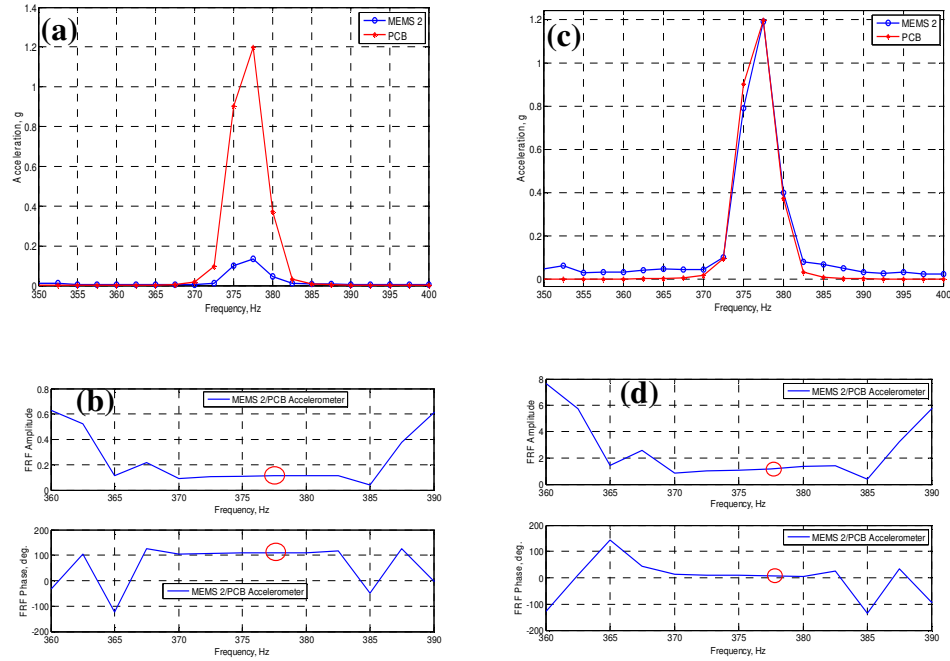


Figure 6.19 Comparison of the amplitude spectra and FRF of the MEMS 2 (line with circle) and the reference accelerometer (line with star) for the sinusoidal signal at 377Hz, (a) & (b) before correction, (c) & (d) after correction

6.4 Practical Application of the Correction Method

Since this method produced good results, it has been further tested on an experimental rig. The picture of the rig is shown in Figure 6.20. It consists of two steel shafts connected by a rigid coupling and supported through four ball bearings. The shaft lengths are 1m and 0.5m and the diameter is 20mm. The 1m shaft is connected to an electric motor through a flexible coupling. There are three balance disks made of steel with dimensions 125mm (OD) x 15mm (thickness), 2 disks on the long shaft and 1 disk on the short shaft.

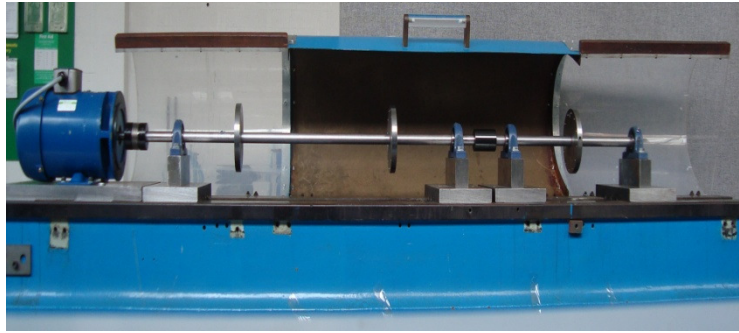


Figure 6.20 The experimental rig

The measurement has been carried out at the bearing-2 pedestal in the lateral direction when the shaft was running at 2400RPM (40Hz). Here a capacitive type MEMS accelerometer with the technical specifications, 167mV/g, frequency range 2 kHz and the acceleration range of $\pm 2g$ has been used. A conventional ICP type accelerometer (as reference) has also been mounted at the same location for comparison. Figure 6.21 shows the mounting of both accelerometers at the bearing-2 pedestal.

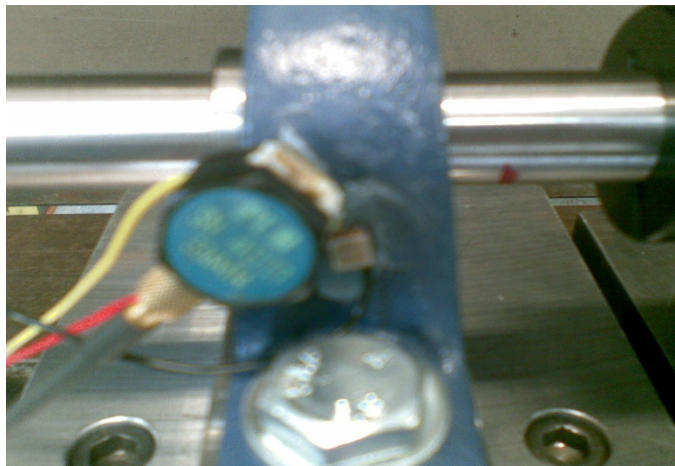


Figure 6.21 Mounting of the MEMS and the reference accelerometers at the bearing-2 of the rig

The amplitude spectra of the MEMS and the reference accelerometers, and their FRF plot are shown in Figures 6.22 and 6.23 which show significant deviation in both amplitude (0.1) and phase (-42.47 deg.) at the rotating frequency of 40Hz of the rig. Here again, the CF for this MEMS accelerometer has been generated from the test setup facility shown in Figure 6.1 and then correction in the measured MEMS signals has been applied. The amplitude spectrum and the FRF plot with respect to the conventional ICP accelerometer after correction are shown in Figures 6.24 and 6.25 respectively. Now it can be seen from both figures that error at 40Hz reduced significantly to the negligible level. Hence, the proposed method seems to be useful.

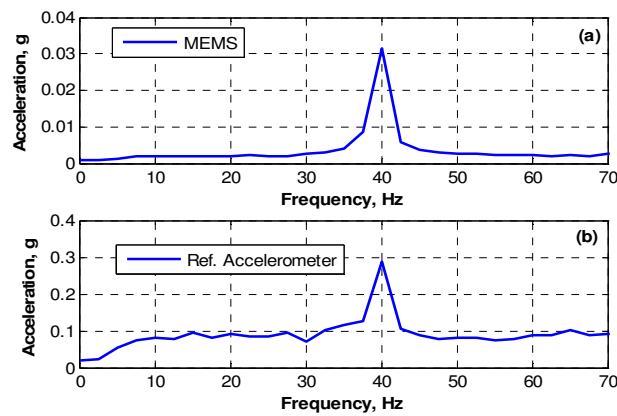


Figure 6.22 Typical comparison of the amplitude spectrum for the MEMS accelerometer (a) before correction with the reference accelerometer (b) for the rig

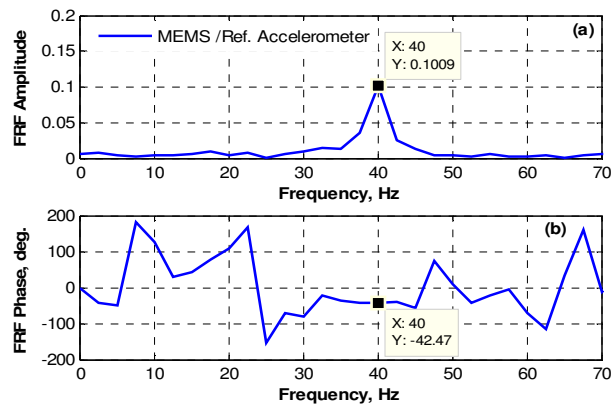


Figure 6.23 FRF plot of the MEMS accelerometer before correction) with respect to the reference accelerometer, (a) Amplitude, (b) Phase

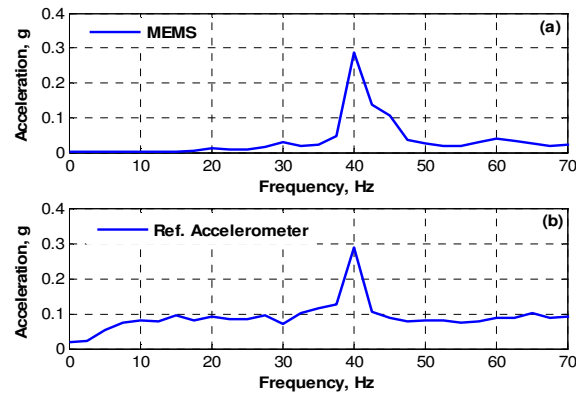


Figure 6.24 Typical comparison of the amplitude spectrum for the MEMS accelerometer (a) after correction with reference accelerometer (b) for the rig

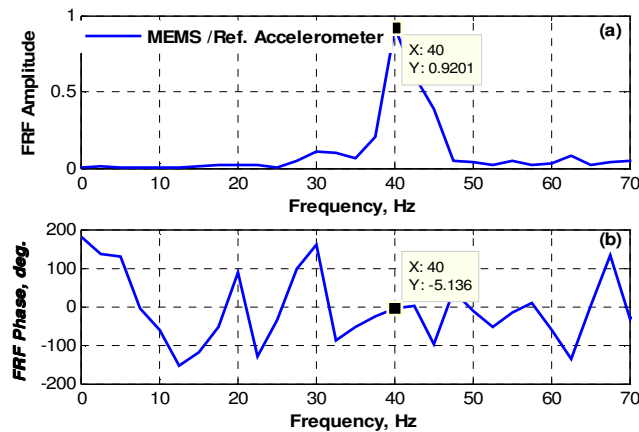


Figure 6.25 FRF plot of the MEMS accelerometer (after correction) with respect to the reference accelerometer, (a) Amplitude, (b) Phase

6.5 Enhancing the Frequency Range of Measurement for an Accelerometer

Multiple data collection points are generally required in most of the condition monitoring systems and for vibration based diagnosis purpose for machines and structures. The different field applications demand the proper selection of accelerometers, for example, the frequency range of measurement. Let's say, there is a requirement of simultaneous measurement at 10 locations and the

frequency range of interest is up to 6 kHz or more, but the available accelerometers can measure up to say, 4 kHz within the error of 0.6 dB as shown in Figure 6.26. This simply indicates that either a compromised measurements can be taken with the available accelerometers knowing that the measured signals will show error in phase and amplitude beyond 4 kHz or other alternative is to buy accelerometers meeting the requirements. The later option is definitely going to be costly. Hence, a viable approach has been suggested to enhance the working frequency range of measurement of an accelerometer depending upon the accelerometer resonance frequency [111]. For example, the frequency range can be enhanced to 8 kHz for a typical accelerometer whose frequency response characteristic curves shown in Figure 6.26 for two different mounting resonances. Here again, a CF up to 8 kHz for the accelerometer can be generated by conducting experiment in the lab with a reference accelerometer and then this CF can be used to correct the measured signals up to 8 kHz as per method suggested in section 6.2.2.

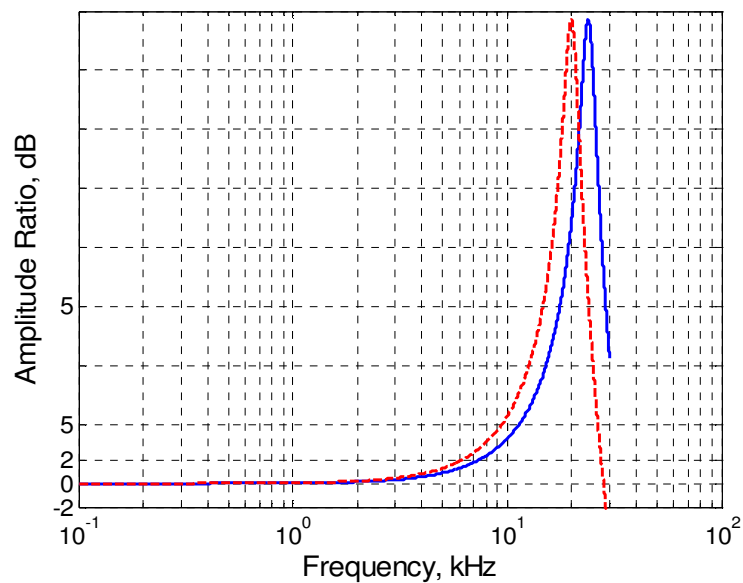


Figure 6.26 Characteristic response curves of a typical accelerometer for two different mounting resonance frequencies

6.6 Conclusion

Repeatability between the single sinusoidal response and the sweep-sine response measurement by the MEMS accelerometers was observed, but the measured amplitude and phase deviates significantly when compared with well known Accelerometer. Hence, a simple method for correcting both amplitude and phase response of any accelerometer in frequency domain has been adopted which has been discussed in the chapter. The method is based on the generation of a characteristic function (CF) using well known reference accelerometer in Laboratory test which needs to be preserved so that the measured signals by MEMS Accelerometer can be corrected/calibrated in the frequency domain using this CF. The usefulness of the present study has been successfully brought out through two typical case studies on two different MEMS accelerometers. However, the poor performance of the MEMS accelerometers, mainly related to the random vibration measurements needs further investigation. However, consistent performance has been observed for the MEMS for sinusoidal inputs, hence these accelerometers can be used confidently with the correction/calibration method in the condition monitoring of rotating machines where vibrations are generally related to harmonics and sub-harmonics of the rotating speed.

CHAPTER 7

ACCELEROMETER MODELLING

Reformatted version of papers:

1. MODAL ANALYSIS OF MEMS ACCELEROMETER

Authors:

Abdellatef Badri and Jyoti K. Sinha

Paper published in:

17th International Congress on Sound and Vibration (ICSV17), Cairo, Egypt, 18-22 July 2010.

2. Dynamics of MEMS Accelerometer and Possible Design Modification for Future Improvement

Authors:

Abdellatef Badri, Jyoti K. Sinha, and A. Albarbar

Paper submitted to:

Measurement Journal

Keywords: MEMS Accelerometer, Vibration Measurement, Finite Element (FE) Analysis, Modal Analysis, MEMS Accelerometer Design

Abstract

The use of the MEMS (Micro-Electro Mechanical System) concept for manufacturing accelerometers is relatively new technology. However earlier studies suggest that the measured signals by the MEMS accelerometers generally show deviation when

compared with the conventional accelerometer. Hence, a simple Finite Element (FE) model of a MEMS accelerometer has been constructed and the modal analysis has been carried out. The cantilever beam mode of finger used in MEMS capacitive type accelerometers observed in the modal analysis highlights the possibility of errors in measurement. Hence, few modifications in finger design have been suggested to improve the performance of the MEMS accelerometer.

7.1 Introduction

The MEMS (Micro-Electro Mechanical System) accelerometers have been receiving attention in the recent years due to their low cost and small size [30, 37]. The micromachined accelerometer was initially introduced in 1988 by NovaSensor which was based on piezoresistive sensing mechanism [30]. The Wheatstone bridge principle was used to measure the acceleration of the vibrating objects [30, 56, 107]. Thereafter the concept of capacitive sensing has also been introduced in the MEMS accelerometers [54, 57, 73, 108-110]. A typical capacitive MEMS accelerometer is composed of capacitors formed between the proof mass and fixed conductive electrodes. The proof mass is free to move in the vibration direction. This mass movement creates unbalance in the differential capacitor resulting in an output which is proportional to acceleration of the vibrating object. The capacitance change due to acceleration is then converted into voltage with appropriate signal conditioning through on chip circuitry [54, 57, 73, 108-110]. Sections 2 and 3 briefly discussed the principle of a conventional piezoelectric accelerometer and the capacitive type MEMS accelerometer.

However, the performance of such accelerometers has not been rigorously

tested to enhance the confidence level for the industrial applications. A few earlier researches compared the performance of MEMS and conventional accelerometers. It has been observed that the measured vibration signals by the MEMS accelerometer often show a difference from the signals measured by the well-accepted conventional accelerometer [21, 23, 111]. Hence the present attempt is to understand the dynamics of the present design used for the MEMS accelerometer so that appropriate modification, either in the mechanical design or in the associated electronic circuitry, can be proposed to improve the performance of the MEMS accelerometer in future. In the present study the dynamic behaviour of the sensing element of capacitive type MEMS accelerometer has been studied. Hence, a simple Finite Element (FE) model of a MEMS accelerometer has been constructed and the modal analysis has been carried out. The cantilever beam mode of finger used in MEMS capacitive type accelerometers observed in the modal analysis highlights the possibility of errors in measurement. Hence, a few modifications in finger design have been suggested to improve the performance of the MEMS accelerometer.

7.2 A conventional Piezoelectric Accelerometer

A typical design of a conventional piezoelectric accelerometer is shown in Figure 7.1. It consists of a small mass, a spring made of piezoelectric crystal and a damping of around 0.7. For this configuration, if the natural frequency of the accelerometer is f_n then the linearly frequency range of measurement is approximately 20% of the natural frequency, f_n .

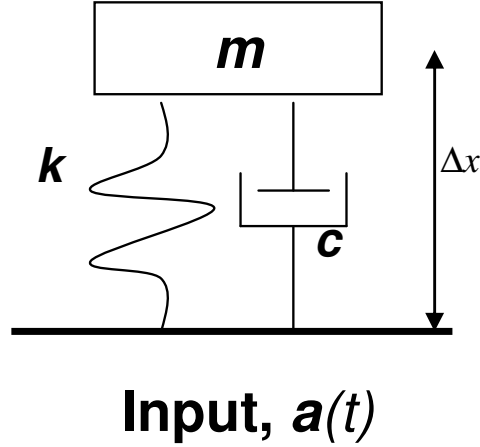


Figure 7.1 The conventional piezoelectric accelerometer

The input acceleration of a vibrating object causes the vibration of the accelerometer mass, m which results in the relative motion, $\Delta x(t)$, between the mass and the object in the piezoelectric spring generates the proportional electric charge, $\Delta Q(t)$. Mathematically it can be written as:

$$\Delta x(t) \approx \frac{a(t)}{\omega_n^2} \propto \Delta Q(t) \quad (7.1)$$

where $\omega_n = 2\pi f_n$. Hence the charge, $\Delta Q(t)$, is proportional to the acceleration of the vibrating object which is then converted into the voltage as the output for the accelerometer.

7.3 A Capacitive Type MEMS Accelerometer

The working principle of a capacitive type MEMS accelerometer is also same as the

conventional piezoelectric accelerometer. However the output of the MEMS accelerometer uses the change in the capacitance and not to the charge. A typical design configuration of a MEMS accelerometer is shown in Figure 7.2 [112].

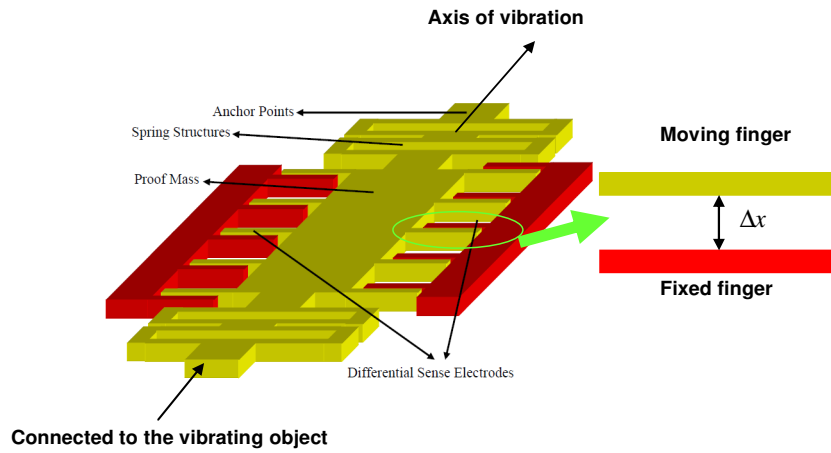


Figure 7.2 Typical constructional details of a capacitive type MEMS accelerometer [112]

The MEMS accelerometer also consists of a spring and a mass both made of a material commonly poly-silicon. However, the concept of converting the mechanical vibration into electrical signal is different. Here numbers of fingers are attached to the mass which are generally called as the “Moving fingers” and number of fingers attached to the fixed frame of the accelerometer, called “Fixed fingers”. The arrangement is such that a pair of the fixed and moving fingers constitutes a parallel capacitor. Here again, the input acceleration of a vibrating object causes the vibration of the accelerometer mass, m which results in the relative motion, $\Delta x(t)$, between the moving and fixed fingers which generates a proportional change in the capacitance, $\Delta C(t)$. Mathematically it can be written as:

$$\Delta x(t) \approx \frac{a(t)}{\omega_n^2} \propto \Delta C(t) \quad (7.2)$$

where the change in the capacitance, $\Delta C(t) = C_0 \cdot \left(\frac{\Delta x(t)}{d_0}\right)$ [10]. The change in capacitance $\Delta C(t)$ is proportional to the acceleration of the vibrating object which is then converted into the voltage as the output for the accelerometer. Often a number of the fixed and moving fingers are used to strengthen the electrical output, which means the sensitivity of the accelerometer.

7.4 Earlier Studies on MEMS Accelerometers Performance

Performance tests for several MEMS accelerometers have been carried out using test set-up shown in Figure 6.1 [23, 24, 113]. The test setup consists of a small shaker (M/s GW make) together with a shaker power amplifier, signal generator and a PC based data acquisition for data collection and storage for further signal processing. In every test, the MEMS accelerometer (Test accelerometer) was attached back to back with an Integrated Circuit Piezoelectric (ICP) conventional accelerometer (Reference accelerometer) on the armature of the shaker.

Responses of MEMS accelerometers showed significant deviation in both amplitude and phase compared to the responses of the reference accelerometer and this deviation is changing with the frequency. A few typical examples for measured responses of MEMS accelerometers compared with the reference accelerometer are shown in Figures 4.8, 5.2, and 4.19 for the impulsive, random and sinusoidal excitations respectively.

More details can be found in [23, 24, 113]. A typical example on a rotating rig in Figure 6.20 also shows deviation in the MEMS measurement compared to the measurement by the conventional accelerometer which is shown in Figure 6.22 and Figure 6.23.

It has been observed that the frequency contents in the spectra of the MEMS accelerometers are same as the conventional reference accelerometer; however the amplitude and phase at each frequency significantly different when compared with the conventional reference Accelerometer. A couple of methods have been suggested earlier [24, 113] to improve the measured signals of the MEMS accelerometers. However it is always good to understand the dynamics of the MEMS accelerometer to know the reason for such error so that the possible improvement in the design can be made.

7.5 Limitations in the existing design of MEMS accelerometer

It is important to understand the present design limitations in the MEMS accelerometer, hence the effect of present mechanical design and the conversion into the electrical signal has been studies separately and the results of these studies are discussed here.

7.5.1 3-D Finite Element Model

The typical design configuration shown in Figure 7.2 has been modelled in 3D, but only two moving fingers of 154 μm length and 4 μm width have been used. Three fixed fingers of the same moving fingers dimensions are attached to the mass which is 28 μm

of length and $152\text{ }\mu\text{m}$ width. The gap between each moving finger and fixed finger is $4\text{ }\mu\text{m}$. The mass is fixed to the frame through two folded beams one on the top and the other on the bottom. The element type used in this model is Continue 3-Dimensions 4 node (C3D4), the material properties of polysilicon used are, density $\rho = 2.3\text{ g/cm}^3$, Poisson's ratio $\mu = 0.22$, and Young's modulus $E = 170\text{ GPa}$. The accelerometer model is shown in Figure 7.3 and the 1st mode shape in Figure 7.4. The modal analyses were carried out with the accelerometer base fixed. The mode shape shows that the moving fingers act as a beam resulting in the distance between the moving and fixed finger become nonlinear. As can be seen in Figure 7.5 where the mode shape is zoomed, the gap d_1 is not equal to the gap d_2 . This finger motion makes the formed capacitors between moving and fixed fingers non parallel plate capacitors. The non parallel plates have an effect on capacitance, sensitivity, electrostatic force, electrostatic spring constant, and the overall accelerometer operation [114, 115].

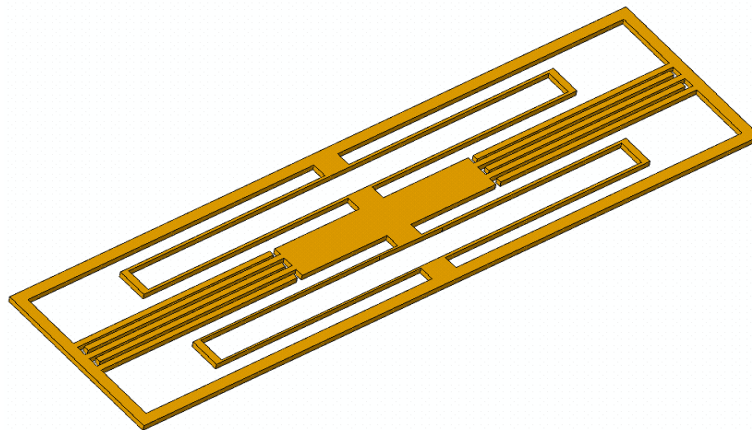


Figure 7.3 A 3D model for a typical MEMS accelerometer

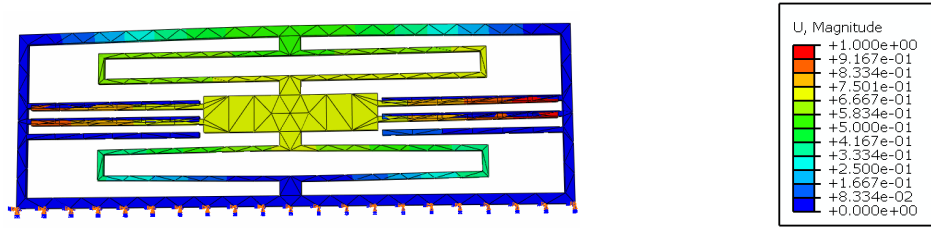


Figure 7.4 The 1st mode shape in vertical direction

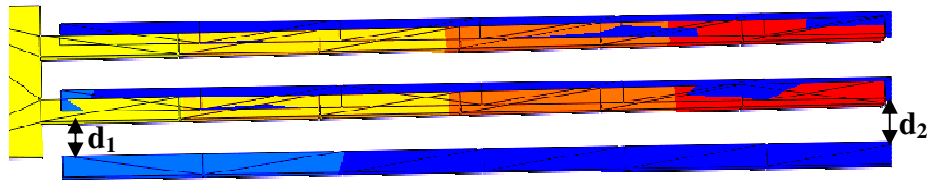


Figure 7.5 zoomed view

7.5.2 Conversion of the Capacitance into Voltage

Several types of detection circuits such as the diode-bridge, switch capacitor and synchronized detection circuit have been developed to detect the capacitance changes in capacitive type sensors and convert it into voltage signal [116]. However, the synchronized detection circuit is the most common concept which is used in capacitive MEMS accelerometers. In this circuit, amplitude modulation is used, where a carrier of high frequency is modulated by the change in capacitance and then synchronous demodulator and a low pass filter are used to extract the voltage signal which is proportional to the applied acceleration.

7.5.2.1 Modulation and Demodulation

Let $x_c(t)$ be the carrier signal generated by local oscillator and $m(t)$, the modulating signal. Linear amplitude modulation is achieved by multiplying these two signals to generate amplitude modulated signal $s(t)$. In synchronous demodulation, $s(t)$ is multiplied by the same signal which is used as the carrier signal assuming that they are synchronised in both amplitude and phase. Figure 7.6 shows a simplified block diagram for synchronised detection circuit.

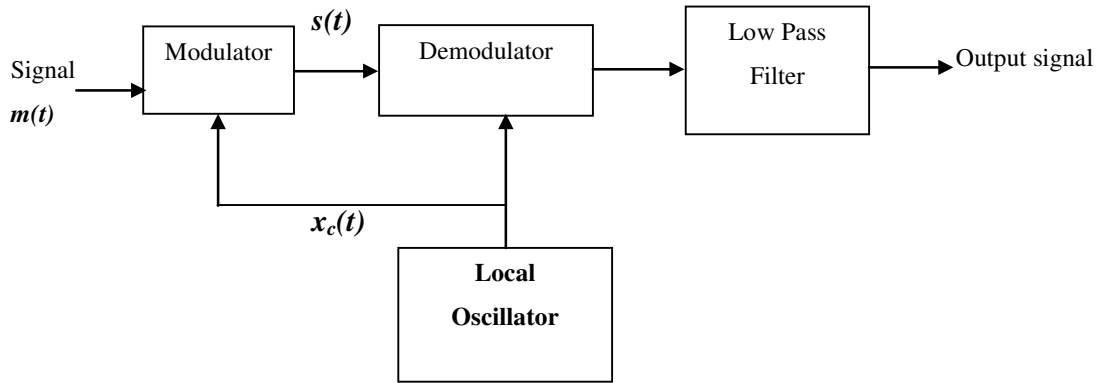


Figure 7.6 Block diagram for synchronised detection circuit

However, it is usually found that the oscillator output has a phase error ϕ which varies randomly with time [117]. Therefore, the output of the demodulator, after low pass filtering, can be written as:

$$v_o(t) = \frac{1}{2} A_{osc} A_c \cos(\phi) m(t) \quad (7.3)$$

where, A_c and A_{osc} are the amplitudes of the carrier and oscillator signals

respectively. The phase error ϕ in the local oscillator causes the demodulator output to vary with time by a factor equal to $\cos(\phi)$. In addition, the dc offset in analogue multiplier can decrease the multiplier's gain, degrade and increase the nonlinearity and distortion introduced by the multiplier in the modulation or demodulation process [118]. In general, the amplitude modulation/demodulation process causes amplitude and phase shift in the modulating signal. This has been examined by experimental work carried out on demodulation of amplitude modulated signal using envelope detector method.

7.5.2.2 Modulation and Demodulation Experiment

Modulation and demodulation experiment has been carried out using test facilities shown in Figure 7.7. A carrier signal of 100 kHz has been modulated by low frequency signal (modulating signal) at different frequencies from 100 to 2000Hz. The amplitude and phase for FRF have been computed between the original signal (before modulation) and the output signal (after demodulation). The values of amplitude and phase for the FRF at each frequency are listed in Table 7.1, and their plots are shown in Figure 7.8.

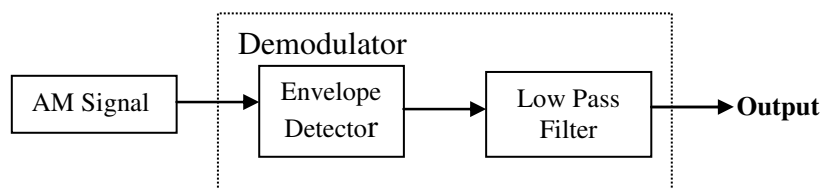
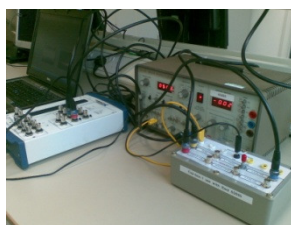


Figure 7.7 Modulation and demodulation experiment facility

Table 7.1 Amplitude and phase values for the FRF

Frequency	Amplitude (ratio)	Phase (degree)
100Hz	5.825	1.015
300Hz	6.087	2.662
500Hz	6.147	3.983
1000Hz	6.284	7.385
1250Hz	6.551	9.14
1500Hz	6.558	10.95
2000Hz	6.911	13.67

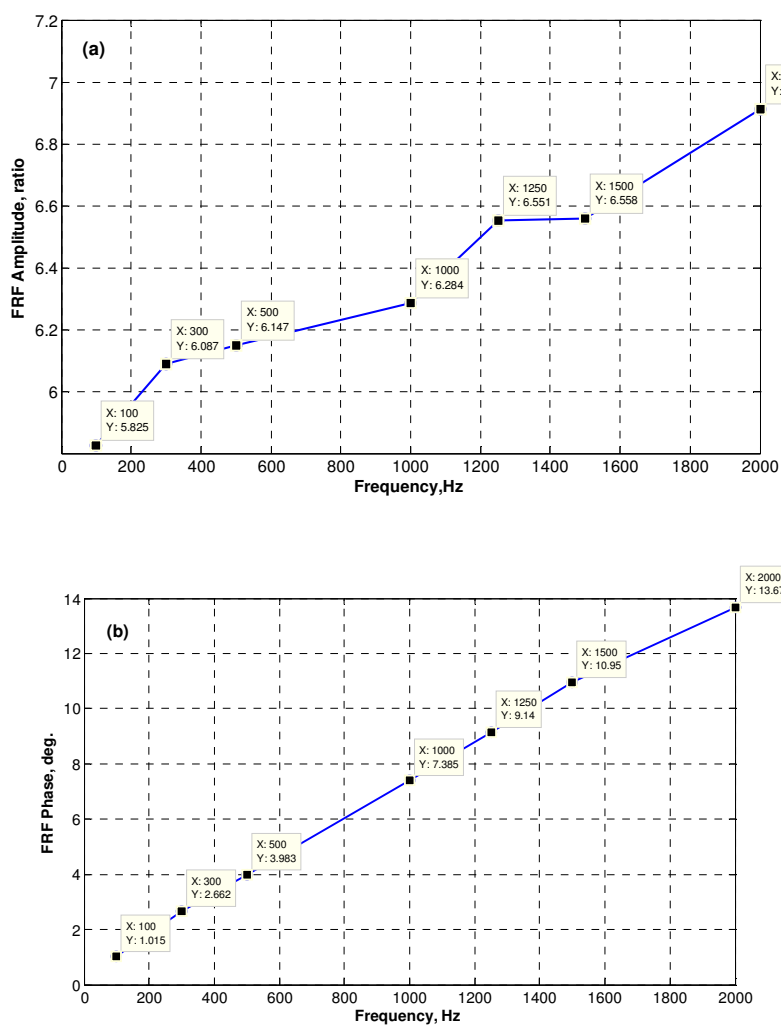


Figure 7.8 Amplitude of FRF (a), Phase of FRF (b)

7.6 Possible Improvement in Mechanical Design

Having known that the fixed fingers have the rigid body motion, hence a simple model of a MEMS accelerometer has been considered here. A single spring equivalent to the upper and lower springs shown in Figure 7.2 has been assumed and just two moving fingers (one on each side of the mass) were used instead of number of fingers. The simplified model is shown in Figure 7.9. Table 7.2 lists the physical dimensions and material properties of the model parameters which are partially taken from [119].

Table 7.2 Physical dimensions and material properties of the MEMS accelerometer

Model parameters	Dimensions
Mass (m_p)	0.42 ng
Movable finger width (W_f)	4 μm
Movable finger length (L_f)	160 μm
Movable finger thickness (t)	4 μm
Equivalent spring stiffness k	1.874 N/m
Young's modulus of poly-Si	$1.70 \times 10^{11} \text{ Pa}$
Density of poly-Si	$2.33 \times 10^3 \text{ kg / m}^3$

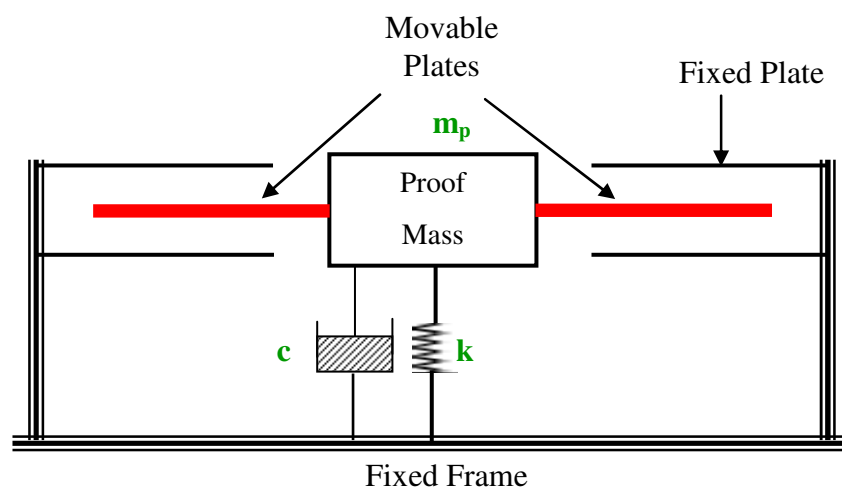


Figure 7.9 Simple model

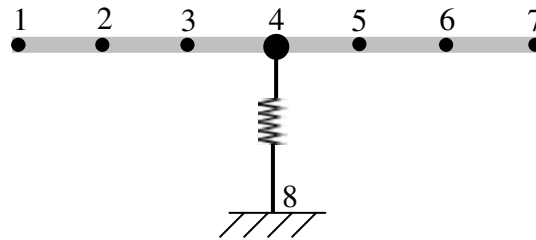


Figure 7.10 FE Model

The Finite Element (FE) modelling approach has been used to model the mechanical parts of the accelerometer. The finger has been modelled like beam using a 2-node beam element divided into 6 elements; the proof mass and the equivalent linear spring stiffness have been added at node-4 and node-8 assumed to be fixed. The FE model is shown in Figure 7.10. The modal analysis of the FE model has been carried out to find out the natural frequencies and mode shapes. Figure 7.11 shows the first two mode shapes for this model. The 1st mode natural frequency calculated at 10.631 kHz can be considered as the natural frequency of the MEMS accelerometer; hence, the working range for this accelerometer should be up to 2 kHz (often 1/5th of the natural frequency).

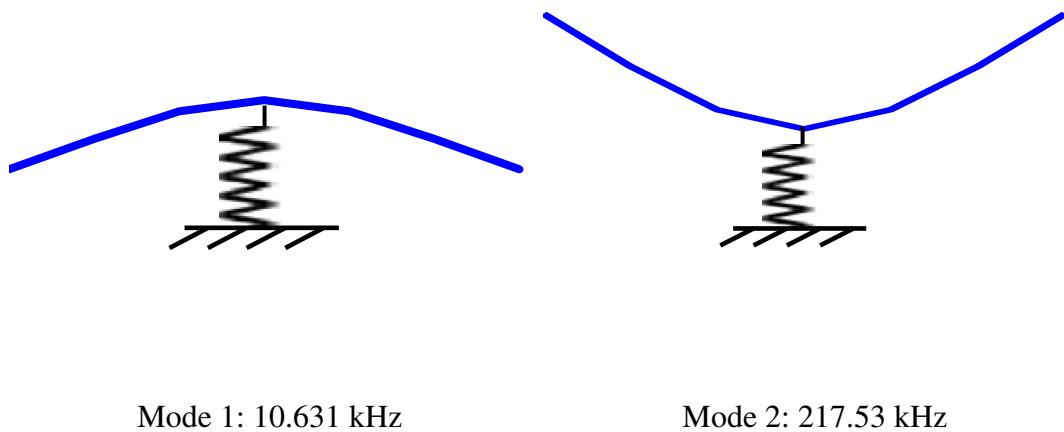


Figure 7.11 Mode shapes

As can be seen, the fingers behave as the cantilever beam at mode 1 which may leads to

non-parallel-plates capacitor. Hence, it can be suspected as the reason of observed measurement errors. Therefore, modification to the original finger design has been carried out using trapezoidal shape of the fingers to achieve rigid body motion [120]. The modified finger shape is shown in Figure 7.12. Four different dimensions have been used for the shape thicknesses as listed in Table 7.3.

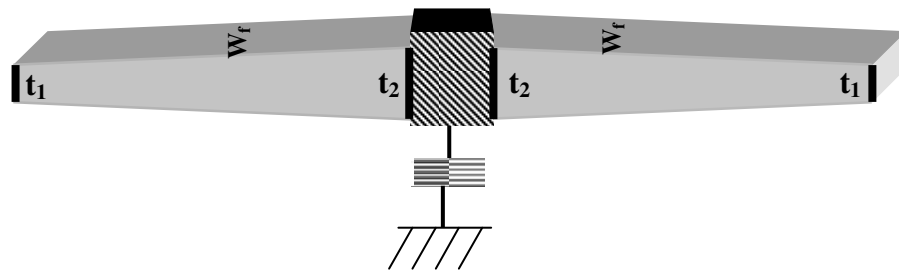


Figure 7.12 Modified design

Table 7.3 Dimensions of modified designs and expected improvement

	t_1 (μm)	t_2 (μm)	Expected improvement %
Original	4	4	
Modification 1	3	5	28.17
Modification 2	2	6	54.93
Modification 3	1	7	66.76
Modification 4	0	8	67.32

The modal analysis of the FE model for the modified finger design has been carried out. The natural frequencies of each mode for the modified designs are listed in Table 7.4. As can be seen from Table 7.4, these modifications in finger design have no affect on the natural frequency of the 1st mode. However, natural frequencies for modes 2

and 3 have been changed due to these modifications.

Table 7.4 Natural frequencies for mode shapes of modified designs

	Natural frequencies, kHz				
Mode	Original	Modification 1	Modification 2	Modification 3	Modification 4
1	10.631	10.631	10.631	10.631	10.631
2	217.53	279.12	346.75	416.83	455.28

The 1st mode shapes for the modified finger designs compared with 1st mode shape for the original design are shown in Figure 7.13. Modification 4 showed approximately a rigid body motion as its mode shape show much small deflection compared with the original finger design and other modified finger designs. The expected improvement in the MEMS accelerometer due to these modifications when compared with the original MEMS accelerometer design has been quantified as:

$$Improvement = \frac{\Delta\phi_o - \Delta\phi_M}{\Delta\phi_o} \times 100\% \quad (7.4)$$

where, $\Delta\phi_o$ is the difference of the mode shape between the centre and the finger tip at mode 1 for the original finger design and similarly $\Delta\phi_M$ for the modified finger design. The calculated ‘*Improvement*’ for the different modifications proposed in Table 7.3 shows that the Modification 4 provides 67% improvement for the present case. An

optimised result can be achieved by optimization of different accelerometer parameters listed in Table 7.1.

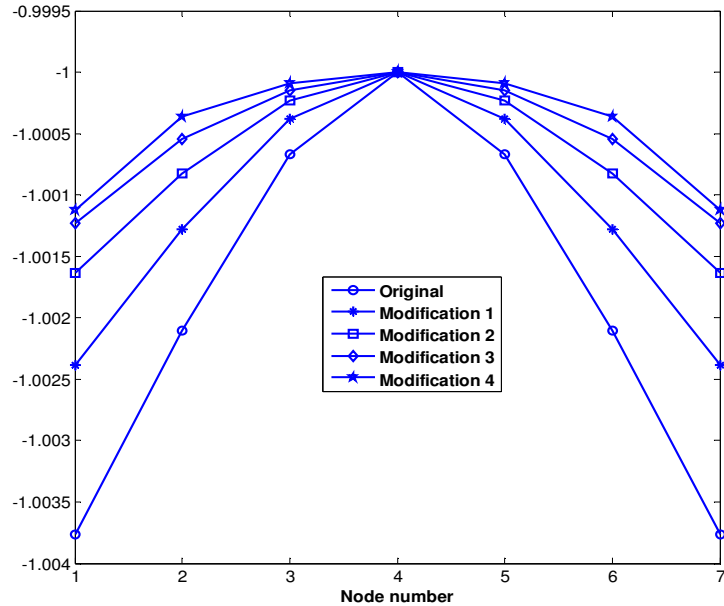


Figure 7.13 1st mode shape for the modified designs compared with original design

7.7 Conclusions

Earlier experimental studies for performance of capacitive type MEMS accelerometers showed deviation in their responses both in amplitude and phase. Modal analysis for a MEMS Accelerometer using a simple FE model has been presented. The modal analysis confirms that the accelerometer fingers behave as the cantilever beam which can be considered as one of major reasons for the error observed in the vibration measurements. Few modifications on finger shape design have been suggested and showed remarkable improvement. However, it is expected that translating the fingers

movement into changes in capacitance and then into output voltage will also introduce some errors.

CHAPTER 8

CONCLUSIONS AND FUTURE WORK

8.1 Conclusions

The use of conventional accelerometers in the condition monitoring is well accepted in practice. However, multiple data collection points are generally required in most of the condition monitoring systems which makes the system costly. Hence, there is a need for cheaper and reliable alternative for the conventional accelerometers. The use of MEMS accelerometers is one of the available options that came to light because of their low cost, and small size. However, the use of MEMS accelerometers is still limited in the field of vibration-based condition monitoring because of lack of confidence level in their performance. The stability, sensitivity, lifetime, mechanical strength, ease of operation and installation, are not attractive enough for the users to switch over. In addition, there are some concerns on the effect of noise and temperature over their accuracy.

Performance improvement of MEMS accelerometers for general applications rather than machine condition monitoring is still under research. Different sensing mechanisms, design parameters and variables, manufacturing process, and packing materials have been investigated and modified to achieve better performance and reliability with the less possible cost. However, A few earlier researches gave comparison of the performance between the MEMS and conventional accelerometers in the field of condition monitoring, mainly related to the frequency content in spectrum of

the measured signals.

8.2 Achieved Objectives

- **Objective 1:** Laboratory tests were carried out to compare the response characteristics between capacitive type MEMS accelerometers and a reference accelerometer when exposed to various forms of excitation. The tests include sinusoidal, band limited random and impulsive excitation. All tests were conducted well within the technical specifications of both the MEMS accelerometers under test and the reference accelerometer. The observations were based on the amplitude and phase of the FRF assuming the response from MEMS accelerometer as an output and the reference accelerometer response as the input. A significant deviation has been noticed in the amplitude and phase responses of MEMS accelerometers compared with a reference accelerometer. Moreover, it has been observed that MEMS accelerometers give repeated measurement for sinusoidal input excitation only.
- **Objective 2:** A correction method has been proposed by developing a filter based on the Characteristic Function (CF) obtained experimentally in the Laboratory experiments. Such filter can be incorporated in the accelerometer design itself if deviation observed during calibration. The application of the proposed method showed improvement of the measure signals in time domain. Hence the proposed method is useful in practical applications for reliable and credible signals.

- **Objective 3:** A simple method for correcting both amplitude and phase response of any MEMS accelerometer in frequency domain has been presented. The method is based on the generation of a characteristic function (CF) using well known reference accelerometer in Lab test and then this CF has been used in correcting the signals in frequency domain. The method has been qualified through number of tests on MEMS accelerometers and further tested on an experimental rig.
- **Objective 4:** A fine mesh FE model has been carried out to understand the dynamics of capacitive type MEMS accelerometer. It has been observed that the moving fingers behave like a cantilever beam while the fixed fingers showed rigid body motion. Based on these observations, a simple FE model; with a spring, a moving mass, and two moving fingers; has been developed in order to modify the design of the fingers. Few modifications on finger shape design have been suggested which showed remarkable improvement. Moreover, the effect of using synchronous amplitude modulation and demodulation in the readout circuit has been studied. The experimental study showed that this circuit introduces errors in amplitude and phase of the output signal compared with the input signal.

8.3 Overall Conclusion

MEMS accelerometers showed deviation compared with conventional accelerometers. Two methods have been suggested, one for correction in time domain and other in frequency domain. Either of these two methods can be used for the exciting MEMS accelerometers or any accelerometer showing some error. The reason of such error in MEMS accelerometer has also been identified and design modification for the fingers has been suggested for future manufacturing.

8.4 Future Work

1. In the present research, the proposed correction methods are only tested on lab experiments and one typical example on test rig. However, the real application may be field measurement. Hence, the methods must be further be tested and qualified for real application like machine condition monitoring.
2. MEMS accelerometer has two parts, mechanical design and electronic read out circuit. Modification in the moving and fixed fingers has already been suggested to improve the performance. However, the present read out circuit also introduces error in measurement. Hence, improvement in readout circuit needs to be investigated.

REFERENCES

1. Liang B., Condition Monitoring and Fault Diagnosis of Induction Motors, PhD Thesis, Manchester School of Engineering, Manchester, UK, 2000.
2. Harris M., and Charles E., Shock and Vibration Handbook, McGraw-Hill Book Company, New York, 1987.
3. Brüel and Kjær, Shock and Vibration Measurement, Denmark, 1998.
4. Brüel and Kjær, Frequency Analysis, Denmark, 1992.
5. Hargis C., Gaydon G., and Kamash K., The Detection of Rotor Defects in Induction Motors, In: Proc. Int. Conf. on Electrical Machines- Design and Applications, IEE, London, Vol.213, July 1982, pp. 216-220.
6. Sinha J. K., Health Monitoring Techniques for Rotating Machinery, PhD Thesis, University of Wales Swansea, 2002.
7. Sinha J. K., Friswell M. I., Lees A. W., The identification of the unbalance and the foundation model of a flexible rotating machine from a single run down, Mechanical Systems and Signal Processing, Vol.16, Issue 2-3, 2002, 255–271.
8. Rama R. A., Sinha J. K., Moorthy R. I. K., Vibration problems in vertical pumps- need for integrated approach in design and testing, Shock and Vibration Digest, Vol.29, No. 2, 1997, pp. 8–15.
9. Sinha J. K., Lees A. W., Friswell M. I., Estimating unbalance and misalignment of a flexible rotating machine from a single run-down, Journal of Sound and Vibration, Vol.272, Issue 3-5, 2004, pp. 967–989.
10. Moorthy R. I. K., Rao A. R., Sinha J. K., Kakodkar A., Use of an unconventional technique for seismic qualification of equipments, Nuclear Engineering and Design, Vol.165, Issue 1-2, 1996, pp. 15–23.
11. Sinha J. K., Simplified method for the seismic qualification using measured modal data, Nuclear Engineering and Design, Vol.224, Issue 2, 2003, pp. 125–129.
12. Sinha J. K., Moorthy R. I. K., Combined experimental and analytical method for a realistic seismic qualification of equipment, Nuclear Engineering and Design, Vol.195, Issue 3, 2000, pp. 331–338.
13. Moorthy R. I. K., Sinha J. K., , Dynamic qualification of complex structural

-
- components of nuclear power plants, Nuclear Engineering and Design, Vol.180, Issue 2, 1998, pp. 147-154
14. Moorthy R., Sinha J., Rao A., Sinha S., Kakodkar A., Diagnostics of direct CT-PT contact of coolant channels of PHWRs, Nuclear Engineering and Design, Vol.155, Issue 3, 1995, pp. 591-596.
15. Sinha J., Sinha S., Moorthy R., Diagnosis of the bearing failure in a Pillger Mill, Shock and Vibration Digest, Vol.28, No. 2, 1996, pp. 11-14.
16. Sinha J., Friswell M., Model updating: a tool for reliable modelling, design modification and diagnosis, Shock and Vibration Digest, Vol.34, No. 1, 2002, pp. 27-35.
17. Sinha J., Friswell M., The use of model updating for reliable finite element modelling and fault diagnosis of structural components used in nuclear plants, Nuclear Engineering and Design, Vol. 223, Issue 1, 2003, pp. 11-23.
18. Sinha J., Rao A., Moorthy R., Significance of analytical modelling for interpretation of experimental modal data: a case study, Nuclear Engineering and Design 220 (2003) 91-97.
19. Goldman S., Vibration Spectrum Analysis: A Practical Approach, Second Edition, Industrial Press Inc., New York, 1999.
20. Mehregany M., Microelectromechanical Systems, IEEE Circuits and Devices Vol. 9 Issue 4, 1993, pp 14-22.
21. Thanagasundram S, Schlindwein F, Comparison of integrated micro-electrical-mechanical system and piezoelectric accelerometers for machine condition monitoring, IMechE Journal of Mechanical Engineering Science, Part C, 220, 2006, pp. 1135-1146.
22. Albarbar H, Mekid S, Starr A, Pietruszkiewicz R, Suitability of MEMS Accelerometers for Condition Monitoring: An experimental study, Sensors, 8 (2), 2008, pp. 784-799.
23. Albarbar A, Abdellatef Badri, Sinha J. K., Starr A, Performance evaluation of MEMS accelerometers, Measurement, vol.42, Issue 5, Jun 2009, pp. 790-795.
24. Abdellatef E. Badri, Jyoti K. Sinha, Correcting Amplitude and Phase Measurement of Accelerometer in Frequency Domain, Proceeding of The Fifth International Conference on Condition Monitoring & Machinery Failure Prevention
-

-
- Technologies, Heriot-Watt University, Edinburgh, 15-18 July, 2008, pp. 94-100.
25. Fraden J., Handbook of Modern Sensors, Physics, Designs, and Applications, 3rd ed., Springer-Verlag, Inc., pp. 305.
26. Gardner J. W., Microsensors Principles and Applications, John Wiley & Sons Ltd, West Sussex, England, 1994.
27. Wilson J S, Sensor technology handbook, Elsevier Newnes.
28. Bentley J., Principles of Measurement Systems, 3rd Edition, Longman Scientific & Technical, Essex, England.
29. Reilly S., Leach R., Cuenat A., Lowe M., Overview of MEMS sensors and the metrology requirements for their manufacture, NMS Programme for Engineering Measurement 2005 – 2008, NPL Report DEPC-EM 008, October 2006.
30. Barth P.W., Pourahmadi F., Mayer R., Poydock J., Petersen K., A monolithic silicon accelerometer with integral air damping and over range protection, Solid-State Sensor and Actuator Workshop, Technical Digest., IEEE, 1988, pp. 35 – 38.
31. Roszhart T. V., Jerman H., Drake J., and Cotiis C. de, An Inertial-Grade Micromachined Vibrating Beam Accelerometer, The 8th International Conference on Solid-State Sensors and Actuators, Eurosensors IX. Transducers '95. , Stockholm, Sweden, 1995, pp. 656-658.
32. Seshia A. A., Palaniapan M., Roessig T. A., Howe R. T., Gooch R. W., Schimert T. R., and Montague S., A vacuum packaged surface micromachined resonant accelerometer, Journal of Microelectromechanical Systems, Vol.11, Issue 6, 2002, pp. 784-793.
33. Leung A. M., Jones J., Czyzewska E., Chen J., Woods B., Micromachined accelerometer based on convection heat transfer, Proceedings of The Eleventh Annual International Workshop on Micro Electro Mechanical Systems, MEMS 98, pp. 627-630.
34. MEMSIC, Thermal Accelerometers Temperature Compensation, Application Note #. 00MX-002, <http://www.memsic.com/data/pdfs/an-00mx-002.pdf>.
35. Kenny T.W., Waltman S. B., Reynolds J. K., Kaiser W. J., A micromachined silicon electron tunneling sensor, IEEE Proceedings of An Investigation of Micro Structures, Sensors, Actuators, Machines and Robots Micro Electro Mechanical Systems, 1990, pp. 192-196.
-

-
36. Yeh C., Najafi K., A low-voltage tunneling-based silicon microaccelerometer, IEEE Transactions on Electron Devices, Vol.44, Issue 11,1997, pp. 1875-1882.
 37. Dong H., Jia Y., Hao Y., Shen S., A novel out-of-plane MEMS tunneling accelerometer, Sensors and Actuators A: Physical, Vol.120, 2005, pp. 360-364.
 38. Cheng-Hsien Liu, Kenny T. W., A high-precision, wide-bandwidth micromachined tunneling accelerometer, Journal of Microelectromechanical Systems, Vol.10, Issue 3, 2001, pp.425-433.
 39. Uttamchandani D., Liang D., Culshaw B., A micromachined silicon accelerometer with fibre optic interrogation, IEE Colloquium on Fibre Optics Sensor Technology, 1992, pp. 4/1-4/4.
 40. DeVoe D.L., Pisano A.P., Surface micromachined piezoelectric accelerometers (PiXLs), Journal of Microelectromechanical Systems, Vol.10, Issue 2, 2001, pp. 180-186.
 41. Kunz K., Enoksson P., Stemme G., Highly sensitive triaxial silicon accelerometer with integrated PZT thin film detectors, Sensors and Actuators A: Physical, Vol.92, 2001, pp. 156-160.
 42. Abbaspour-Sani E., Huang Ruey-Shing, Yee Kwok Chee, A linear electromagnetic accelerometer, Sensors and Actuators A: Physical, Vol.44, Issue 2, 1994, pp. 103-109.
 43. Chien Chao-Heng, Chen Shi-Hao, Fabrication comb-drive device by MEMS and electroplating, Proceedings of the Symposium on Design, Test, Intergation & Packing of MEMS/MOEMS, Cannes-Mandelieu, 5-7 May 2003.
 44. Khine Myint Mon A., Tin Thet Nwe B., Zaw Min Naing C. Dr., Yin Mon Myint D. Dr., Analysis on Modeling and Simulation of Low Cost MEMS Accelerometer ADXL202, Proceedings of World Academy of Science, Engineering and Technology, Vol.32, August 2008, pp. 389-601.
 45. Xingguo Xiong, Yu-Liang Wu, Wen-Ben Jone, Design and Analysis of Self-Repairable MEMS Accelerometer, Proceedings of the 20th IEEE International Symposium on Defect and Fault Tolerance in VLSI Systems (DFT'05), 2005.
 46. Starr J. B., Squeeze-film damping in solid-state accelerometers", IEEE, 1990. pp. 44-47.
 47. Beeby S., Stuttle M., White N. M., Design and fabrication of a low cost

-
- microengineered silicon pressure sensor with linearized output, Science, Measurement and Technology, IEE Proceedings, Vol.147, Issue 3, May 2000, pp. 127-130.
48. Martin Handtmann, Robert Aigner, Andreas Meckes, Gerhard Wachutka, Sensitivity enhancement of MEMS inertial sensors using negative spring and active control, Sensors and Actuators A, 97-98, 2002, pp. 153-160.
49. Sazzadur Chowdhury, Ahmadi M., Miller W. C., Nonlinear Effects in MEMS Capacitive Microphone Design, Proceeding of the International Conference on MEMS, NANO and Smart Systems (ICMENS'03), 2003.
50. Xuesong Jiang, Feiyue Wang, Michael Kraft, Bernhard E. Boser, An Integrated Surface Micromachined Capacitive Lateral Accelerometer with $2\mu\text{G}/\sqrt{\text{Hz}}$ Resultion, Solid-State Sensor, Actuator and Microsystems Workshop Hilton Head Island, South Carolina, June 2-6, 2002, pp. 202-205.
51. Yasin F., Korman C., Nagel D., Measurement of noise characteristics of MEMS accelerometers, Solid-State Electronics, 47, 2003, pp. 357-360.
52. Badariah Bais, Burhanuddin Yeop Majlis, Low-g Area-changed MEMS Accelerometer Using Bulk Silicon Technique, American Journal of Applied Sciences 5 (6), 2008, pp. 626-632.
53. Wei Tech Ang, Si Yi Khoo, Pradeep K. Khosla, Cameron N. Riviere, Physical Model of a MEMS Accelerometer for Low-g Motion Tracking Applications, Proceeding of the 2004 IEEE, International Conference on Robotics & Automation, New Orleans, LA, April 2004, pp. 1345-1351.
54. Sergey Edward Lyshevski, MEMS and NEMS Systems-Devices and Structures, CRC PRESS, 2001.
55. Los Santos H., Introduction to Microelectromechanical Microwave Systems, ARTECH HOUSE, INC.
56. Plaza J., Collado A., Cabruja E., Esteve J., Piezoresistive accelerometers for MCM package, Journal of Microelectromech. Systems, Vol.11, No. 6, Dec. 2002, pp. 794–801.
57. Xie H., Fedder G., CMOS z-axis capacitive accelerometer with comb-finger sensing, Proc. IEEE Micro Electro Mechanical Systems (MEMS), 2000, pp. 496–501.
-

-
58. Biefeld V., Buhrdorf A., Binder J., Laterally driven accelerometer fabricated in single crystalline silicon, *Sensors & Actuators A*, Vol.82, No. 1, May 2000, pp. 149–154.
 59. Yazdi N., Ayazi F., Najafi K., Micromachined inertial sensors, *Proc. IEEE*, Vol.86, No. 8, August 1998, pp. 1640–1659.
 60. Li L., Xu Y., Zhao Y., Liang C., Wei T., Yang Y., Micromachined accelerometer based on electron tunnelling, *Proc. SPI-International. Society Optical Engineering*, Vol.3891, 1999, pp. 121–125.
 61. Gao R., Zhang L., Micromachined microsensors for manufacturing, *IEEE Instrumentation & Measurement Magazine*, Vol.7, Issue 2, 2004, pp. 20-26.
 62. Packirisamy M., Microfabrication influence on the behaviour of capacitive type MEMS sensors and actuators, *Sensor Review*, 26/1, 2006, pp. 58-65.
 63. Wan W., Lowther D., Design and synthesis of wide tuning range variable comb drive MEMS capacitors, *COMPEL*, Vol.26, No. 3, 2007, pp. 689-699.
 64. Bogue R., MEMS sensors: past, present and future, *Sensor Review*, 27/1(2007) 7-13.
 65. Felnhofer D., Khazeni K., Mignard M., Tung Y., Device physics of capacitive MEMS, *Microelectronic Engineering*, 84, 2007, pp. 2158-2164.
 66. Lee I., Yoon G., Park J., Seok S., Chun K., Lee K., Development and analysis of the vertical capacitive accelerometer, *Sensors and Actuators A*, 119, 2005, pp. 8-18.
 67. Meunier D., Desplats R., Benbrik J., Perez G., Pellet C., Etsève D., Benteo B., Electrical characterization and modification of a MicroElectroMechanical System (MEMS) for extended mechanical reliability and fatigue testing, *Microelectronics Reliability*, 38, 1998, pp. 1265-1269.
 68. Yee Y., Park M., Kim S., Chun K., Integrated Silicon Accelerometer with MOSFET-type Sensing Element, *Journal of the Korean Physical Society*, Vol.33, November 1998, pp. S419-S422.
 69. Wu J., Sensing and Control Electronics for Low-Mass Low Capacitance MEMS Accelerometers, PhD Thesis, 2002.
 70. Sung S., Lee J., Kang T., Development and test of MEMS accelerometer with self-sustained oscillation loop, *Sensors and Actuators A*, 109, 2003, pp. 1-8.
 71. HA B., OH Y., Song C., A Capacitive Silicon Microaccelrometer with Force-

-
- Balanced Electrodes, *Jpn. J. Appl. Phys.*, Vol.37, 1998, pp. 7052-7057.
72. Xie H., Fedder G., Pan Z., Frey W., Design and Fabrication of An Integrated CMOS-MEMS 3-Axis Accelerometer, *Nanotech*, 2003, Vol.2, pp. 420-423.
73. Coulate J., Fox C., McWilliam S., Malvern A., Application of optimal and robust design methods to a MEMS accelerometer, *Sensors and Actuators A*, 142, 2008, pp. 88-96.
74. Rao P., Babu P., Rani A., Reddy D., Design of Two Beam Capacitive Micromachined Acceleration Sensor and Its Displacement and Stress Analysis, *Asian J. Exp. Sci.*, Vol.22, No. 3, 2008, pp. 351-356.
75. Natarajan V., Bhattacharya S., Chatterjee A., Alternate Electrical Tests for Extracting Mechanical Parameters of MEMS Accelerometer Sensor, *Proceedings of the 24th IEEE VLSI Test Symposium (VTS'06)*, 2006.
76. Luo H., Zhang G., Carley L., Fedder G., A Post-CMOS Micromachined Lateral Accelerometer, *Journal of Microelectromechanical Systems*, Vol.11, No. 3, June 2002.
77. Qu H., Fang D., Xie H., A Monolithic CMOS-MEMS 3-Axis Accelerometer With a Low-Noise, Low-Power Dual-Chopper Amplifier, *IEEE Sensors Journal*, Vol.8, No. 9, September 2008.
78. Chattaraj D., Swamy K., Sen S., Design and Analysis of Dual Axis MEMS Accelerometer, *International workshop on Physics of Semiconductor Devices*, 2007, pp. 718-720.
79. Bell D., Lu T., Fleck N., Spearing S., MEMS actuators and sensors: observation on their performance and selection purpose, *Journal of Micromechanics and Microengineering*, 15, 2005, pp. 153-164.
80. Dias Pereira JM, Carlos Banha, Octavian Postolache, Silva Girao P., Improving Accelerometers Performance Using Smart Sensing Techniques, *IEEE SENSORS 2006, EXCO, Daegu, Korea / October 22-25, 2006*.
81. Fadi M. Alsaleem, Mohammad I. Younis, Mahmoud I. Ibrahim, A Study for the Effect of the PCB Motion on the Dynamics of MEMS Devices Under Mechanical Shock, *Journal of Micromechanical Systems*, vol.18, No. 3, June 2009.
82. Alexander A. Trusov, Andrei M. Shkel, A Novel Capacitive Detection Scheme With Inherent Self-Calibration, *Journal of Micromechanical Systems*, Vol.16, No. 6, December 2007.
-

-
83. Tetsuya Kajita, Un-Ku Moon, Gábor C. Temes, A Two-Chip Interface for a MEMS Accelerometer, IEEE Transaction on Instrumentation and Measurement, Vol.51, No. 4, August 2002.
 84. Xiaowei LIU, Haifeng ZHANG, Guangming LI, Weiping CHEN, Xilian WANG, Design of Readout Circuits Used for Micro-machined, Proceedings of the 2nd IEEE International Conference on Nano/Micro Engineered and Molecular Systems January 16 - 19, 2007, Bangkok, Thailand.
 85. Xiaowei Liu, Chen Hong, Chen Weiping, System Damping Ratio Analysis of a Capacitive Micromechanical Accelerometer, IEEE. 6th International Conference on Electronic Packaging Technology, 2005.
 86. Guchuan Zhu, Lahcen Saydy, Mehran Hosseini, Jean-François Chianetta, Yves-Alain Peter, A Robustness Approach for Handling Modelling Errors in Parallel-Plate Electrostatic MEMS Control, Journal of Micromechanical Systems, Vol.17, No. 6, December 2008.
 87. Marinov Marin, Todor Djamiykov, Ivan Topalov, Volker Zerbe, Remote Machine Condition Monitoring Based on Wireless Connectivity, ELECTRONICS' 2004, 22-24 September, Sozopol, Bulgaria.
 88. Pandiyan J., Umapathy M., Balachandar S., Arumugam M., Ramasamy S., Gajjar N., Design of Industrial Vibration Transmitter Using MEMS Accelerometer, Journal of Physics: Conference Series, 34, 2006, pp. 442-447.
 89. Inzarulfaisham Abd. Rahim, Muhamad Azman Miskam, Othman Sidek, Shahril Azwan Zaharudin, Mohammad Zaidi Zainol, Shukri Korakkottil Kunhi Mohd, Development of a Vibration Measuring Unit Using a Microelectromechanical System Accelerometer for Machine Condition Monitoring, European Journal of Scientific Research, Vol.35 No.1, 2009, pp. 150-158.
 90. Ratcliffe C., Heider D., Crane R., Krauthauser C., Yoon M., Gillespie J., Investigation into the use of low cost MEMS accelerometers for vibration based damage detection, Composite Structures , 82, 2008, pp. 61-70.
 91. Tjiu W., Ahanchian A., Majlis B., Development of Tire Condition Monitoring System (TCMS) Based on MEMS Sensors", ICSE2004 Proc. 2004, Kuala Lumpur, Malaysia.
 92. Erwin Peiner, Condition monitoring with axle box bearings using resonant

-
- microelectromechanical sensors, *Journal of Micromechanics and Microengineering*, 12, 2002, pp. 479–485.
93. Vogl Andreas, Dag T. Wang, Preben Storås, Thor Bakke, Maaïke M.V. Taklo, Allan Thomson, Lennart Balgård, Design, process and characterisation of a high-performance vibration sensor for wireless condition monitoring, *Sensors and Actuators A*, 153, 2009 pp. 155–161.
94. Wright Paul, David Dornfeld, Nathan Ota, Condition Monitoring in End-Milling using Wireless Sensor Networks (WSNs), *Transactions of NAMRI/SME*, Volume 36, 2008.
95. Huang S., Zhang D. H., Chan H. L., Goh K. M., Evaluation of WSN-based accelerometer for tool condition monitoring, *SIMTech technical reports (STR_V10_N2_04_MEC)*, Vol.10, No. 2, Apr-Jun 2009.
96. ISO 5347, Methods for the calibration of vibration and shock pick-ups—Part 0: Basic concepts, 1987.
97. Sinha Jyoti K., On Standardisation of calibration procedure for accelerometer”, *Journal of Sound and Vibration*, 286, 2005, pp. 417-427.
98. Liu C., Kenny T.W., A high-precision, wide-bandwidth micromachined tunneling accelerometer, *Journal of Microelectromechanical Systems*, 10, 3, 2001, pp. 425–433.
99. Albarbar A., Starr A., Pietruszkiewicz R., Towards the implementation of integrated multimeasurand wireless monitoring system, *Proceedings of Second World Congress on Engineering and Asset Management*, 2007, pp. 96–105.
100. Suryam B.C.B.N., Meher K.K., Sinha J. K., Rao A., Coherence measurement for early contact detection between two components, *Journal of Sound and Vibration* 290 ,2006, pp. 519–523.
101. Sinha J. K., Vibration based diagnosis techniques used in nuclear power plants: an overview of experiences, *Nuclear Engineering and Design*, Vol.238, Issue 9, 2008, pp. 2439–2452.
102. Badri Abdellatef, Sinha J.K., Albarbar A., A method to calibrate the measured responses by MEMS accelerometers. *Strain* (2010), doi:10.1111/j.1475-1305.2010.00764.x.
103. Oppenheim A.V., Schafer R.W., *Discrete-Time Signal Processing*, Prentice-
-

-
- Hall, 1989, pp. 203–5.
104. Simon Haykin, Adaptive Filter Theory, Prentice-Hall, 1996.
 105. Mathworks, MatLab Signal Processing Toolbox.
 106. Lynn P.A., Introductory Digital Signal Processing with Computer Applications, John Wiley & Sons Ltd., 1999, pp. 109–110.
 107. Ferrari V., Ghisla A., Marioli D., Taroni A., MEMS Accelerometer with Multiaxial Response by Dynamic Reconfiguration of Peizoiresistive Bridges, Proceedings of Eurosensors Conference, Sweden, 2006, ISBN/ISSN:97891-631-9281-4.
 108. Boga B., Ocak I. E., Kulah H., Akin T., Modelling of a Capacitive Σ - Δ MEMS accelerometer system including the noise components and verification with test results, MEMS 2009, IEEE 22nd Int. Conf. 2009, 821-824.
 109. Sun C., Wang C., Fang W., On the sensitivity improvement of CMOS capacitive accelerometer, Sensors and Actuators A, 2008, 141, pp. 347-352.
 110. Acar C., Shkel A. M., Experimental evaluation and comparative analysis of commercial variable-capacitance MEMS accelerometers, J. Micromech. Microeng. 2003, 13, pp. 634-645.
 111. Badri A., Sinha J. K., Albarbar A., Enhancing the frequency range of measurement for an accelerometer, Noise & Vibration Worldwide, Volume 40, Number 6, June 2009, pp. 33-36.
 112. ERİŞMİŞ M. A. MEMS Accelerometers and Gyroscopes for Inertial Measurement Units, MSc Thesis, The Graduate School of Natural and Applied Sciences of Middle East Technical University, 2004.
 113. Badri A. E., Sinha J. K., Improvement of Measured Signals of MEMS Accelerometer, 3rd International Conference on Integrity, Reliability and Failure, Porto/Portugal, 20-24 July 2009, Paper Ref: S1146_P0507.
 114. Tay F. E. H., Jun Xu, Liang Y. C., Logeeswaran V. J., Yufeng Yao, The effects of non-parallel plates in a differential capacitive microaccelerometer, J. Micromech. Microeng, 9, 1999, pp. 283–293.
 115. Linxi Donga, Lufeng Cheb, Lingling Suna, Yuelin Wang, Effects of non-parallel combs on reliable operation conditions of capacitive inertial sensor for step and shock signals, Sensors and Actuators A, 121, 2005, pp. 395–404.

-
116. Asrulnizam Bin Abd Manaf, Yoshinori Matsumoto, Low voltage charge-balanced capacitance–voltage conversion circuit for one-side-electrode-type fluid-based inclination sensor, *Solid-State Electronics*, 53, 2009, pp. 63–69.
 117. Simon Haykin, *Communication Systems*, 4th edition, John Wiley & Sons, Inc, USA, 2001, pp. 90-96.
 118. Maziar Tavakoli, Rahul Sarpeshkar, An Offset-Canceling Low-Noise Lock-In Architecture for Capacitive Sensing, *IEEE Journal of Solid-State Circuits*, Vol.38, No. 2, February 2003.
 119. Sharma K., Macwan I. G., Zhang L., Hmurcik L., Xiong X. Design Optimization of MEMS Comb Accelerometer,
http://www.asee.org/documents/zone1/2008/student/ASEE12008_0050_paper.pdf
 120. Badri A E., Sinha J. K., Dynamics of MEMS Accelerometer, The 17th International congress on sound & vibration, Cairo, Jul. 2010.

(This page is intentionally left blank)